Lead-Free KNN-based Piezoelectric Ceramics

By:

Fayaz Hussain

A thesis submitted in partial fulfilment of the requirements for the degree of Doctor of Philosophy

Supervisors: **Prof. Ian M Reaney**

Prof. Derek C Sinclair

Faculty of Engineering

Department of Materials Science and Engineering

October 2016

" لاَ عَقْلَ كَالتَّدْبِيرِ وَلاَ وَرَعَ كَالْكَفِّ وَلاَ حَسَبَ كَحُسْنِ الْخُلُقِ "

"There is no wisdom like reflection, and no honour like good manners."

(Sunan Ibn Majah Vol. 5, Book 37, Hadith 4218)

Dedications

(Late) My Father, whose prayers are always with me!

My Mother, every time wants to see me successful in every good step of life! Missing me a lot! Is happy with me like father!

(Alhamd-u-lillah)!

Wife, made a happy life here in Sheffield with lot of love, showed patience and served delicious foods! Fazal & Iqra, filled the colours of father into me to say good bye to sadness!

Sister, was so helpful like mother in our life!

Brothers, organised the life wonderful in absence of me in Pakistan!

And to all relatives, friends (M.Ameen is also included in brothers!)

Acknowledgements

In the name of Allah Who is the most Merciful and Bountiful to all Mankind!

I am very thankful and obliged to my supervisor Prof. Ian M. Reaney. His polite and highly professional way of research encouraged me to write thesis for PhD to successfully finish the project. Thanks a lot to Prof. Derek C Sinclair, for learning Impedance Spectroscopy and to Prof. Tony West for Solid State Chemistry concepts during group meetings. I am also very grateful to Dr. Iasmi Isterianou, particularly for her very detailed guidance and training of equipment used in research and her expert ideas that were very helpful. Learning tape casting, screen printing and multilayer stacking was facilitated by Dr Denis Cumming and from Mr Alireza Mehranjani; thanks a lot both of you! My gratitude is also for Mr Amir Khesro for his technical discussions, working-together in the labs and for help in strain measurement. The good relationship of our families made life easier. Towards the end of the PhD I had very positive interaction with Dr Dawei Wang. Dr Nik Reeves helped hugely with X-ray diffraction. I will not forget his technical help, learning sessions and emails of polite instruction. I am thankful to Mr Mohammed Elbadawi for his help with scanning electron microscopy. I would like to mention my other colleagues in the Functional Materials and Devices group (Nouf, Adil, Ibtsam, Yang, Jack, Shunsuke, Greg, Simon, Rouzbeh, John, Leo, Bo etc.), all of whom at some stage contributed to me submitting my thesis.

I am also thankful to Mr. Andrew Mould for training on equipment and up-to-date information of status of laboratories as the Sorby Centre for their patience in training me. And sincere regards go to the all staff members of the MSE department who were directly or indirectly linked with technical services of my research work (Ann, Kurn, Bev, Bell, Ma, etc.).

I am appreciative to the Ex-Head of Department, Prof. Mark Rainforth, for facilitating a fee waiver so that I could commence my Ph.D. It is great pleasure to thank Mr. Abdul Haque Kandhro to his surety (through Mother-in-Law) for my Scholarship and our Dean (CPE) Prof. M. Tufail Jokhio.

Finally, I am very gratified to the NED University of Engineering and Technology for funding support. A special thank you is awarded to all my friends (Dr. Sheraz, Dr. Bilal, Ameen, Kashif, Shakeel etc.) and colleagues for their support.

Publications

On Different ratios of KNN with BNZ:

- Wang, D., **Hussain, F**, Khesro, A, et al., *Composition and temperature dependence of piezoelectricity in* $(1-x)(K_{1-y}Na_y)NbO_3$-$x(Bi_{1/2}Na_{1/2})ZrO_3$ *lead-free ceramics.* American Ceramic Society, 2016: p. 1-9.

MLA Fabricated with this study's Novel method (WMM):

- Khesro, A., Wang, D, **Hussain, F**, et al., *Temperature Stable and Fatigue Resistant Lead-free Ceramics for actuators,* Applied Physics Letters, 2016. 109(14).

Conferences

- **Fayaz Hussain**, Iasmi Sterianou, Derek C Sinclair, Ian M Reaney, *Properties of* $K_{0.50}Na_{0.50}NbO_3$ *Sintered in* N_2 *and Air*, Ferroelectrics UK, 17-18 January 2013, IOP, University of Sheffield, Sheffield, UK.
- **Fayaz Hussain**, Iasmi Sterianou, Derek C Sinclair, Ian M Reaney, *Semiconductor Behaviour of* $K_xNa_{(1-x)}NbO_3$ $(0.49 \leq x \leq 0.51)$ *as a function of* $P(O_2)$, Electroceramics-XIV Conference, 16-20 June 2016, Bucharest, Romania.
- Shunsuke Murakami, Amir Khesro, **Fayaz Hussain**, Dawei Wang, Derek C Sinclair and Ian M Reaney, "*Doping Effects in Lead-free Piezoelectric BT-BF based Ceramics*", Sustainable Functional Materials April 2016, Scarborough, UK
- Dawei Wang, **Fayaz Hussain**, Amir Khesro, Antonio Feteira, Ye Tian and Ian M Reaney, "*Composition and Temperature Dependence of*

Piezoelectricity in KNN-based Lead-free Ceramics". 2016 Joint IEEE International Symposium on the Applications of Ferroelectrics, European Conference on Applications of Polar Dielectrics, Darmstadt Germany.

Summary

In many commercial devices, there are a number of ways in which energy is wasted or dissipated. This waste energy can, in principle, be harvested by using the correct functional material. In the case of vibrational energy, the logical materials of choice are piezoelectric ceramics. However, all current commercial piezoelectrics contain lead oxide which is classed as a restricted material in environmental legislation. The main contenders for lead free piezoelectrics are based on $K_{0.5}Na_{0.5}NbO_3$ (KNN) and $Na_{0.5}Bi_{0.5}TiO_3$. The former however, has the advantage in that it is compatible with cheap Ni-based internal electrodes and thus it is feasible to manufacture low cost KNN based multilayer devices provided formulations do not deteriorate in the reducing condition required to suppress the formation of NiO. Consequently, KNN based lead free piezoelectric ceramics have been studied from the perspective of optimising their performance for multilayer actuators, potentially for energy harvesting applications. To this end, the defect chemistry of KNN has been investigated under different sintering conditions, dopants (acceptors: Mn^{2+}, Ti^{4+}, Sn^{4+} in KNN_50/50 ratio; Donor: Sr^{2+} in KNN_50/50 ratio; Ta^{5+} as an isovalent in KNN-51/49 ratio; and co-dopants: Bi^{3+} and Zr^{4+} in KNN_50/50 ratio) have been incorporated into KNN to enhance the piezoelectric performance and prototype multilayers of 10 and 16 layers with inner Pt electrodes have been fabricated to demonstrate the potential of 0.942KNN-0.058BNZ+ZrO_2 for the fabrication of multilayer actuators. This lead free composition has the potential to replace PZT-4 and PZT-8 in piezoelectric devices for room temperature applications. To fabricate the multilayers, a novel Wet-Multilayer-Method (WMM) was also developed to overcome the issues of delamination during firing of MLCCs.

Contents

Chapter 1 Introduction and Aims

1.1 Introduction and Aims

Piezoelectric ceramics are an important class of functional materials. However, the majority of piezoelectrics are based on $Pb(Zr,Ti)O_3$ (PZT) which contains lead oxide. According to European environmental legislation, lead is toxic and not environmentally friendly. There is therefore, significant focus on lead free piezoelectric materials. Potassium Sodium Niobate (KNN) is one of the leading candidates to replace PZT but there are many fundamental science and processing issues to be understood before it can be used commercially. The main issue in, e.g., the fabrication of KNN multilayer actuators for potential use in energy harvesting applications, is the optimisation of its piezoelectric properties during co-firing with Ni based internal electrodes. The use of base metal electrodes is highly desirable since they are cheap and have been extensively developed for the capacitor industry but to prevent oxidation during sintering they require low $P(O_2)$. Consequently, inert or reducing atmospheres are commonly used. KNN is an ideal starting material for the fabrication of PbO free piezoelectrics since it follows a sequence of ferroelectric phase transitions on cooling, Figure 1-1, which are similar to better known compounds such as $BaTiO_3$.

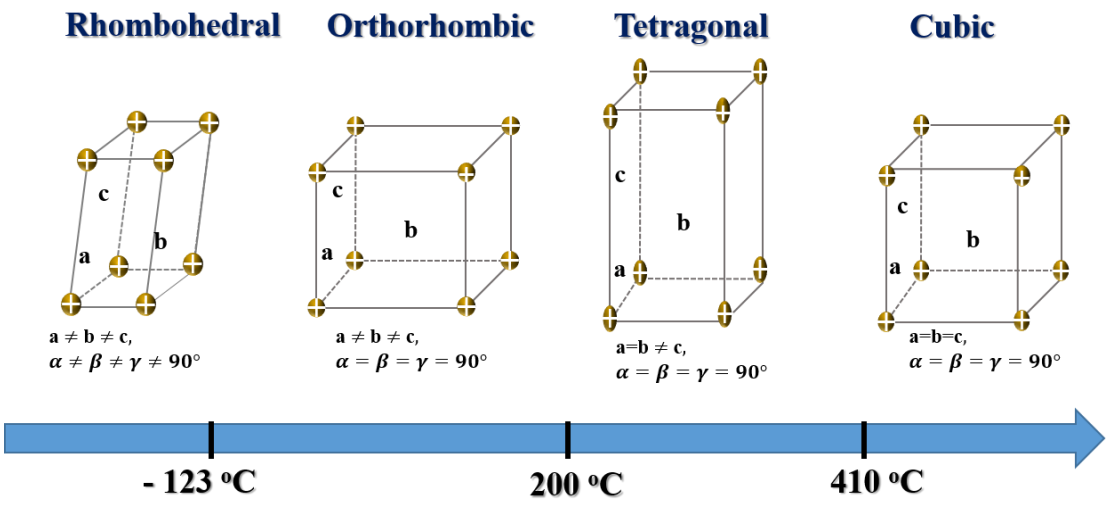

Figure 1-1 The phase transitions in KNN with respect to the temperature

At high temperature, KNN (50:50) is cubic but below 410 °C, it transforms to a ferroelectric tetragonal structure with subsequent transitions to orthorhombic (210 °C) and rhombohedral (-123 °C) on further cooling, Figure 1-1.

The flexibility of the structure means that the properties of KNN can be modified by suitable dopants and domain engineered to have superior properties in a manner reminiscent of PZT. However, K and Na are volatile at high temperatures and there are difficulties anticipated in high temperataure fabricaion of actuators. Moreover, the defect chemistry of KNN sintered at differerent atmospheres is not well understood.

The aim of this project therefore was to develop KNN based compositions whose piezoelectric properties are optimised and in the long term not affected by firing in inert/reducing conditions. To this end, the effect of processing atmosphere on the properties of KNN have been investigated. In addition, the role of dopants has been studied in the enhancement of piezoelectric properties with a view to developing prototype multilayers in the latter part of the project.

Chapter 2 Literature Review

2.1 Perovskite Structure (ABX_3)

This perovskite structure was discovered by Geologist Gustav Rose in 1830, named After Russian Mineralogist, C. L. A. Von Perovski. In this structure A and B are metallic cations, and X is non-metallic anion, typically O or a halide. The ideal perovskite has a primitive cubic structure with $Pm\bar{3}m$ symmetry, in which $R_A >> R_B$ and $R_A \approx R_O$ where R_A, R_B and R_O are the ionic radii of the A-, B- and O-site ions respectively [1].The tolerance factor (t) was first used by Goldschmidt (1926) to establish combination of ions likely to form the perovskite structure,

$$t = \frac{R_A + R_O}{\sqrt{(R_B + R_O)}}$$

and for an ideal cubic crystal such as $SrTiO_3$, $t \approx 1$.

2.2 Piezoelectric and Dielectric Properties

Piezoelectric properties can only be obtained from crystals which are non-centrosymmetric. From 32 crystal classes or point groups, 21 are non-centrosymmetric (i.e., without centre of symmetry) but only 20 are piezoelectric, as described in detail in Figure 2-1 and Figure 2-3. From the piezoelectric point groups, only 10 are polar and exhibit piezoelectricity and pyroelectricity simultaneously and within this there is a subgroup which exhibits spontaneous reversible polarization. This latter group are simultaneously pyroelectric, ferroelectric and piezoelectric.[2]

Mainly ceramics are composed of randomly oriented grains and are said to be isotropic. To induce pyro- or piezoelectricity therefore, they require ‘poling’ which is usually carried out a high field 2 MV/m and at elevated temperatures to encourage the reorientation of electric dipoles and domains within the crystal structure and grains. At a morphotropic phase boundary (MPB), the reorientation of dipoles and

domains is comparatively easy and thus the properties of ceramics are optimised. MPBs in typical KNN-based compositions are considered to arise at the T_{O-T} and T_{O-R-T} phase boundaries [3]

In addition to piezoelectric properties being optimised at an MPB, the relative permittivity (ε_r) is often at a maximum. In principle ε_r is independent of electric field strength but may depend on frequency of AC field, crystal structure, defect chemistry, temperature and pressure. ε_r is an effective measure of the ability of a dielectric to store charge within a simple parallel plate capacitor and its value is determined by magnitude and type of polarizability. Electronic, ionic, dipolar and space charge dominate ε_r and tanδ in the approximate frequency ranges, 10^{12-15}, 10^{9-12}, 10^{4-9} and $<10^3$, respectively, and are briefly described in Figure 2-2. Tanδ or the dielectric loss is a measure of the dissipation of heat during the storage of charge in a dielectric.[2-5]

Dipolar behaviour in ferroelectric materials arises from the onset of spontaneous polarisation from a centro- to non-centrosymmetric state at its Curie temperature (T_C) which for KNN is from a non-polar cubic to polar tetragonal structure. Polarisation of the low temperature ferroelectric structure is defined as the total dipole moment per unit volume.

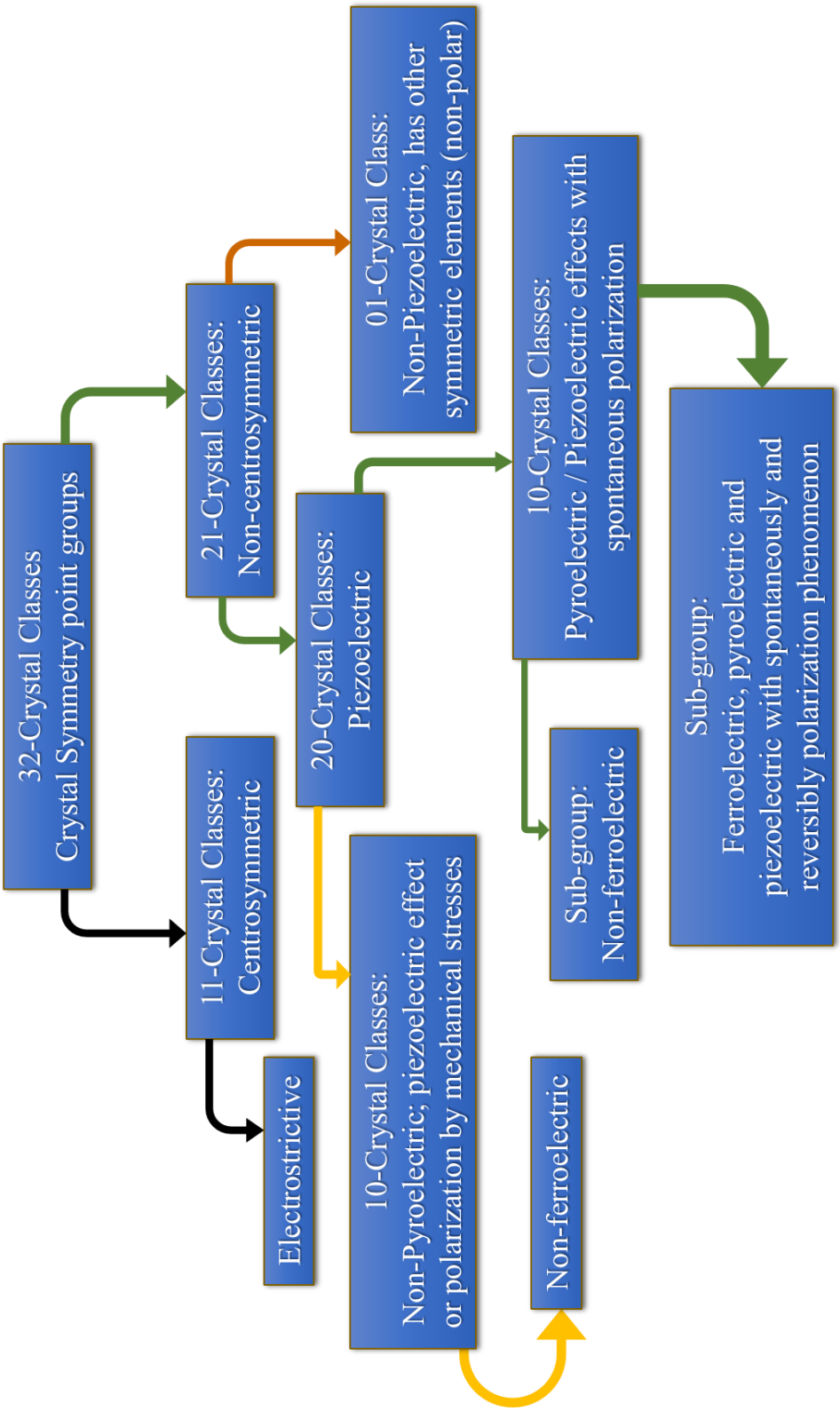

Figure 2-1 Crystal classes according to their respective properties [2, 6]

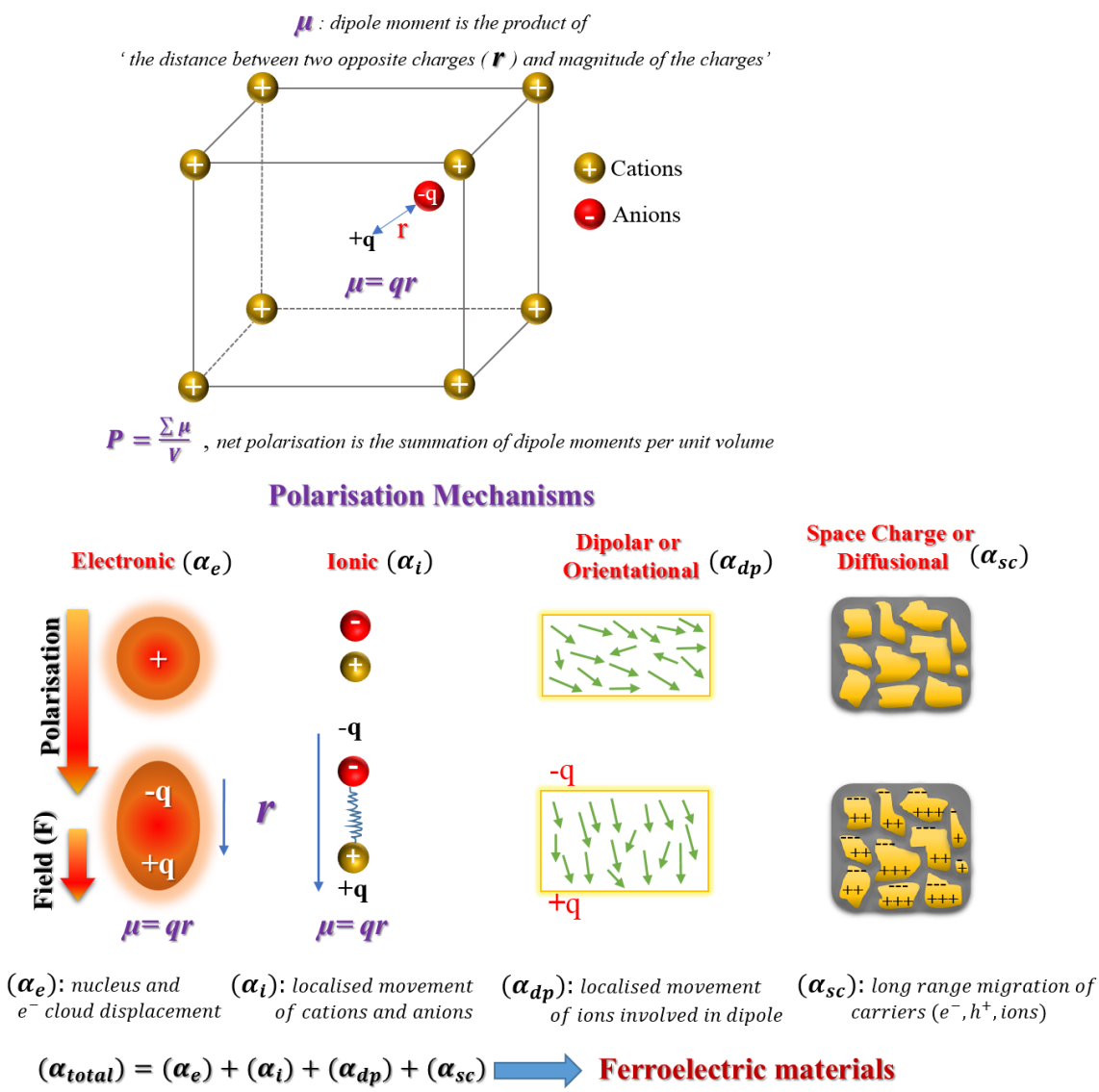

Figure 2-2 Explanation of dipole moment and polarisation mechanisms, re-drawn from[3, 5]

The efficiency of piezoelectric materials can be measured in the ratio of 'electrical energy converted into mechanical energy' to 'input electrical energy' or vice versa, which is known as the electro-mechanical coupling factor (k). k is always expressed as a fraction or percentage. For quartz, k = 0.1, for barium titanate 0.4 whereas for PZT, it is around 0.7.

$$k^2 = \frac{(output)\,Electrical\ energy\ into\ mechanical\ energy}{(input)\ electrical\ energy}$$ [1]

Or

$$k^2 = \frac{(output)\,Mechanical\ energy\ into\ electrical\ energy}{(input)\ mechanical\ energy}$$

Crystal system	Crystal class	Symmetry elements	Degree of symmetry	Laue classes (center of symmetry)	Piezo - pyro
Triclinic	$\bar{1}$	$\bar{1}$	2	Yes	No
	1	1	1	No	Pyro
Monoclinic	2/m	2/m	4	Yes	No
	2	2	2	No	Pyro
	m	m	2	No	Pyro
Ortho-rhombic	mmm	2/m2/m 2/m	8	Yes	No
	222	222	4	No	Piezo
	mm2	mm2	4	No	Pyro
Tetragonal	4/mmm	4/m2/m 2/m	16	Yes	No
	422	422	8	No	Piezo
	4mm	4mm	8	No	Pyro
	$\bar{4}$ 2m	$\bar{4}$ 2m	8	No	Piezo
	4/m	4/m	8	Yes	No
	4	4	4	No	Pyro
	$\bar{4}$	$\bar{4}$	4	No	Piezo
Trigonal	$\bar{3}$m	$\bar{3}$2m	12	Yes	No
	32	32	6	No	Piezo
	3m	3m	6	No	Pyro
	$\bar{3}$	$\bar{3}$	6	Yes	No
	3	3	3	No	Pyro
Hexagonal	6/mmm	6/m2/m 2/m	24	Yes	No
	622	622	12	No	Piezo
	6mm	6mm	12	No	Pyro
	$\bar{6}$ 2m	$\bar{6}$ 2m	12	No	Piezo
	6/m	6/m	12	Yes	No
	6	6	6	No	Pyro
	$\bar{6}$	$\bar{6}$	6	No	Piezo
Cubic	m$\bar{3}$m	4/m $\bar{3}$ 2/m	48	Yes	No
	432	432	24	No	No
	$\bar{4}3m$	$\bar{4}3m$	24	No	Piezo
	m$\bar{3}$	2/m $\bar{3}$	24	Yes	No
	23	23	12	No	Piezo

Figure 2-3 Nomenclature of piezoelectric and pyroelectric crystal classes [6].

[1] Dimensionless factor

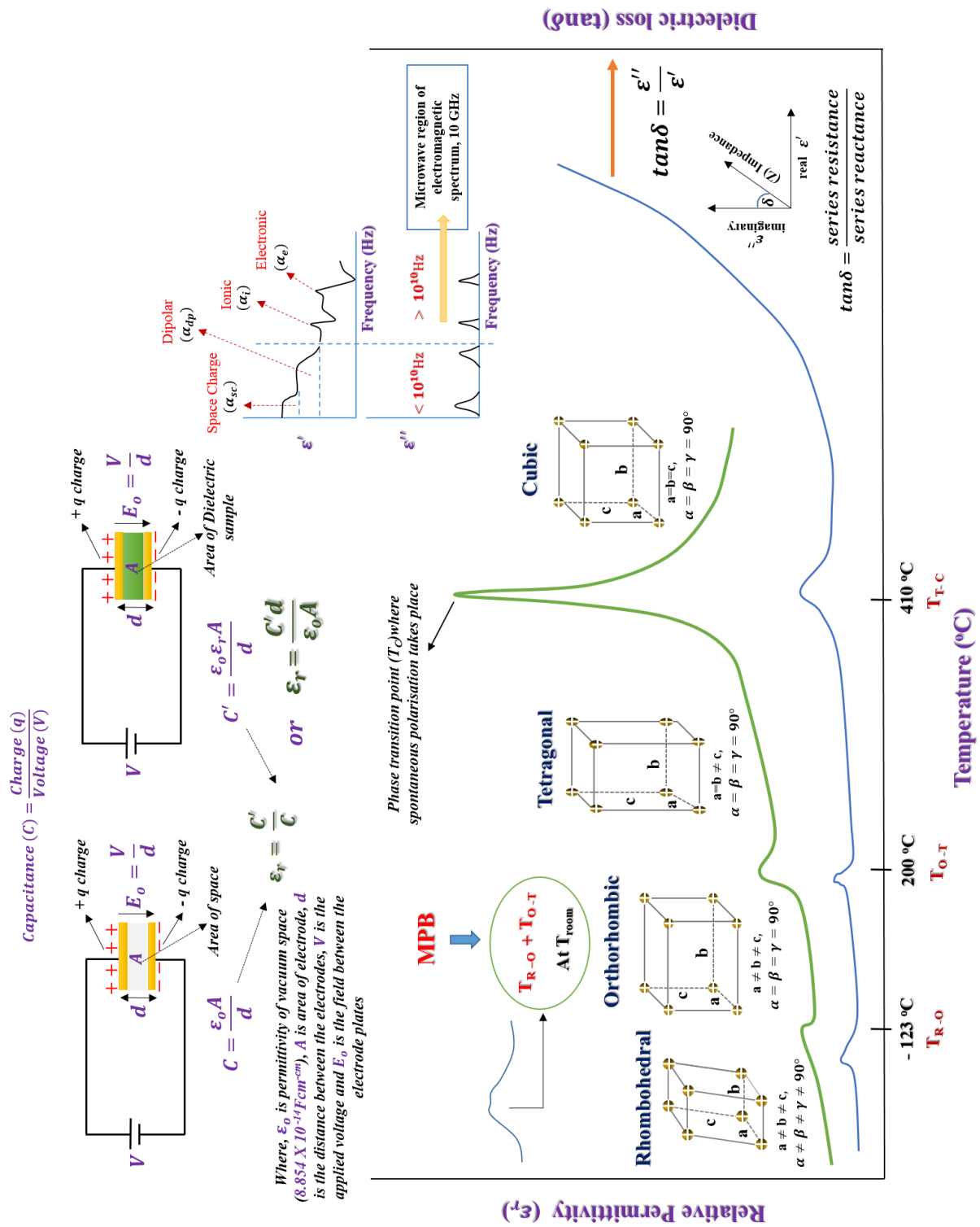

Figure 2-4 Basic concepts and relationships of ε_r and tanδ with ε_r and tanδ modelled in the case of KNN [7, 8].

Piezoelectric properties are anisotropic because they depend on crystal orientation. Hence, the piezoelectric coefficient, d and k, require tensor notation in order to have a useful meaning. d_{33}, for example, denotes that the applied stress/field are in the same direction as the measured strain/charge, Figure 2-6. d may also be defined in two different ways,

$$d = \frac{\text{electric charge generated}}{\text{Applied stress}} \quad \text{or} \quad d = \frac{strain\ generated}{\text{applied electric field}} \quad \text{(unit: [2] pC/N)}$$

Similarly, the piezoelectric voltage coefficient, g, may be defined as:

$$g = \frac{\text{Strain generated}}{\text{Applied charge density}} \quad \text{or } g = \frac{\text{electric field produced}}{\text{Mechanical stress}} \quad \text{(unit: [3] Vm/N)}$$

Piezoelectric properties and equations are further defined in Table 2-1.

[2] Pico-Coulombs / Newton
[3] Volt-meter/Newton

Table 2-1 Mathematical equations to calculate piezoelectric constants from different relationships

Piezoelectrical properties	Relationships to calculate these properties
Electro-mechanical coupling factors	$k_{31} = \sqrt{(\frac{\pi}{2}\frac{fa}{fr}\frac{1}{\frac{\pi fa}{2fr} - \tan\frac{\pi fa}{2fr}})}$, $k_p \cong \sqrt{(2.51\frac{fa-fr}{fr} - (\frac{fa-fr}{fr})^2)}$, $k_t = \sqrt{(\frac{\pi}{2}\frac{fr}{fa}\cot\frac{\pi}{2}\frac{fr}{fa})}$; where f_a is anti-resonant frequency, f_r is resonant frequency
Piezoelectrical charge coefficients	$d = k\sqrt{(\varepsilon^T S^E)}$ (C/N), $d_{31} = k_{31}\sqrt{(\varepsilon_{33}^T S_{11}^E)}$, $d_{33} = k_{33}\sqrt{(\varepsilon_{33}^T S_{33}^E)}$, $d_{15} = k_{15}\sqrt{(\varepsilon_{11}^T S_{55}^E)}$, where k is the coupling factor, ε^T is the permittivity at constant stress, S^E is the elastic compliance with closed circuit,
Piezoelectrical voltage coefficients	$g = \frac{d}{\varepsilon^T}$ (V-m/N), $g_{31} = \frac{d_{31}}{\varepsilon_{33}^T}$, $g_{33} = \frac{d_{33}}{\varepsilon_{33}^T}$, $g_{15} = \frac{d_{15}}{\varepsilon_{11}^T}$,

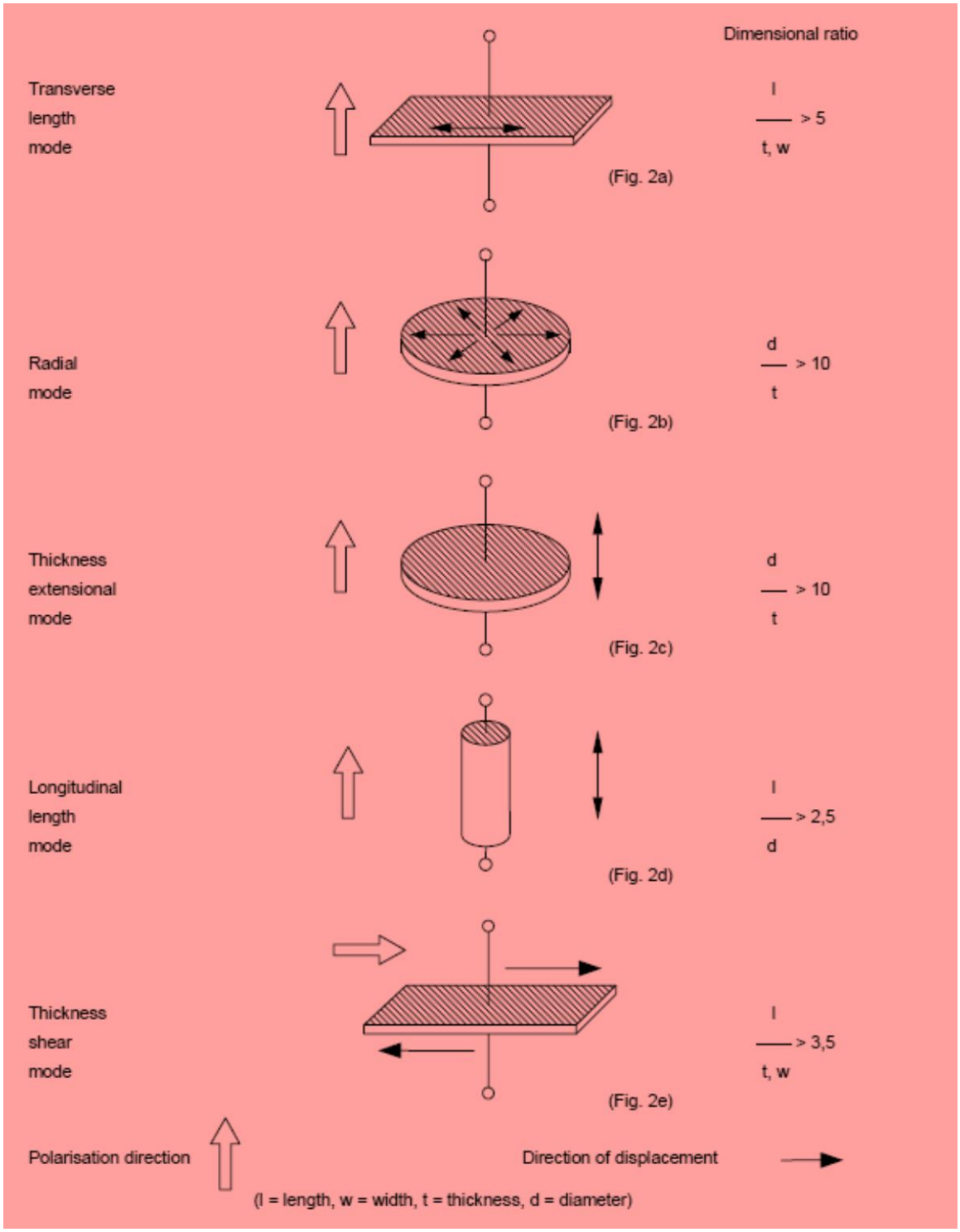

Figure 2-5 Piezoelectric vibrational modes vs. shapes with dimensional ratios [9]

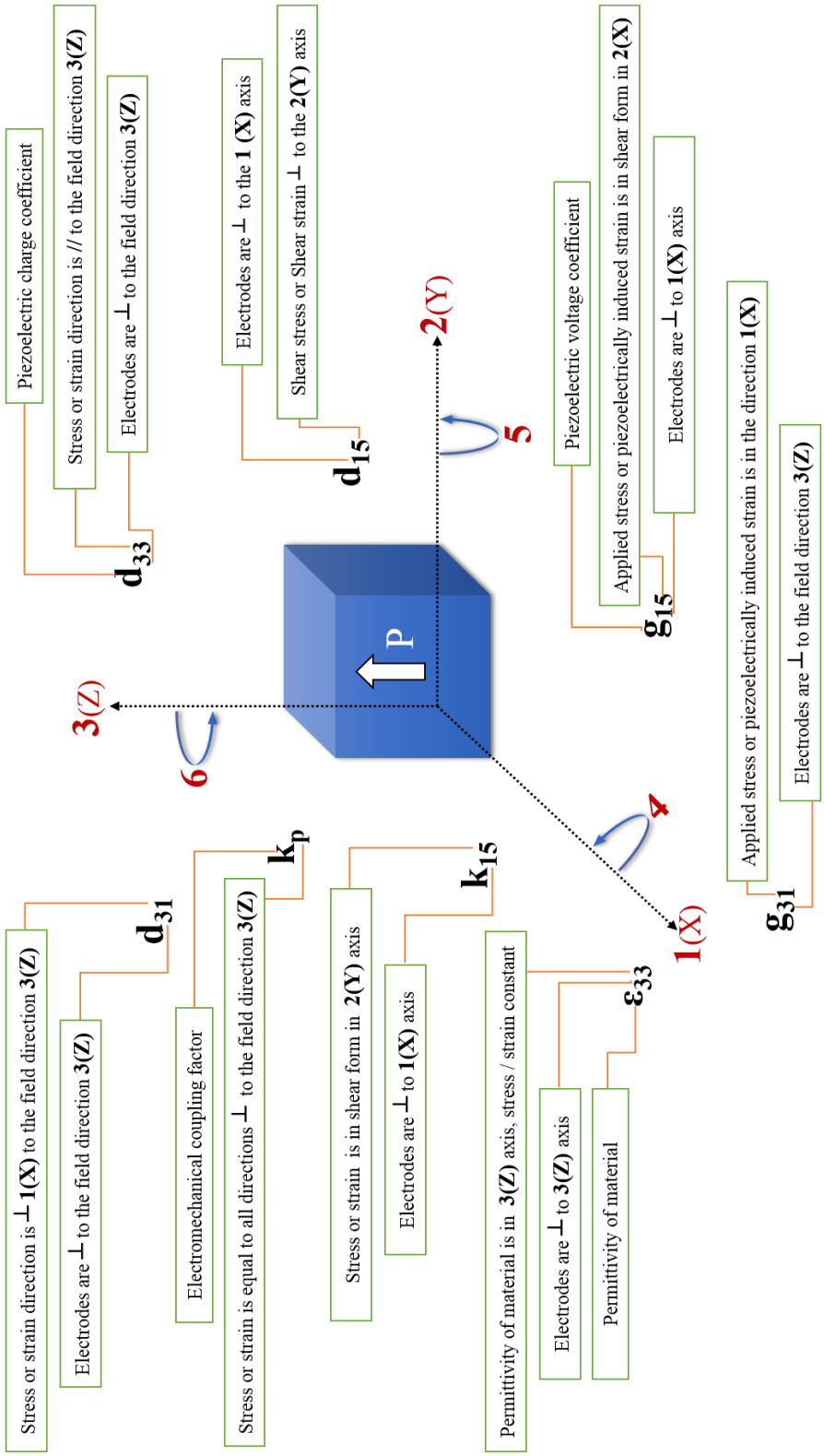

Figure 2-6 Tensor notations of piezoelectric properties, redrawn from [2-4, 10]

2.2 Piezoelectric Materials

The history of piezoelectrics began thousands of years ago when certain types of minerals were known to generate sparks when rubbed together to light fires. The direct piezoelectric effect which leads to the generation of charge was first demonstrated however, by two French brothers Pierre and Jacques Curie in 1880 by pressing in certain directions crystals such as tourmaline, zinc blende, sodium chlorate, boracite, tartaric acids, calamine, topaz, quartz, cane sugar and Rochelle salt. [11]

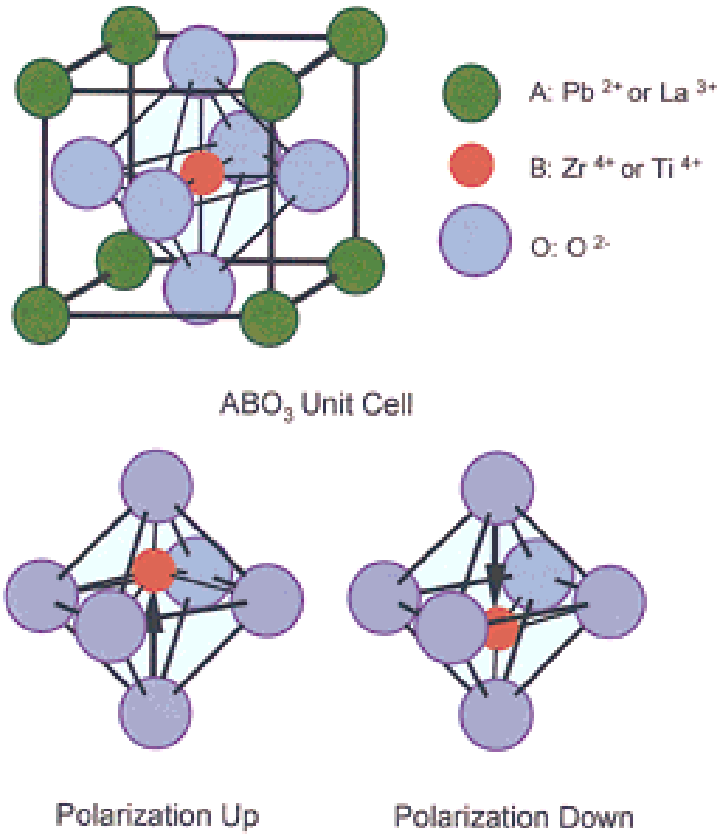

Figure 2-7 Perovskite ABO_3 unit cell for PZT or PLZT, illustrating 180° polarization reversal for two of the six possible polarization states produced by displacement of the central cation in the tetragonal plane.[12]

Today, most of commercial piezoelectrics with the exception of quartz are synthesised and generally have the perovskite structure with an ABO_3 formula unit, as some of them are shown in Figure 2-7. The T_Cs and piezoelectric properties of some early synthetic piezoelectrics material are listed in Table 2-2. Note that even amongst these early compositions, PZT is clearly the most performant piezoelectric. The piezoelectric coefficients of PZT have significantly improved since the 1950's when it was first discovered and many publications have shown that its properties are influenced by crystal structure, grain size and domain structure.

Table 2-2 Properties of some piezoelectric ceramics compositions are defined, along with the transition temperatures for each composition.[11]

Materials*	BT	BZ	BPC	LZ4A	LZ5A	SCN2O	SCN25	PBN30	PBN40
Density (10^3 kg/m^3)	5.72	5.44	5.3	7.6	7.5	4.3	4.4	5.9	5.9
Compliance	8.55	11	13	14.6	14.8	10.5	9.0	10.9	11.5
Radial frequency constant-frequency × dia (10^3m/s)	-	2.9	3.2	2.2	2.2	3.2	3.4	2.65	2.6
Relative permittivity (ε_r)	1900	1400	600	1200	1500	2000	2000	900	1500
Power factor (Low fields)	-	0.02	0.007	0.005	0.02	0.01	0.01	0.02	0.01
Resistivity ($10^6\Omega$m) (20C) **(250C)**	- -	- -	- -	10^5 0.1	10^5 300	- -	- -	10^5 10	10^5 10
Coupling Factors: • **Radial mode (disc) k_r** • **Length mode (bar) k_{31}** • **Thickness mode k_t**	 0.35 0.21 0.49	 0.28 0.15** 0.40**	 0.22 0.12** 0.30**	 0.55 0.30 0.76	 0.54 0.32 0.67	 0.30 0.17** 0.42**	 0.26 0.14** 0.35**	 0.24 0.13** 0.33	 0.38 0.22** 0.55**
Mechanical Q-factor (radial mode)	-	200	350	500	75	-	-	350	250
Piezoelectric strain constants: • **d_{31}(pC/N)** • **d_{33}(pC/N)** • **g_{31} (mV/N)** • **g_{33} (mV/N)**	 -79 191 4.7 11.4	 -60 150** -4.8 12.1**	 -35 90** -7.3 18**	 -130 300 -12.3 28.3	 -140 320 -10.6 24.4	 -80 200** -4.5 11.3**	 -60 150** -3.4 8.5**	 -40 100** -5.0 12.5**	 -90 220** -6.8 16.5**
Curie Temperature (°C) **Other transitions**	120 10 & -80	105 50 & 5	160 -- --	320 -- --	350 -- --	240 -10 --	200 -56 --	340 -- --	260 -- --

All quantities other than resistivity measured at room temperature.
** Estimated.

Abbreviations used in this table:
$BaTiO_3$(**BT**), $Ba(Ti_{0.95}Zr_{0.05})O_3$ (**BZ**), $(Ba_{0.80}Pb_{0.08}Ca_{0.12})TiO_3$(**BPC**), $Pb(Ti_{0.48}Zr_{0.52})O_3$ (**LZ**), **LZ4A** & **LZ5A** are commercial names, $(Na_{0.80}Cd_{0.10})NbO_3$ (**SCN20**), $(Na_{0.75}Cd_{0.125})NbO_3$ (**SCN25**), $(Pb_{0.70}Ba_{0.30})Nb_2O_6$ (**PBN30**), $(Pb_{0.60}Ba_{0.40})Nb_2O_6$ (**PBN40**).

2.2 Lead Zirconate Titanate (PZT)

$PbZr_xTi_{1-x}O_3$ (PZT) is a well-known commercially-used perovskite ferroelectric material. Key compositions with optimised piezoelectric coefficients lie at the morphotropic phase boundary (MBP, x= 0.52) between rhombohedral and tetragonal phases [13, 14]. Table 2-3 and Figure 2-8 show some recent PZT based compositions using strontium potassium niobate (SKN) as a dopant in comparison with some classic formulations and d_{33} vs T_C of well-established PZT, respectively. The optimum low field value of d_{33} is 510 pm/V for a T_C = 356°C. The exceptional combination of d_{33} vs T_C demonstrated by SKN doped compositions illustrates the difficulty in replacing PZT with PbO-free compositions.

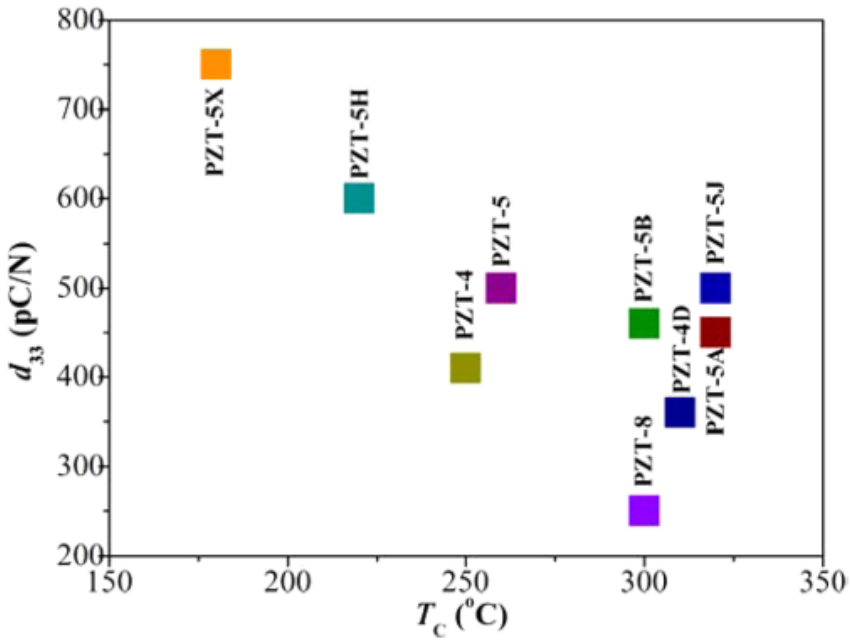

Figure 2-8 d_{33} vs. T_c temperature of well-established PZT piezoelectric ceramics [8]

Table 2-3 Functional Properties of PZT–xSKN Ceramics Sintered at 1250 °C (Standard PZT Compositions at the end of table for comparison) [15]

Mol.(SKN)	Grain Size (μm)	T_C (°C)	ε_{max} (1kHz)	$\varepsilon_{(50^oC)}$ (1kHz)	$\tan\delta_{(50^oC)}$ (1kHz)	$d_{33}^{(High)}$ (pm/V)	$d_{33}^{(Low)}$ (pm/V)	k_p
0.01	11.4±2.9	375	54000	1300	0.018	668	445	0.53
0.02	6.2±2.0	356	40200	1400	0.018	779	510	0.59
0.03	2.8±1.0	341	31100	1430	0.020	713	495	0.58
0.04	1.5±0.5	323	22600	1500	0.023	651	470	0.55
0.05	1.5±0.5	305	15300	1500	0.025	547	395	0.47
0.03 (24h)	2.8±1.0	341	40300	1420	0.022	768	530	0.62
0.05 (24h)	1.2±0.4	305	17300	1460	0.029	559	460	0.52
PZT-6%Sr[1]	--	328		1300	0.004	--	289	0.58
PZT-2.4%Nb[1]	--	365		1700	0.02	--	374	0.60
PZT-5A[11]	--	365		1700	--	--	410	0.60

Where, (SKN = Sr, K, Nb), ε_{max} = maximum relative permittivity at T_C, $\varepsilon_{(50°C)}$ = permittivity at 50 °C, $\tan\delta_{(50°C)}$ = tangent loss at 50 °C, $d_{33}^{(High)}$ (pm/V) = high field value taken from strain diagram and $d_{33}^{(Low)}$ (pm/V) = taken from low field. While PZT-6%Sr, PZT-2.4%Nb and PZT-5A in this table are used as a comparison from other work.

2.3 Lead free piezoceramics versus PZT

The safe disposal of waste electrical and electronic equipment is a major concern in the EU. The European Parliament has adopted the directives 'Waste Electrical and Electronic Equipment' (WEEE) and 'Restriction of the use of certain Hazardous Substances' in electrical and electronic equipment (RoHS) to prevent, reuse, or recycle waste electrical and electronic equipment and to protect human health and environment by the substitution of hazardous substances by safe or safer materials from July 1, 2006 [16, 17]. Lead oxide is classed as toxic and is thus one of the target materials for eradication according to the above legislation. To date, the use of PbO in the fabrication of PZT has received exemptions from this legislation due to extensive lobbying by manufacturers and end-users. However, it is likely that in the long term such exemptions will be more difficult to achieve and thus PbO-free alternatives to PZT are currently being sought.

At present, lead free piezoceramics are replacing Pb containing functional materials in some applications, so the full usage of lead free might be envisaged in the near future. However, there is still a critical need to focus on sustainability, reliability and reproducibility of lead-free piezoceramics to use safely in devices.

The two main contenders for lead free piezoelectric materials also belong to the perovskite family and are based on $K_{0.5}Na_{0.5}NbO_3$ (KNN) and $Na_{0.5}Bi_{0.5}TiO_3$ (NBT). Figure 2-9, Figure 2-12 and Figure 2-13, and Table 2-4, compare the dielectrics vs. T_C and, piezoelectric properties of NBT and KNN with currently available PZT-based formulations [13, 18-21] and illustrates the magnitude of the task. PZT comfortably out-performs PbO-free alternatives for all the key metrics, including ε_r, d_{33}, k_p and T_C.

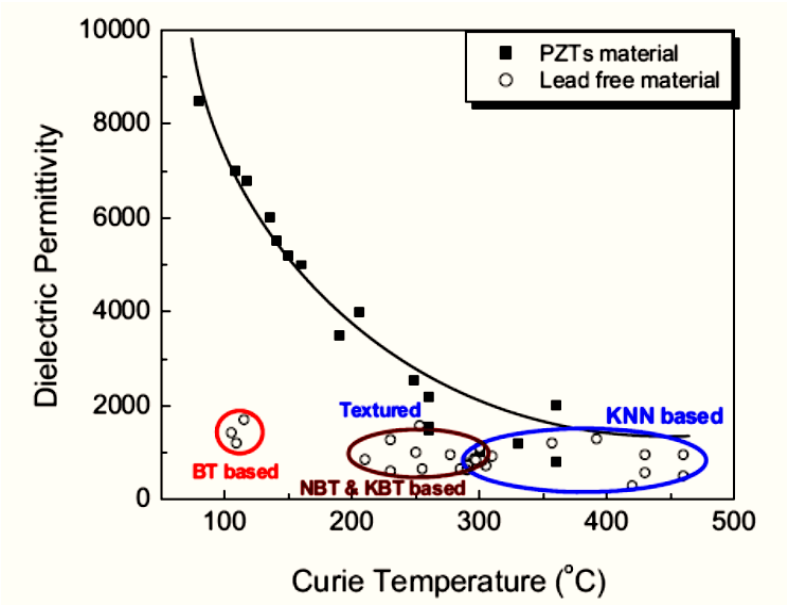

Figure 2-9 Room temperature value of ε_r as a function of T_C for various piezoelectric ceramics [18].

Figure 2-10 shows the number of publications on lead free piezoelectrics per year from 2004 to 2014 Papers on alkali niobates and its phase boundary dominate the research landscape, Figure 2-11

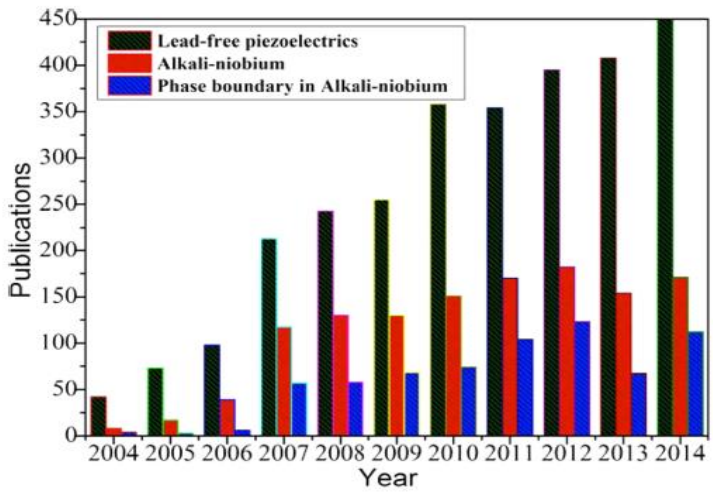

Figure 2-10. Lead free piezoelectrics in general and alkali-niobium with phase boundary in particular, publications from 2004 to 2014 [8]

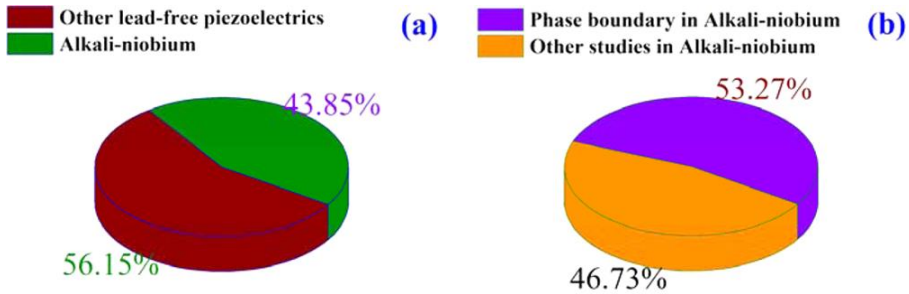

Figure 2-11 Pie charts showing (a) the comparison of alkali-niobium research with other lead free materials, (b) amount of research work done on (MPB) phase boundary of alkali-niobium from 2004 to 2014.

Table 2-4 Dielectric and piezoelectric properties of lead free perovskite Piezo's "past and present."[18]

Materials*	$\varepsilon/\varepsilon_o$	tanδ	d_{33} (pC/N)	k_p	k_{33}	T_C (°C)	$T_{O\text{-}T}/T_d$ (°C)
$BaTiO_3$	1700	0.01	190	0.36	0.5	115	0
$BaTiO_3$-$CaTiO_3$-Co	1420	0.005	150	0.31	0.46	105	- 45
$(Na_{0.50}K_{0.50})NbO_3$ (HP)	500	0.2	127	0.46	0.6	420	--
$(Na_{0.50}K_{0.50})NbO_3$	290	0.40	80	0.35	0.51	420	195
KNN-Li (7%)	950	0.084	240	0.45	0.64	460	~20
KNN-Li (7%)-Ta(20%)	920	0.024	190	0.46	0.615	310	50
KNN-LF4**	1570	--	410	0.61	--	253	25
KNN-$SrTiO_3$ (5%)	950	--	200	0.37	--	277	27
KNN-$LiTaO_3$ (5%)	570	0.04	200	0.36	--	430	55
KNN-$LiNbO_3$ (6%)	500	0.04	235	0.42	0.61	460	70
KNN-$LiSbO_3$ (5%)	1288	0.019	283	0.50	--	392	45
NBT-KBT-LBT	1550	0.034	216	0401	--	350	160
NBT-KBT-BT	820	0.03	145	0.162	0.519	302	224
NBT-KBT-BT (MPB)	730	0.02	173	0.33	0.59	290	162
NBT-KBT-BT	770	0.034	183	0.367	0.619	290	100
SBT-KBT90	870	0.04	110	0.15	0.507	296	--
SBT-KBT85	1000	0.05	120	0.16	0.491	250	--
BBT-KBT90	837	0.05	140	0.23	0.538	297	144
BBT-KBT80	630	0.04	95	0.15	0.361	290	238
$Sr_2NaNb_5O_{15}$**	1100	--	120	--	--	280	--

** Textured; $T_{O\text{-}T}$: Orthorhombic to tetragonal phase transition; HP: Hot Pressed; T_d: depolarisation temperature;
NBT: $(Na_{0.50}Bi_{0.50})\ TiO_3$, **KBT:** $(K_{0.50}Bi_{0.50})\ TiO_3$; **LBT**: $(Li_{0.50}Bi_{0.50})\ TiO_3$; **BT**: $BaTiO_3$; **SBT:** $(Sr_{0.70}Bi_{0.20})\ TiO_3$; **BBT:** $(Ba_{0.70}Bi_{0.20})\ TiO_3$

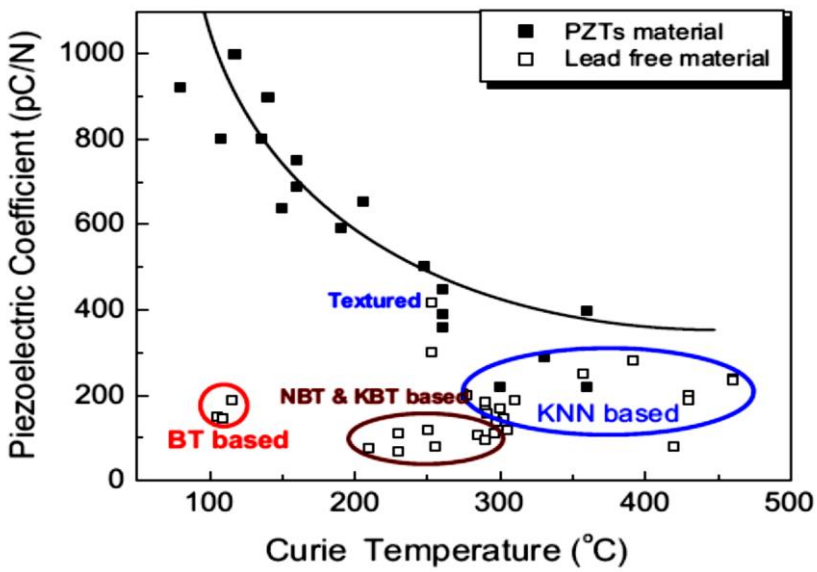

Figure 2-12 Room temperature value of d_{33} as a function of T_C for various piezoceramics[18].

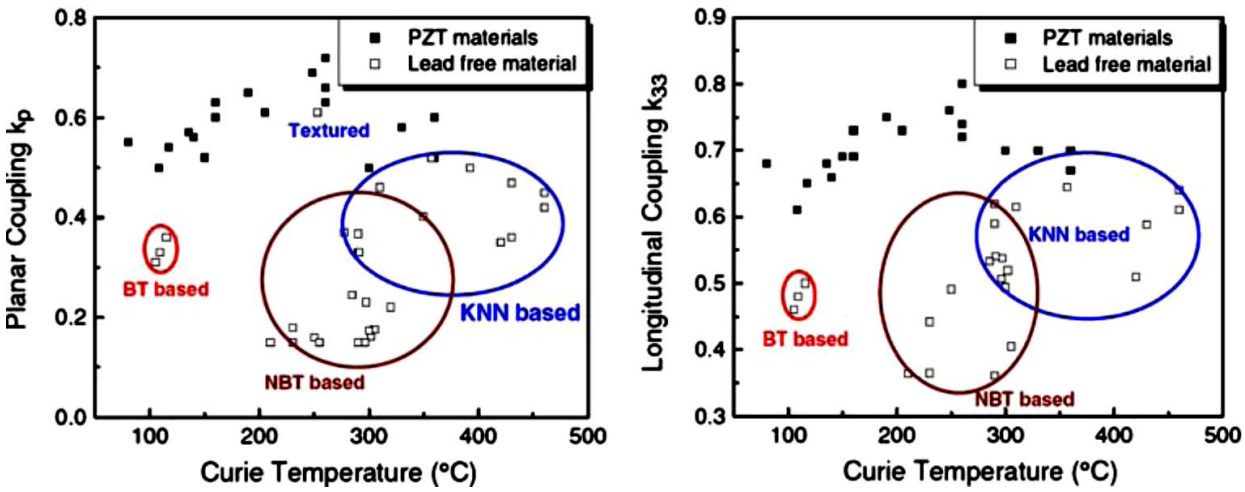

Figure 2-13 Room temperature electromechanical coupling k_p (left) and k_{33} (right) for various piezoelectric ceramics [18].

2.4 Potassium Sodium Niobate (KNN)

2.4.1 Phase Diagrams

Potassium niobate and sodium niobate are ferroelectric crystals that were first studied by Matthias in 1949 but it was not until 1952 that the extensive polymorphism and solid solution of these two crystals was first established [22]. The pseudoternary phase diagram of $KNbO_3$ - $NaNbO_3$ was reported for the 1st time in 1971 by Jaffe et al., Figure 2-14. The phase transitions of interest occur near the so-called MPB composition (KNN50) which itself exhibits rhombohedral to orthorhombic (T_{R-O}), orthorhombic to tetragonal (T_{O-T}) and tetragonal to cubic (T_C) transitions from low temperature to high temperature. At room temperature, MPB composition have a mixture of two orthorhombic phases shown in this diagram as dotted vertical line at nealy 50/50 ratio of K/Na. There is a very narrow region of liquid/solid which may create problems in achieving optimum density through sintering. Since the work of Jaffe et al, [23, 24] a modified phase diagram for KNN (Figure 2-15) has been published which reveals the coexistence of monoclinic and orthorhombic phases at x = 0.5. In this diagram, oxygen tilting superscripts and cation displacements

subscripts for each phase are utilised according to notation taken from Stokes *et al., 2002*.[25] Dotted lines represent changes in the tilt system, and the phases *F* (*Amm*2) and T_2 (*P*4*bm*) correspond to those described by Ahtee and Glazer, 1976, but with updated space groups corresponding to the oxygen tilt and cation displacements observed. [26]

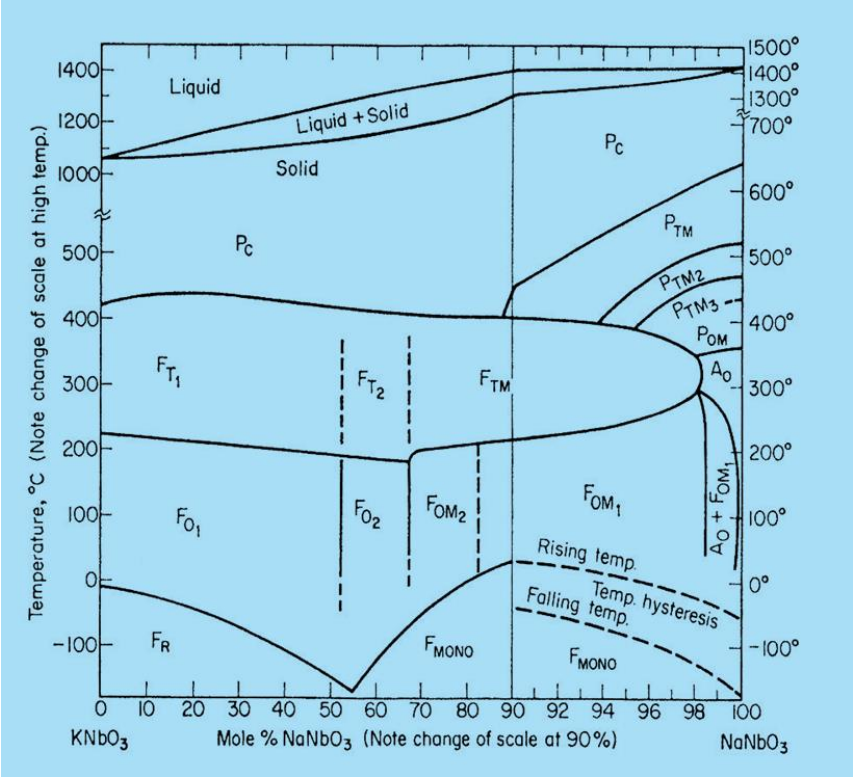

Figure 2-14 Potassium niobate - sodium niobate phase diagram, temperature ºC vs composition.[23]

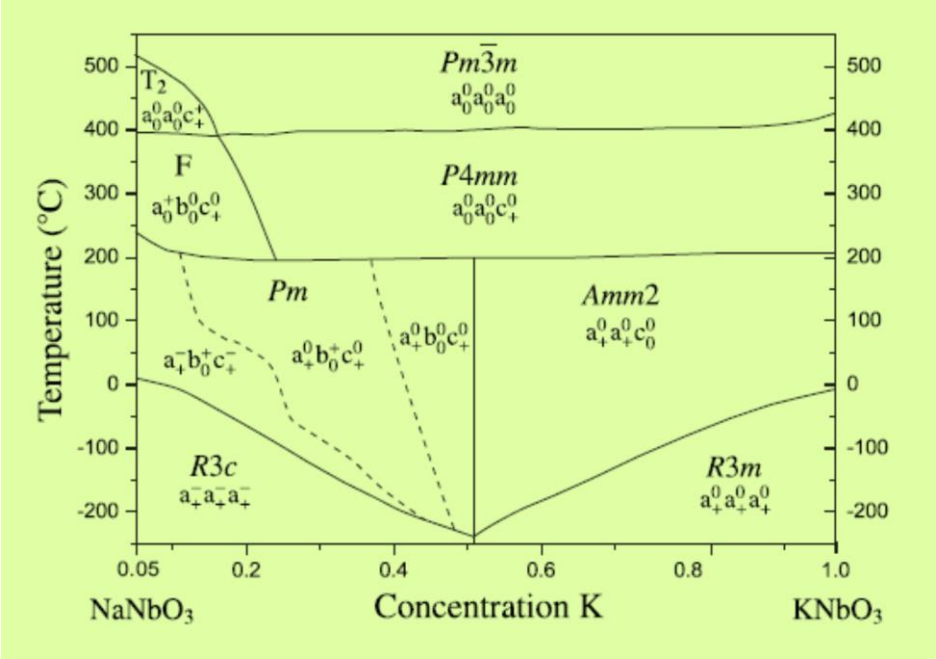

Figure 2-15 Modified phase diagram for KNN, reveals the coexistence of monoclinic and orthorhombic phases at x=0.50 [24]

2.4.2 Un-doped KNN Piezoelectric Ceramics

Birol et al. 2006 conventionally prepared un-doped KNN and obtained d_{33} = 100-110pC/N with 95% dense material. Ferroelectric loops from the work of Birol et al are shown in Figure 2-16. [27] Prior to this, Jaeger et al. 1962improved density only through hot pressing and obtained d_{33} = 160pC/N for 98.8% dense $K_{.50}Na_{.50}NbO_3$.[28] To date, the optimum single crystal of un-doped $(K_{0.56}Na_{0.44})NbO_3$ obtained by slow-cooling method using $0.8(K_{0.5}Na_{0.5})NbO_3$-$0.20K_2CO_3$ as starting powder, has realised a maximum d_{33} = 220pC/N.[29] By using polarized light, the domain structure of orthorhombic where domains in [001]-oriented KNN single crystals were reported non-existent, as shown in Figure 2-17 and dielectric measurements revealed T_{R-O}, T_{O-T} and T_{T-C} to be −100◦C, 214◦C and 433◦C, respectively. [29]

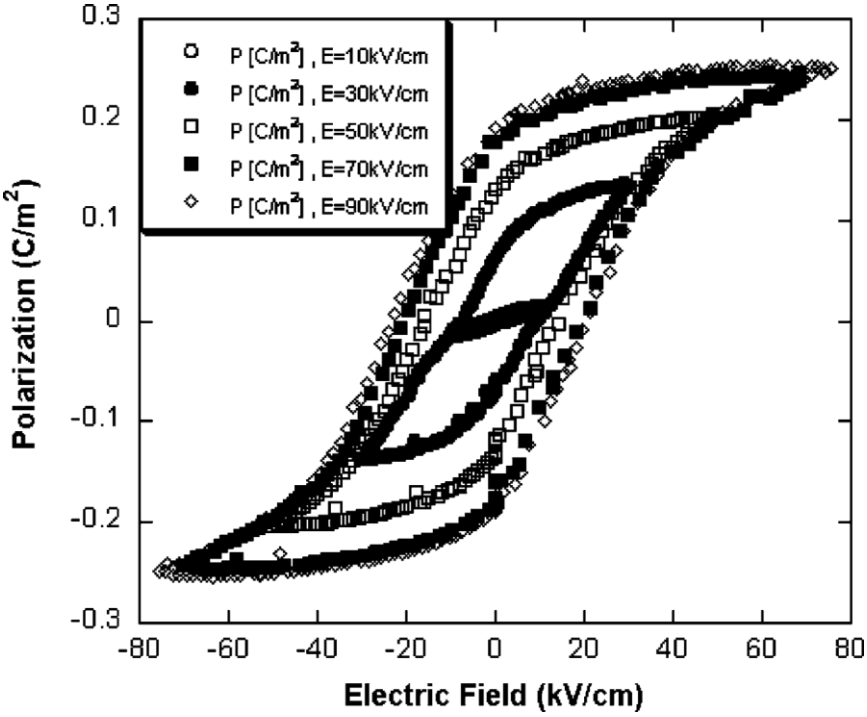

Figure 2-16 Hysteresis loops of KNN-50/50 at room temperature and different applied electric fields. [27]

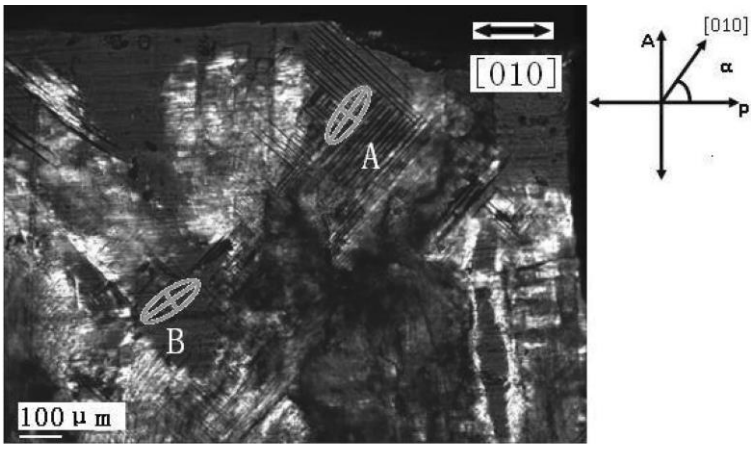

(a)

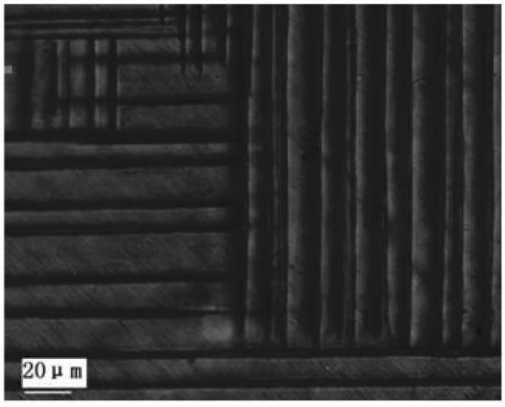

(b)

Figure 2-17 (a) Domain structure of orthorhombic and extinction of [010]-oriented KNN single crystal. (b) Region A is magnified. [29]

2.4.2.1 Volatility issues in KNN-based Ceramics

Many publications raised the issue of volatility in KNN [30-37], particularly with respect to K^+ and Na^+. However, converse to this issue, almost none of the authors have given any direct evidence and thus a meaningful critical review of this topic is difficult. In theory, volatility is the measure of tendency of a substance to vaporize; and this phenomenon happens when the vapour pressure of that substance goes higher than the environmental or atmospheric pressure. So by this definition every material is volatile under certain atmospheric conditions (e.g. pressure, temperature). These conditions vary from compound to compound. More oxidizing and complex compounds are more stable at higher temperatures. Some groups have discussed potassium oxide and sodium oxide separately in terms of volatility but to date none have measured the vapour pressure for KNN [23, 30, 31, 33, 37-40]. LEE Yong-hyun et al 2008 fabricated the ($K_{0.5}Na_{0.5}NbO_3$) composition by conventional solid state processing, and claimed relative densities over 97.4% with excess K^+ of 0.44 mol % and Na^+ of 0.22 mol % to compensate volatility [31]. The piezoelectric constant (d_{33}) and electromechanical coupling factor (k_p) of this ceramic were 0.341 and 126 pC/N, respectively. Moreover, XRD the peak of 45/2θ (Figure 2-18) is clearly changing with excess K^+. The ε_r–T data, reported by these authors, Figure 2-19 suggest that an excess of K^+ ions is however, responsible for a shift in T_C towards higher temperatures. These authors reported the T_{O-T} and T_{T-C} at 230°C and 425°C in contrast with expected values of 200°C and 410°C, respectively [27,31 32, 41-43]. Furthermore, tanδ increased and k_p factor decreased (

Table *2-5*), consistent with excess K and Na in the system, suggesting that the reported volatility is much less prevalent than suggested. It may be concluded that the larger d_{33} value is a result of the $T_{R\text{-}O}$-MPB shifting towards room temperature. In contradiction to the above, most authors report XRD patterns similar to the JCPDS-00-032-0822, as illustrated in Figure 2-20. [27, 32, 41-47]

Table 2-5 Properties of KNN- as a function of excess K/Na [31]

Material	Relative density (%)	k_p (%)	N_p (Hz-m)	Q_m	ε_r (1 kHz)	$\tan\delta\psi$ (%)	d_{33} (pC/N)
KNN	92.9	35.4	3312	86	358	3.7	91
KNN + K (0.26)/ Na (0.13) mol %	96.53	33.3	3314	122	364	5.3	115
KNN + K (0.44)/ Na (0.22) mol %	97.35	34.1	3334	116	361	9.6	126
KNN + K (0.62)/ Na (0.31) mol %	97.06	30.9	3289	123	367	6.4	129

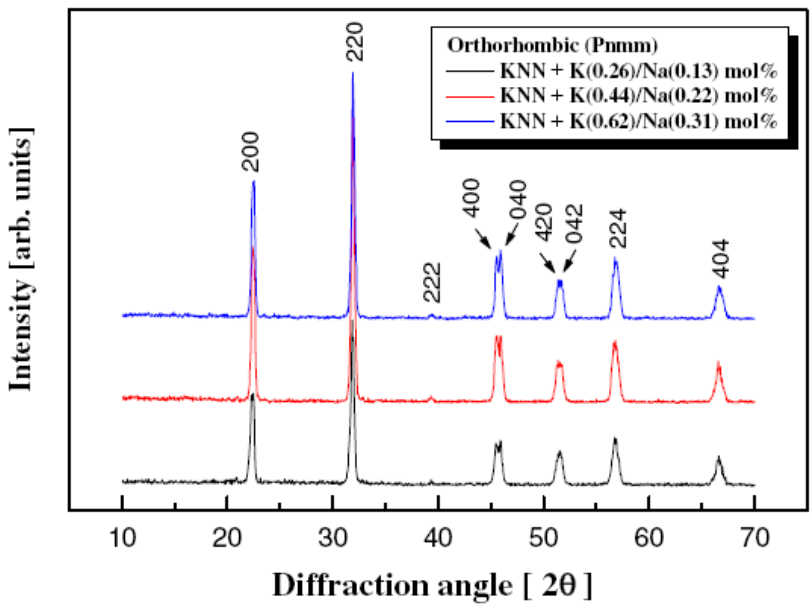

Figure 2-18 XRD pattern of KNN with excess addition of K and Na [31]

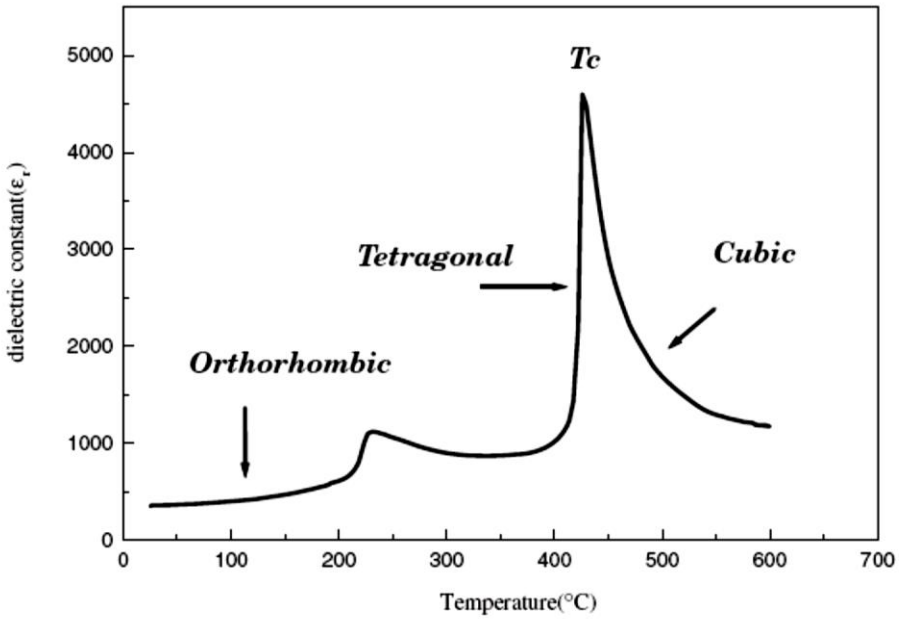

Figure 2-19 ε_r-T relationship of KNN with excess addition of K and Na [31]

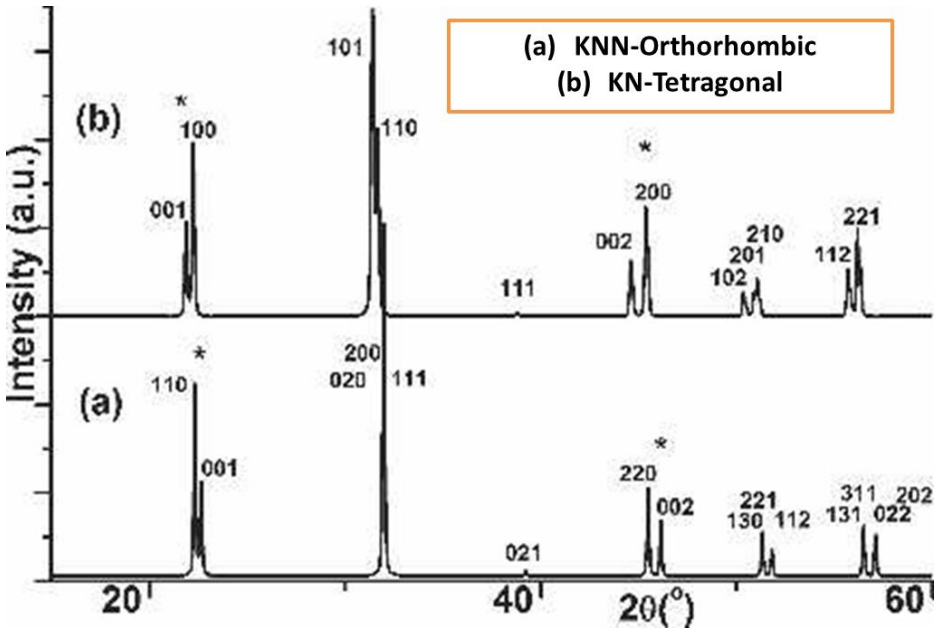

Figure 2-20 XRD pattern of Orthorhombic[48] and tetragonal[49] structures of KN [50, 51]

2.4.3 Modified KNN

The most extensively studied lead free KNN piezoelectric based materials $(K_{0.44}Na_{0.52}Li_{0.04})(Nb_{0.84}Ta_{0.10}Sb_{0.06})O_3$ first time reached at largest d_{33} values (416pC/N) which was first claimed by Saito et al. and was fabricated using a Reactive Templated Grain Growth Method (RTGG) method used for textured ceramics.[52] Following Saito et al's work, Guo et al (2004) and (2005) reported Li and Li-Ta modified KNN respectively[53, 54] and Damjanovic et al [55] discussed Li, Ta modified KNN synthesized by solid state method. They reported piezoelectric properties k_t = 53% and d_{33} = 200 pm/V for the Li-doped ceramics, and k_t = 52% and d_{33} = 300 pm/V for the Li,Ta-co-doped samples. [55] Figure 2-21 and Figure 2-22 show the ε_r-T relationship and uni-polar strain loops for $(K_{0.50}Na_{0.50})_{0.97}Li_{0.03})(Nb_{0.80}Ta_{0.20}O_3$ in comparison with commercial PZ26 (Ferroperm, Denmark).

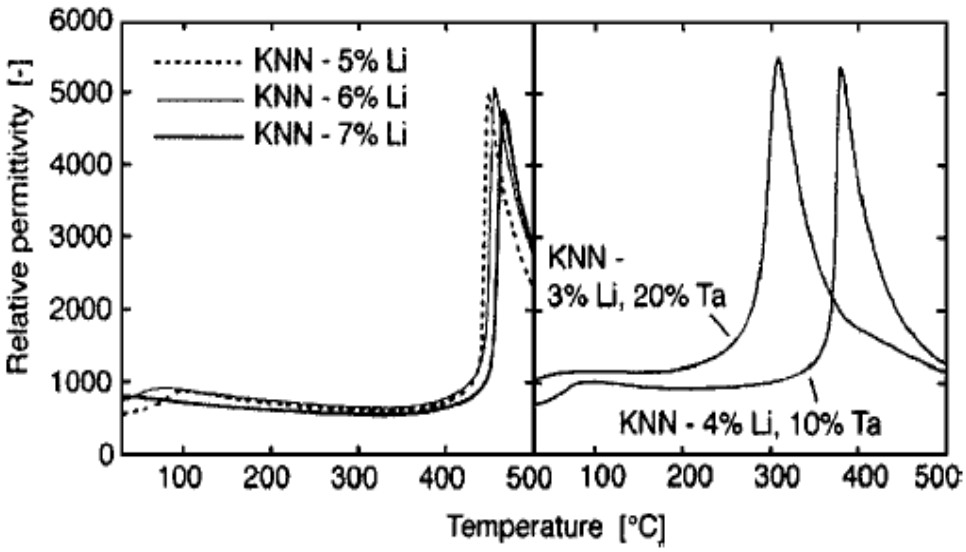

Figure 2-21 ε_r-T relationship for Li, Ta doped KNN [55]

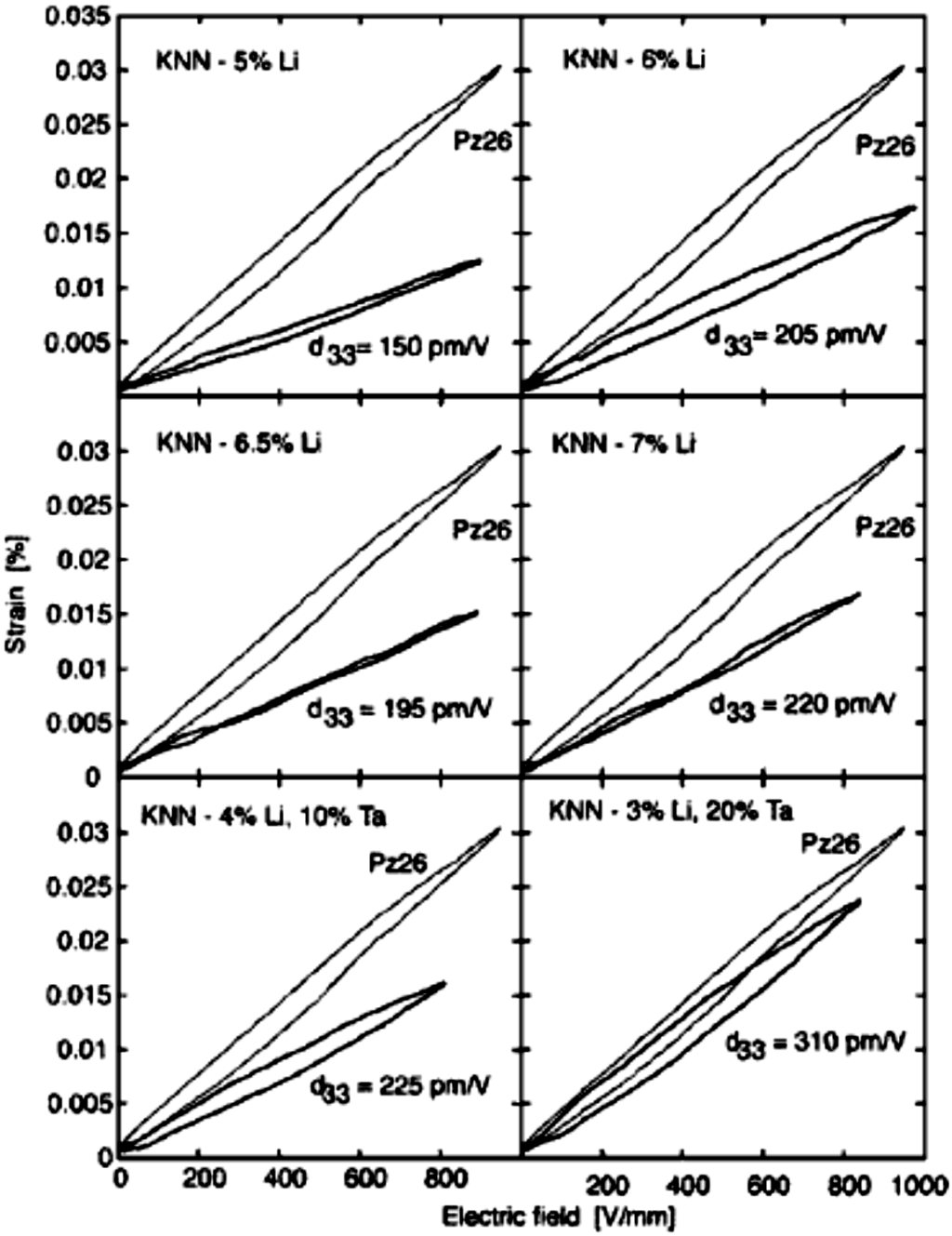

Figure 2-22 Unipolar strain-field loops measured at 1Hz and room temperature; of Li, Ta doped KNN compared with Ferroperm PZ26 hard PZT ceramics [55]

Dunmin et al synthesized $(1-x)(K_{0.5}Na_{0.5})NbO3–xBa(Zr_{0.05}Ti_{0.95})O_3$ (KNN-BZT)with optimum properties obtained for x= 0.06 when 1 mol% of MnO_2 was used as a sintering aid. These authors attributed the excellent properties of KNN-BZT-0.06 to the co-existence of an orthorhombic-tetragonal transition at room temperature

and achieved d_{33}=234pC/N, k_p=0.49, k_t=0.48, ε_r=1191, tanδ =1.20%, and T_C=318 °C, Figure 2-23 and Figure 2-24.[32]

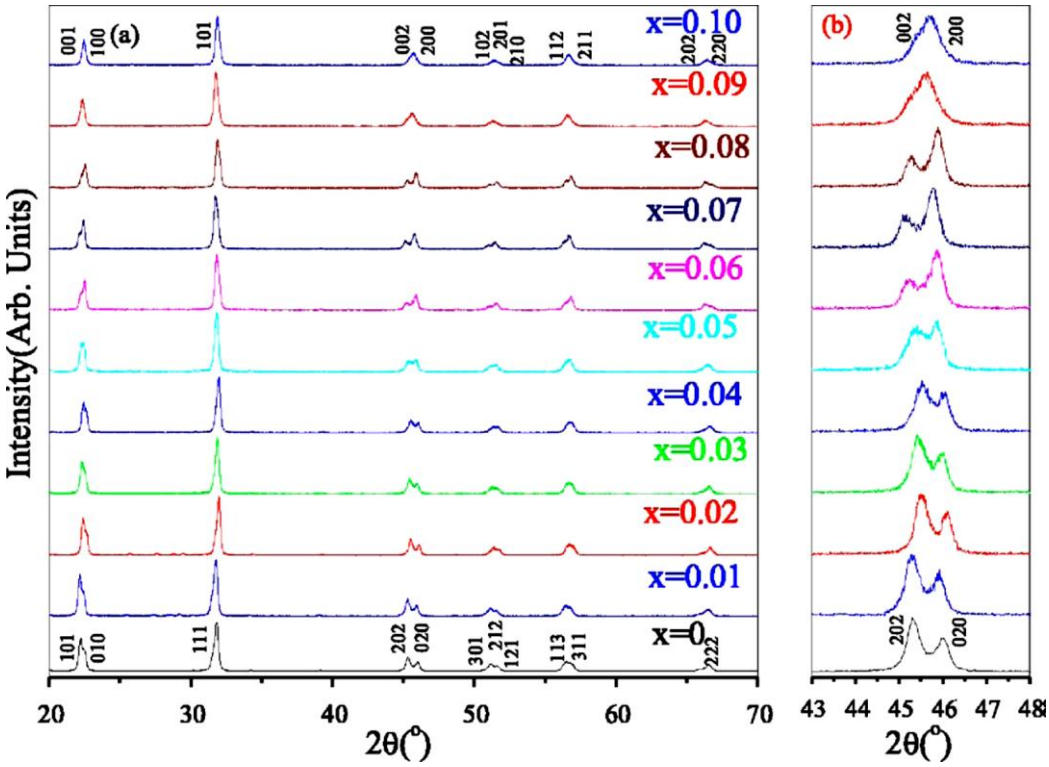

Figure 2-23 XRD data of KNN-BZT, illustrating the structural changes with respect to the x-values [32]

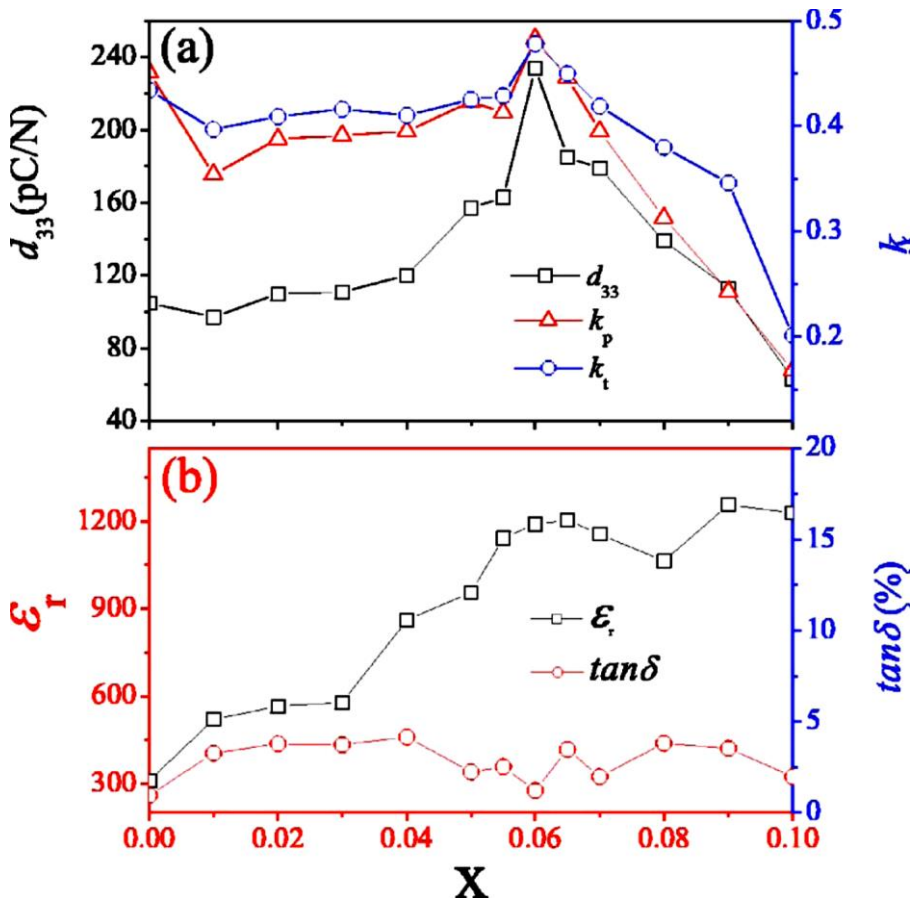

Figure 2-24 Comparison between piezoelectric and dielectric properties of KNN-BZT [32]

In 2011, Jianhua et al [56] prepared $(Na_{0.5}K_{0.5})_{0.94}Li_{0.06}NbO_3$ through a molten salt method and obtained optimum properties ε_r, tanδ, d_{33}, k_p, Q_m (mechanical quality factor), k_t, and T_C of 585, 1.8%, 213 pC/N, 0.35, 500, 0.46 and 381.4°C, respectively. [56]

2.4.4 Giant piezoelectricity in KNN-based Ceramics

After Saito et al, first reported so called 'giant' piezoelectricity in 2004, Wang and co-workers [36, 43, 57] proposed a wide range of KNN-based ceramics that exhibited high levels piezoactivity.

2.4.4.1(1 – x) ($K_{0.5}Na_{0.5}$) NbO_3–x ($Bi_{0.5}Na_{0.5}$) ZrO_3

The optimum piezoelectric properties of (1 – x) ($K_{0.5}Na_{0.5}$) NbO_3–x ($Bi_{0.5}Na_{0.5}$) ZrO_3 ceramics, reported as d_{33} = 360 pC/N, k_p = 32.1%, ε_r = 1429, tanδ = 3.5%, and T_C = 329°C, were obtained through conventional solid state synthesis for x=0.05.[43] The authors reported that for x = 0.05 there is an MPB between the $T_{R\text{-}O}$ / $T_{O\text{-}T}$ transitions at close to room temperature. $(Bi_{0.5}Na_{0.5})^{2+}$ was selected to decrease the temperature of $T_{O\text{-}T}$ transition and Zr^{4+} ions were introduced to increase the temperature of the $T_{R\text{-}O}$ transition. The sintering temperature was reported as 1100-1120°C for 3 hours in air. XRD patterns, P-E loops and LCR data of this composition are shown in Figure 2-25, Figure 2-26 and Figure 2-27, respectively. In addition to this, LCR data showed relaxor behaviour beyond the x=0.050.[43]

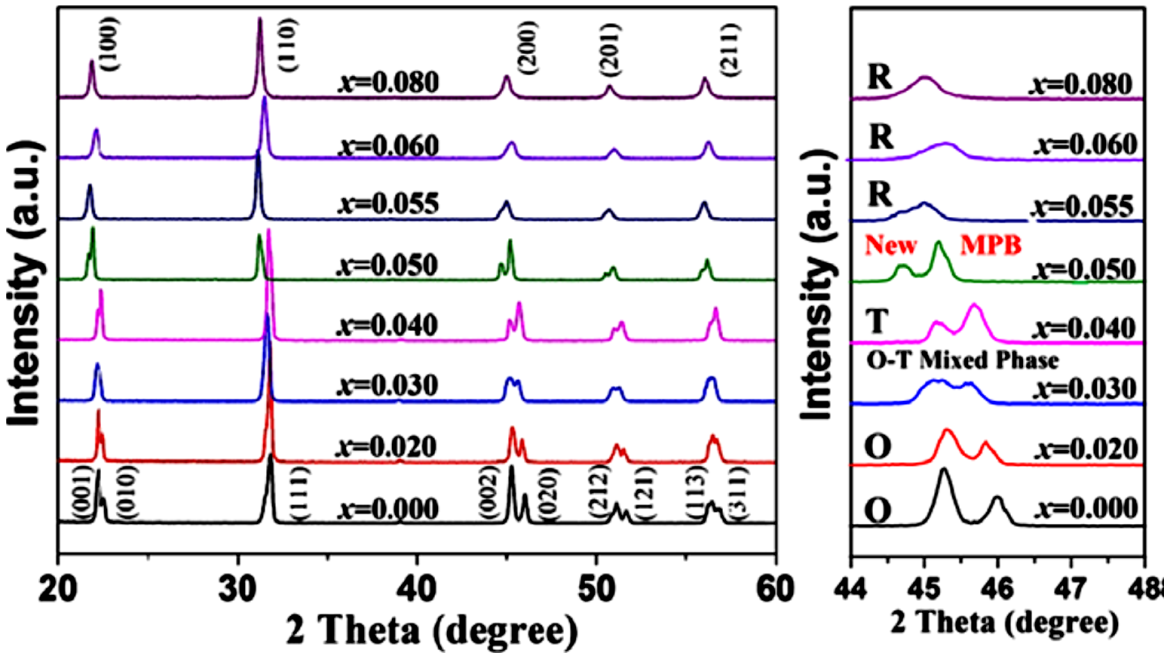

Figure 2-25 XRD of the KNN–xBNZ formulations in the 2θ range of (a) 20°–60° and (b) 44°–48°, respectively [43]

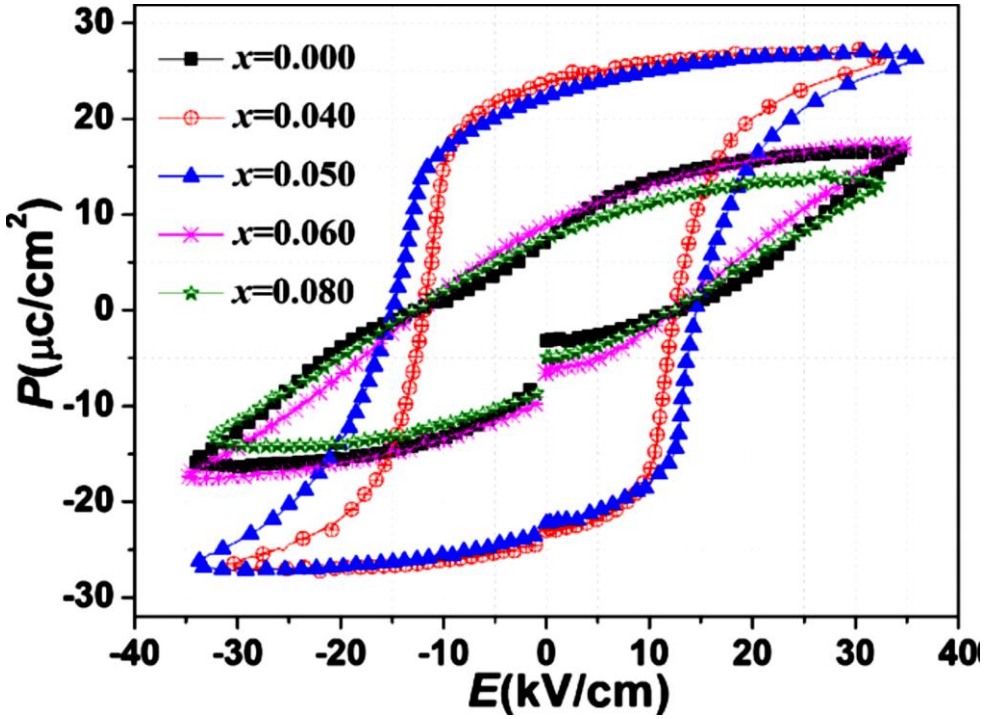

Figure 2-26 Ferroelectric loops of KNN-xBNZ ceramics as a function of x [43]

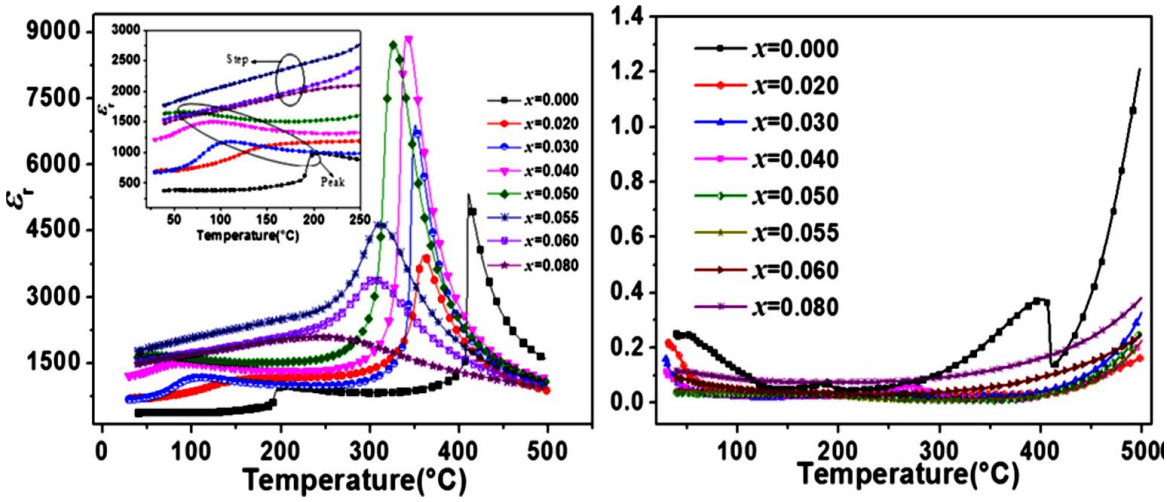

Figure 2-27 (left) Relative permittivity and (right) tanδ loss plots of KNN-xBNZ at 10kHz as a function of temperature [43]

2.4.4.2 $0.96(K_{0.48}Na_{0.52})(Nb_{0.95\_x}Ta_{0.05}Sb_x)O_3$–$0.04Bi_{0.5}(Na_{0.82}K_{0.18})_{0.5}ZrO_3$ or ($0.96KNNTS_x$–0.04BNKZ)

Optimum properties for $0.96KNNTS_x$–0.04BNKZ were obtained for x= 0.04 for ceramics fabricated using conventional solid state synthesis with d_{33}= 460pC/N [58], which is higher than those of the textured ceramics reported by Saito et al [52]. The thermal stability of d_{33} value was also investigated with 354pC/N being recorded at 180°C. Ta^{5+}, BNKZ and Sb^{5+} were considered to be concurrently responsible for the increase in T_{R-O} and the decrease in T_{O-T} transitions of potassium sodium niobate ceramics,

Figure 2-28 and Figure 2-.[58]

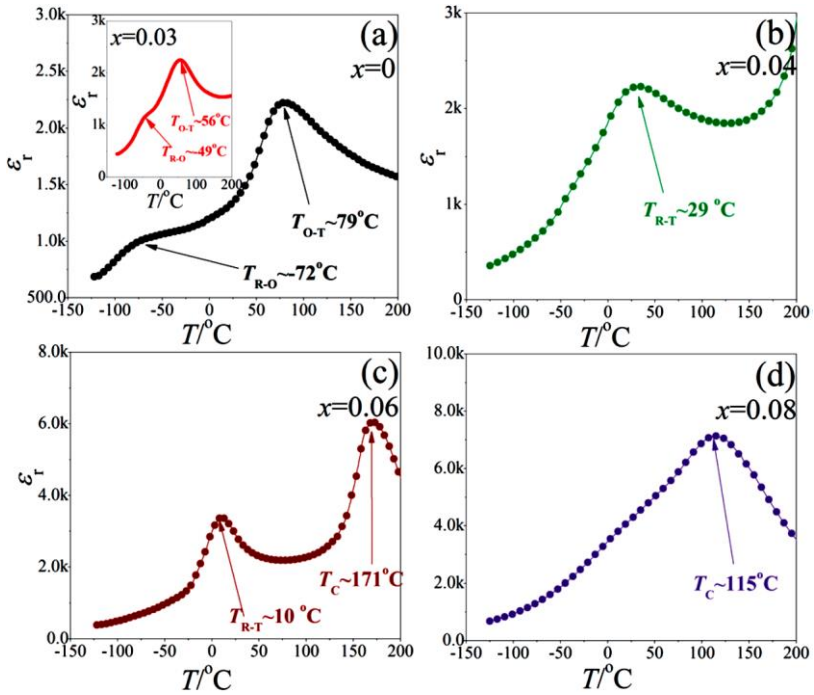

Figure 2-28 ε_r vs T (-150–200°C) for the 0.96KNNTSx–0.04BNKZ ceramics (a) x =0, (b) x = 0.04, (c) x =0.06, and (d) x= 0.08, the inset of (a) is ε_r vs T of the ceramic with x =0.03 [58]

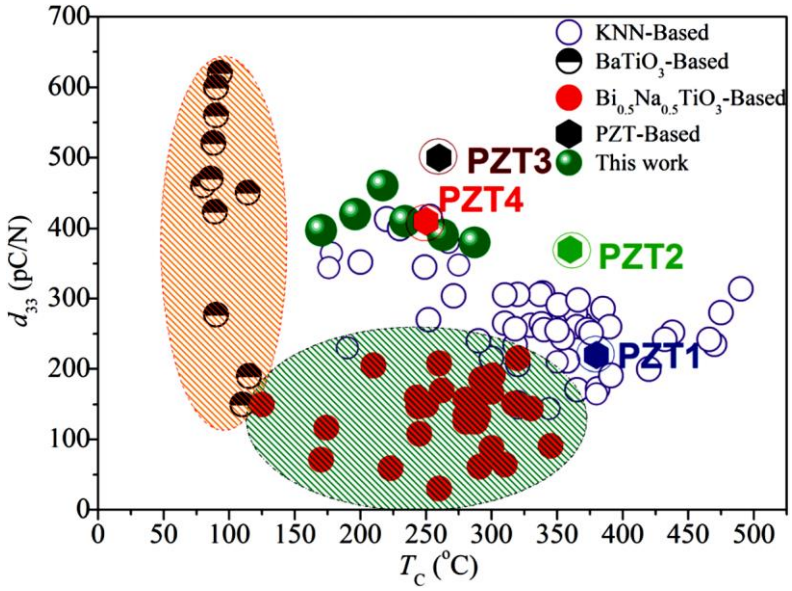

Figure 2-29 Room temperature d_{33}values as a function of T_C for KNN, $Bi_{0.5}Na_{0.5}TiO_3$, $BaTiO_3$, and $Pb(Zr,Ti)O_3$ based piezoceramics [58]

2.4.4.3 $(1-x)(K_{1-y}Na_y)(Nb_{1-z}Sb_z)O_3-xBi_{0.5}(Na_{1-w}K_w)0.5ZrO_3$ ($0 \leq x \leq 0.05$, $0.40 \leq y \leq 0.68$, $0 \leq z \leq 0.08$, and $0 \leq w \leq 1$)

In the above complex formulation, the authors ascribed the function of $[Bi_{0.5}(Na_{1-w}K_w)_{0.5}]^{2+}$ and Zr^{4+} to that of lowering T_{O-T} and raising T_{R-O} of $(K_{1-y}Na_y)(Nb_{1-z}Sb_z)O_3$, respectively, which resulted in the largest d_{33} of ~490pC/N ever claimed so far for KNN-based ceramics. These authors developed a range of compositions with T_C ~217−304 °C which resulted in different d_{33} values by systematically modifying x, y, z and w, in the above formula, thereby creating a number of different MPB compositions, as illustrated in Figure 2-29, , Figure 2-30, Figure 2-31 and Figure 2-32. They also discussed and plotted the direct relationship between d_{33} and $\varepsilon_r.P_r$, Figure 2-. [57]

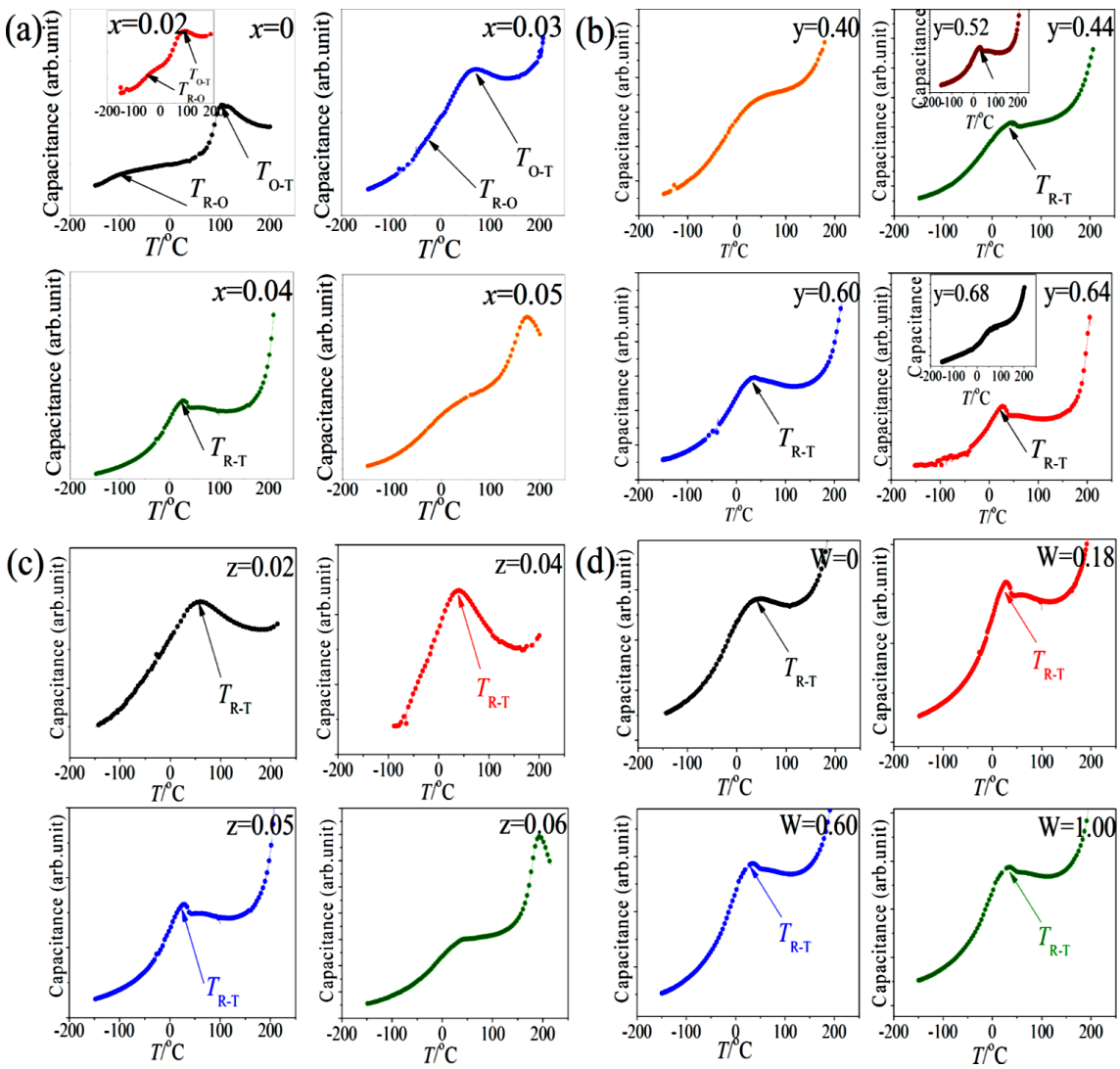

Figure 2-29 Temperature-dependent capacitance of the $(1-x)(K_{1-y}Na_y)(Nb_{1-z}Sb_z)O_3-xBi_{0.5}(Na_{1-w}K_w)0.5ZrO_3$ ceramics with (a) y=0.52, z=0.05, w=0.18, (b) x=0.04, z=0.05, w=0.18, (c) x=0.04, y=0.52, w=0.18, and (d) x=0.04, y=0.52, z=0.05 recorded at 10kHz where the temperature range was of −150−200°C[57]

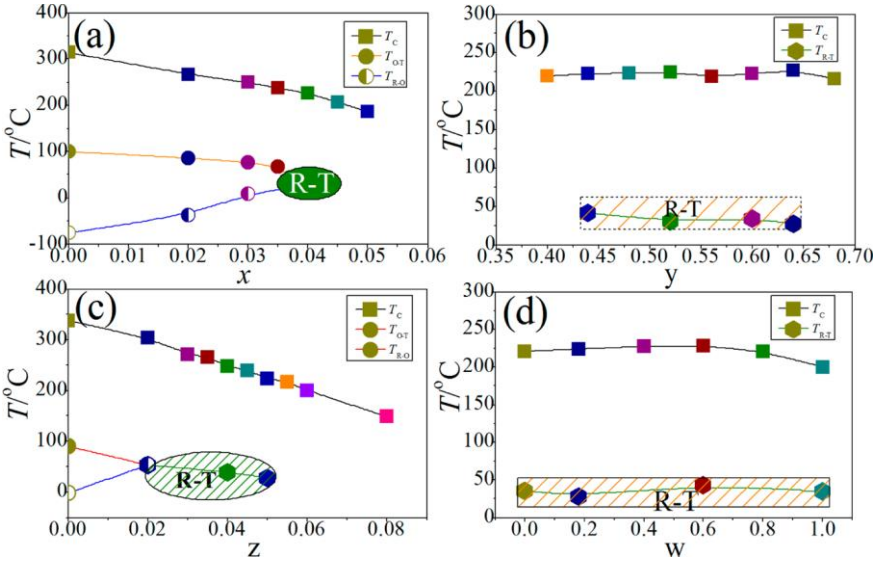

Figure 2-30 MPB-Phase diagrams of the $(1-x)(K_{1-y}Na_y)(Nb_{1-z}Sb_z)O_3 -xBi_{0.5}(Na_{1-w}K_w)0.5ZrO_3$ ceramics of (a) y=0.48, z=0.05, w=0.18; (b) x=0.04, z=0.05, w=0.18; (c) x=0.04, y=0.48, w=0.18; (d) x=0.04, y=0.48, z=0.05[57]

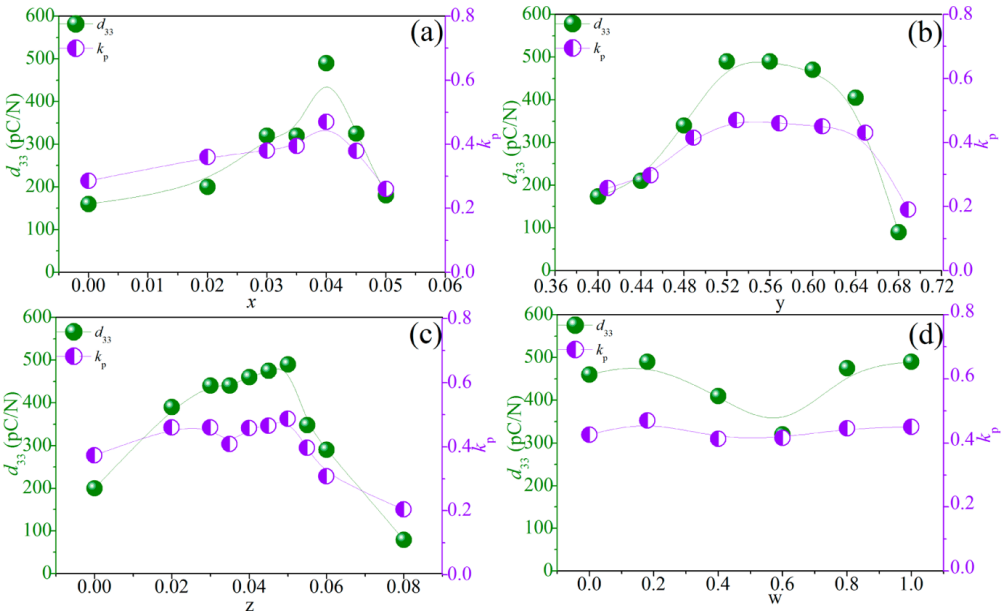

Figure 2-31 d_{33} and k_p of the $(1-x)(K_{1-y}Na_y)(Nb_{1-z}Sb_z)O_3 -xBi_{0.5}(Na_{1-w}K_w)0.5ZrO_3$ ceramics with (a) y=0.52, z=0.05, w=0.18; (b) x=0.04, z=0.05, w=0.18; (c) x=0.04, y=0.52, w=0.18; (d) x = 0.04, y=0.52, z=0.05[57]

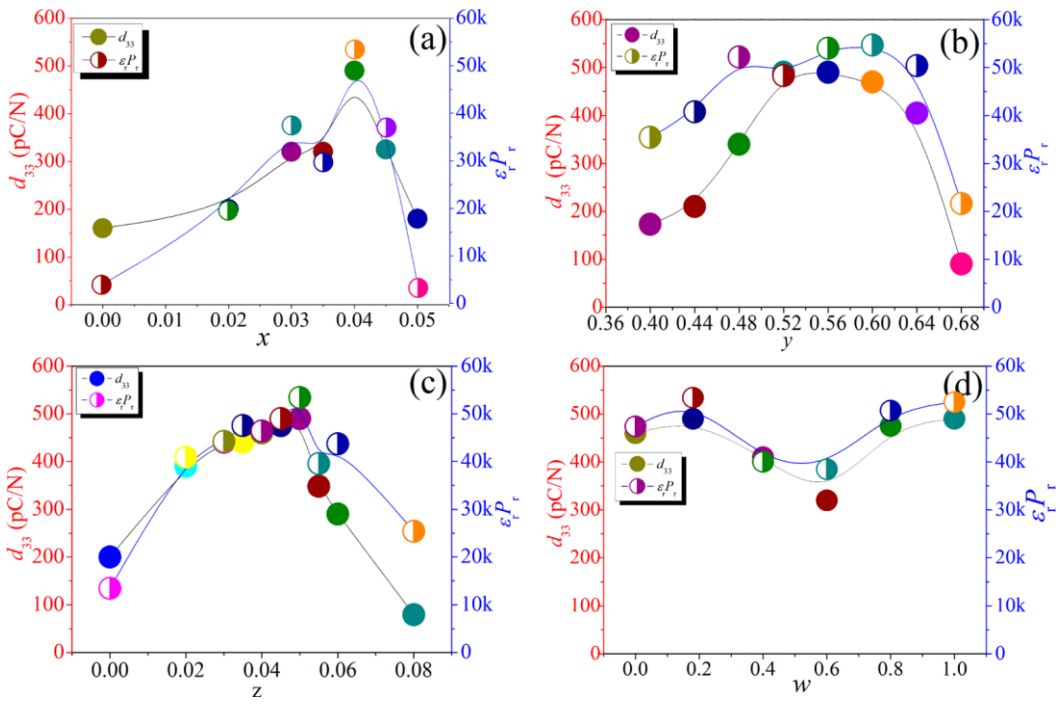

Figure 2-32 ε_r, P_r and d_{33} of the $(1-x)(K_{1-y}Na_y)(Nb_{1-z}Sb_z)O_3-xBi_{0.5}(Na_{1-w}K_w)0.5ZrO_3$ ceramics of (a) y=0.52, z=0.05, w=0.18; (b) x=0.04, z=0.05, w=0.18; (c) x =0.04, y=0.52, w=0.18; (d) x=0.04, y=0.52, z=0.05[57]

2.4.4.4 $0.96K_{0.46}Na_{0.54}Nb_{0.95}Sb_{0.05}O_3$-$0.04Bi_{0.5}(Na_{0.82}K_{0.18})_{0.5}ZrO_3$

The study of this composition mainly focused on attaining an optimum sintering temperature (T_S) and broadening the range of T_S without losing the MPB structure.[36] The authors found the optimum range of T_S was 1060 – 1105°C in which R-T phase coexistence could be achieved. In their XRD results, Figure 2-33, they reported splitting of peaks in the 21-23° and 44-47° 2θ ranges promoted by increasing T_S and proposed to be due to the volatility of alkali ions.

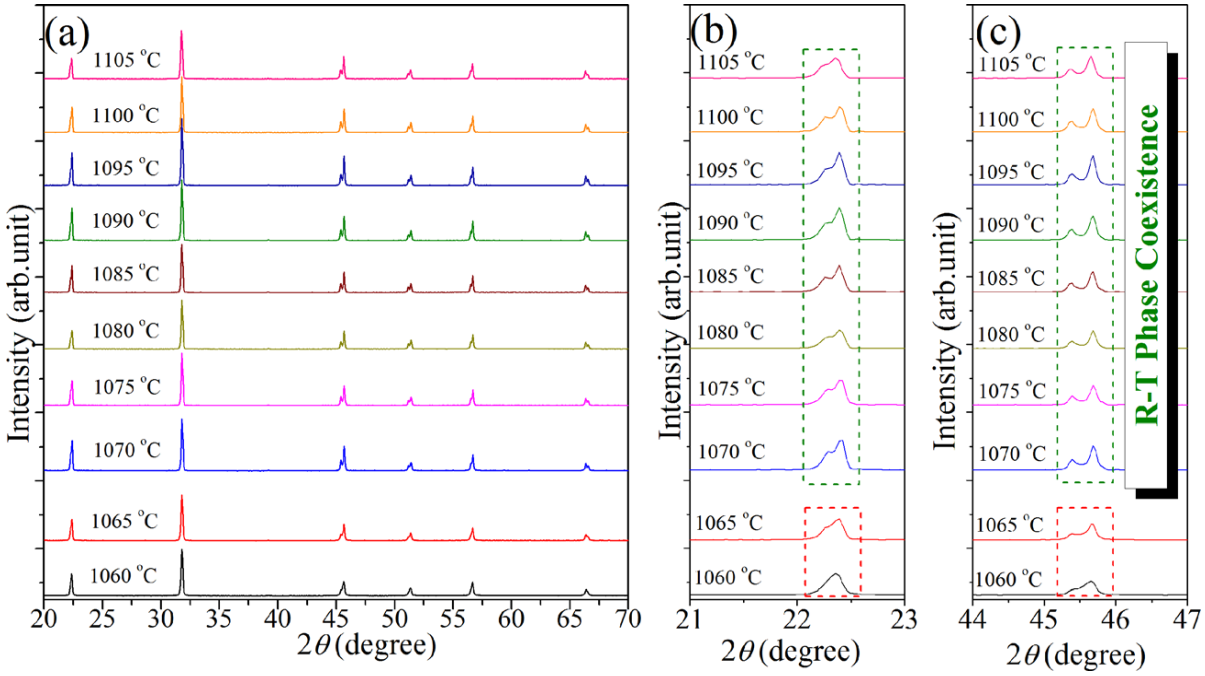

Figure 2-33 XRD result of the systems as a function of T_S, measured at (a) 2θ =20-70°, (b) 2θ= 21-23°, and (c) 2θ=44-47°[36]

The same authors performed energy dispersive X-ray analysis, Figure 2-34, and Figure 2-, to investigate volatility. However, it is unclear whether the data presented relates to volatilisation or to an increase in homogeneity as a function increasing sintering temperature but it noted that the oxygen concentration increases with T_S. Nonetheless, these authors achieved near theoretical densities at around 1080°C with d_{33}=465pC/N, k_p = 0.5, P_r=15μC/cm^2 and low tanδ . The latter seems incongruous with the presumed K^+ volatilisation where loss would be anticipated to increase, Figure 2-.[36]

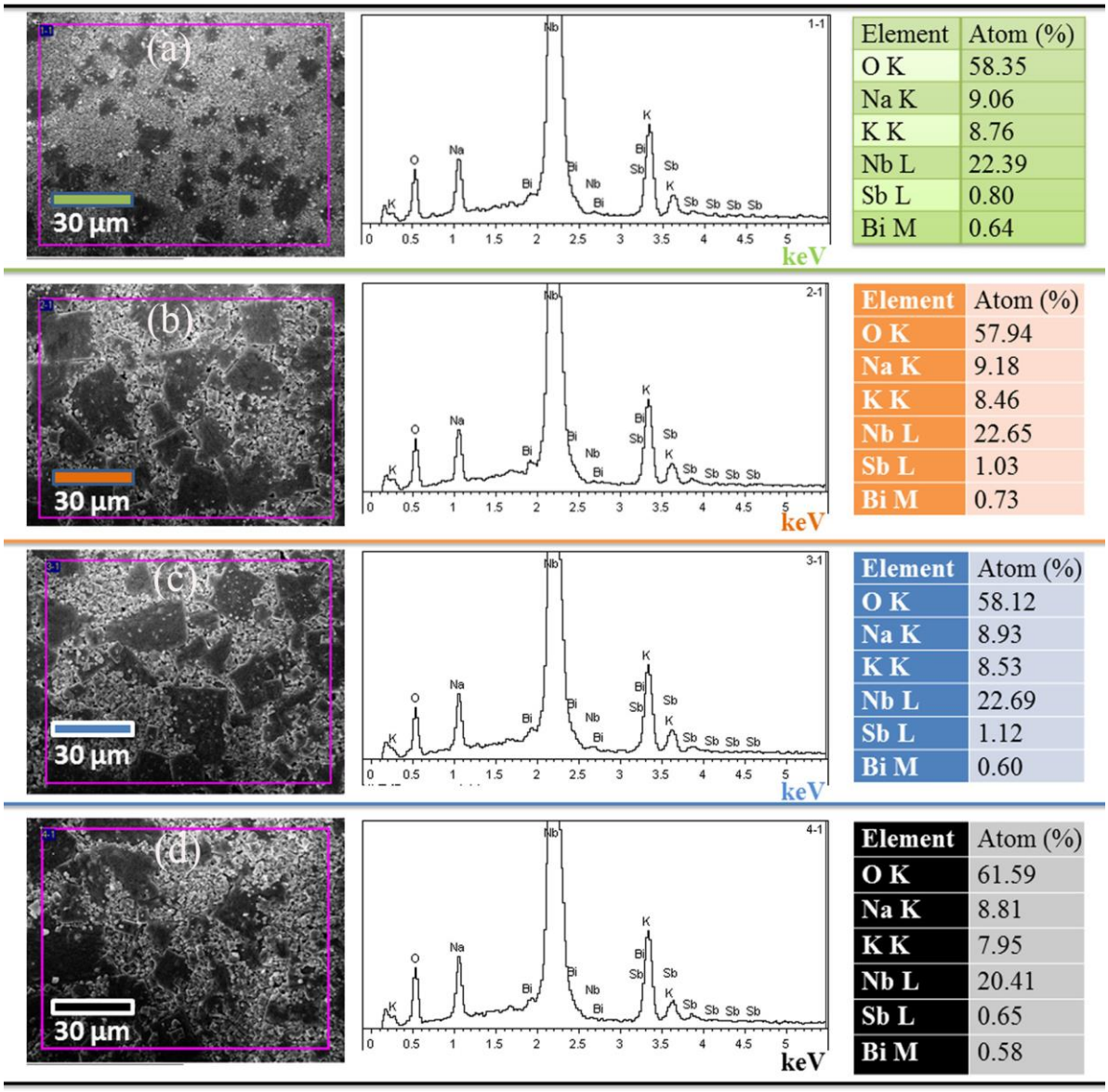

Figure 2-34 EDS analysis of the ceramics sintered at (a) 1060ºC, (b) 1075ºC, (c) 1090ºC, and (d) 1105ºC showing losses of K^{+1} and Na^{+1} [36]

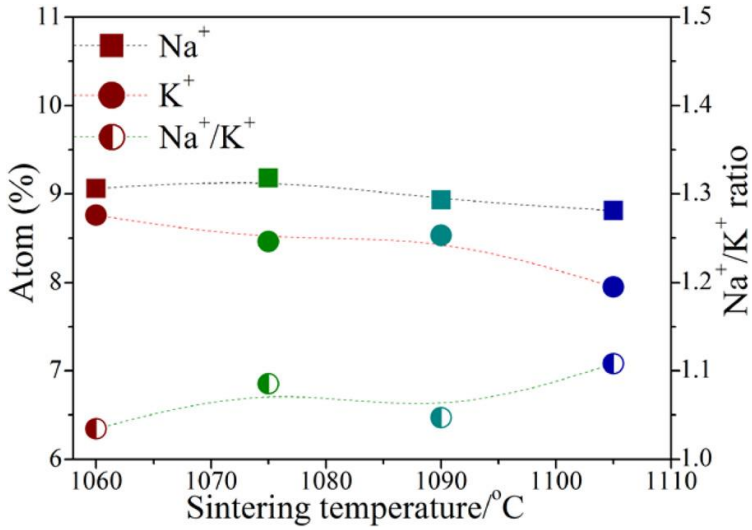

Figure 2-36 Atom percentage of K^+ and Na^+ as well as Na^+/K^+ in the ceramics as a function of T_S, data derived from Figure 2-34 [36]

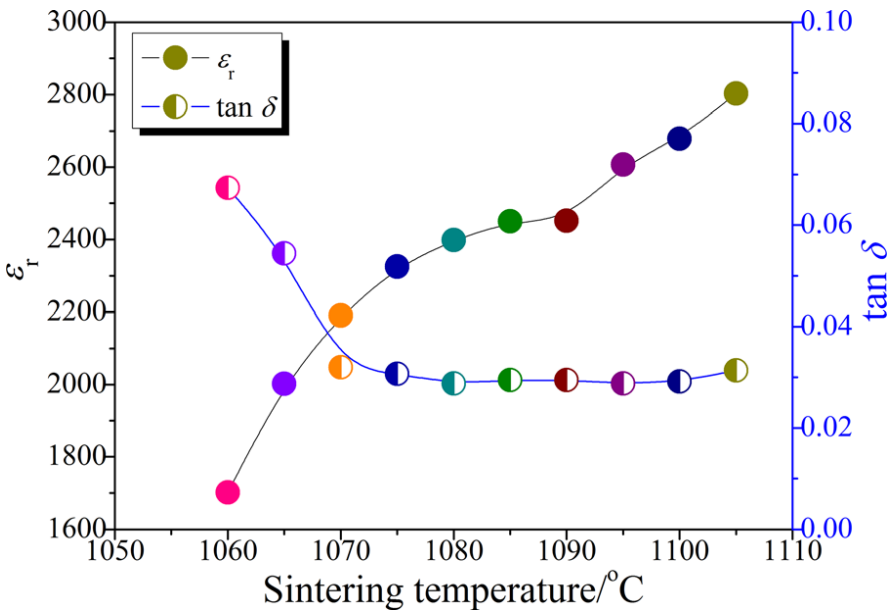

Figure 2-37 ε_r and tanδ vs. sintering temperature [36]

2.4.4.5 0.96 $(K_{0.46}Na_{0.54+x})$ $Nb_{0.95}Sb_{0.05}O_3$–0.04$Bi_{0.5}(Na_{0.82}K_{0.18})_{0.5}$ ZrO_3

The final composition utilising Bi based additions to KNN is $0.96(K_{0.46}Na_{0.54+x})Nb_{0.95}Sb_{0.05}O_3$–$0.04Bi_{0.5}(Na_{0.82}K_{0.18})_{0.5}ZrO_3$[37] Once again the authors report high d_{33} values but there are contradictions in the data and interpretations reported from those in previous publications from the same group.[30,

36] Here, it is claimed that excess of Na^+ = 0.5% enhances d_{33} to obtain 496pC/N with k_p =0.47 but in previous (Figure 2-) studies, K^+ was considered the more volatile species. Thus it is difficult to form a firm perspective on the key compositional and processing factors that lead to enhanced properties in these similar systems. [37]

2.4.5 The Fabrication of KNN-based Multilayers

Multilayers of KNN-5LT (d_{33}=250 pC/N and k_p=0.37) with excess of Li_2O was first reported by Kim et al in 2008 using 70Ag-30Pd internal electrodes. [59] However, the most significant work has focussed on Ni based internal electrodes.

2.4.5.1 Multilayers with Ni Inner Electrode

Kawada, S, et al., in 2009 prepared three KNN-based compounds, namely; 0.96 $(K_{0.5}Na_{0.5})$ NbO_3 – 0.04 $CaTiO_3$ (KNN-CT-1), 0.96 $(K_{0.5}Na_{0.5})$ NbO_3–0.04 $CaZrO_3$ (KNN-CZ-1), and 0.96 $(K_{0.5}Na_{0.5})$ NbO_3–0.04 $CaZrO_3$ + 0.03 Zr (KNN-CZ-2). In each compound, 5 mol% manganese oxide was used as a sintering aid. The (KNN-CZ-2) composition was reported to be more electrically resistive than the others in a low $P(O_2)$ (oxygen partial pressure of $1x10^{-11}$ to $1x10^{-10}$ MPa). These authors multi-layered a stack of 12-ceramic layers and 11-Ni inner-electrodes using KNN-CZ-2 following a conventional tape cast screen print technology. The SEM image of the multilayer and strain-electric field data are shown in Figure 2-35. At the maximum electric field (E_{max}), the maximum strain (S_{max}) gave an effective d_{33}^* = 360 pm/ V, approximately half that of PZT based ceramics.[60]

0.98$(K_{0.5}Na_{0.5})$ NbO_3 - 0.02$CaZrO_3$+0.03Zr (KNN-CZ-2) was also studied by the same group (Hayashi H, et al. 2012) who concluded that the piezoelectric properties,

electric resistance and thermal shock were stable from – 40 ^{0}C to 85 ^{0}C and at high humidity, Figure 2-. [61]

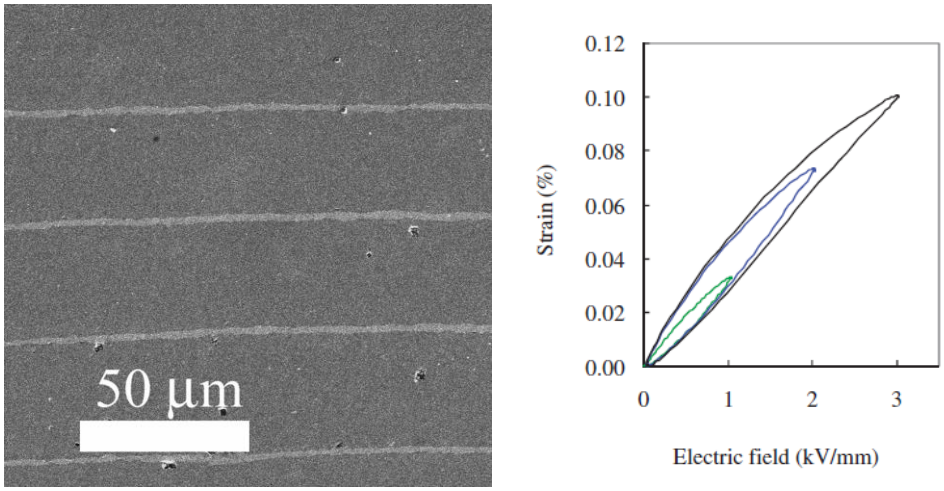

Figure 2-35 (left) SEM image of cross section of KNN-CZ-2 multi-layered with Ni inner electrodes, and (right) the strain versus electric field of KNN-CZ-2[60]

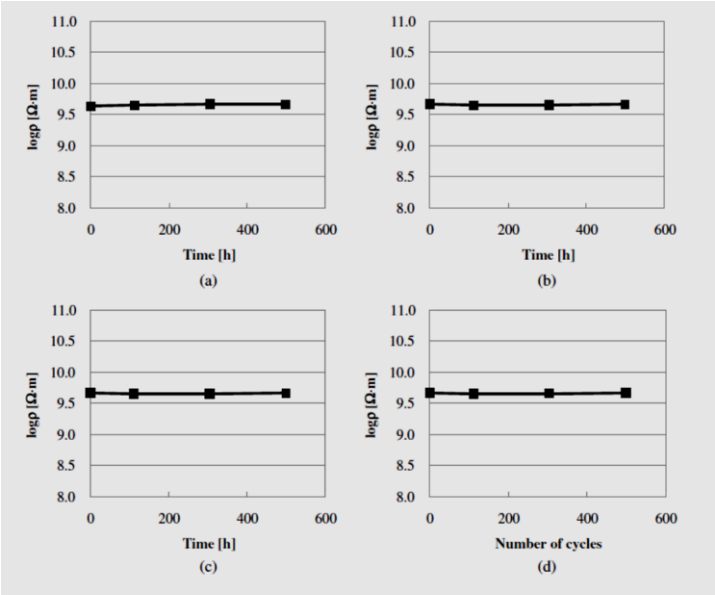

Figure 2-39 Resistivity changes of Modified $0.98(K_{0.5}Na_{0.5})NbO_3$-$0.02CaZrO_3$+0.03Zr (KNN-CZ-2) under different conditions. (a) at 85°C, (b) at -40°C, (c) at 85°C / 85% RH and (d) the thermal shock test (-40°C to 85°C, 1h / cycle) [61]

In 2014, Liu et al [62], prepared multilayers with Ni inner electrodes of (1-x)$K_{0.5}Na_{0.5}$ ($Nb_{0.8}Ta_{0.2}$)O_3 (KNNT) – xNaF-0.5Nb_2O_5, where x =0.02, 0.04, 0.06, Figure 2-36 First they processed KNNT with conventional solid state reaction method and, after calcination the NaF-0.5Nb_2O_5 was added and milled as a sintering aid. By adding this flux, they postulated that V_{Na}' and $V_O^{\bullet\bullet}$ should be lower when processed in low pO_2 compared with air, as described in the Kroger-Vink notation below. They also reported that F^- anions compensate for oxygen vacancies as a donor substitute. The ceramic was sintered in reducing atmosphere (10^{-10} atms) at 1150°C for two hours and followed by annealing (850°C at same partial pressure of oxygen for 8 hours) to improve the resistivity and dielectric loss. The max converse piezoelectric d_{33}^*= 385pC/N was reported for 2NN-KNNT samples of co-fired with Ni inner electrodes. P-E hysteresis loops and unipolar S-E relations are shown in Figure 2-37.[62]

$$\mathbf{NaF + 2V_{Na}' + V_O^{\bullet\bullet} \leftrightarrow Na_{Na}^x + F_O^{\bullet} + V_{Na}'}$$

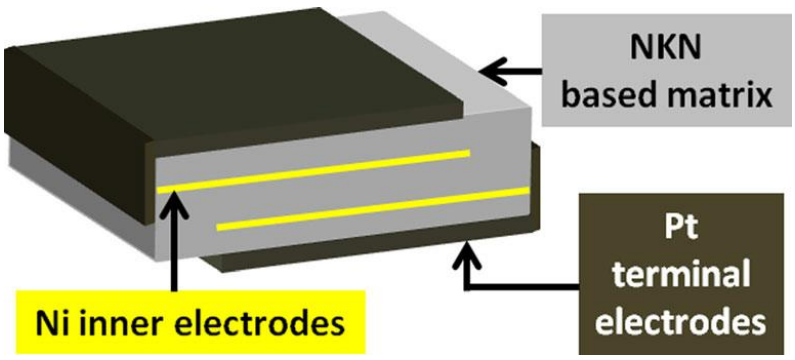

Figure 2-36 Actuator prototype with 3-ceramic and 2-Ni electrodes layers[62]

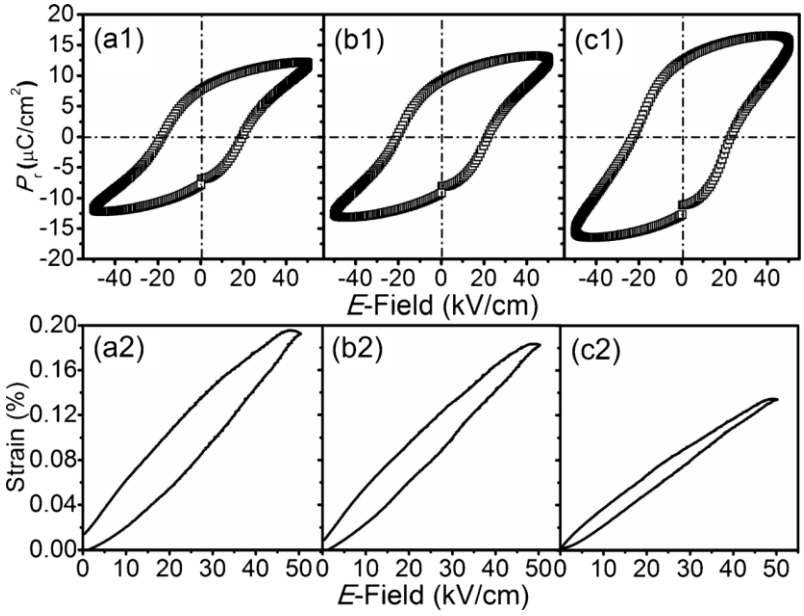

Figure 2-37 Ferroelectric loops and strain data of (a) 2NN-KNNT, (b) 4NN-KNNT and (c) 6NN-KNNT, co-sintered with Ni inner electrodes [62]

2.4.5.2 Ag/Pd co-fired Multilayers of ($Na_{0.52}K_{0.44}Li_{0.04}$) ($Nb_{0.89}Sb_{0.05}Ta_{0.06}$) O_3 (KNNLTS)

Li^{1+}, Ta^{5+} and Sb^{3+} co-doped (KNN-LTS) multilayers with Ag/Pd internal electrodes were synthesized and characterized by Gao et al. (2014) [63]. These authors prepared five active layers and obtained d_{33}^{*} = 452 pm/V in the tetragonal structured KNNLST piezoceramics. At the resonant frequency of 131.8 kHz, a dynamic response of 1839 pm/V was claimed by using a laser as illustrated in Figure 2-38 where the normalised thickness strain (S_{max}/E_{max}) was 369 pm/V.

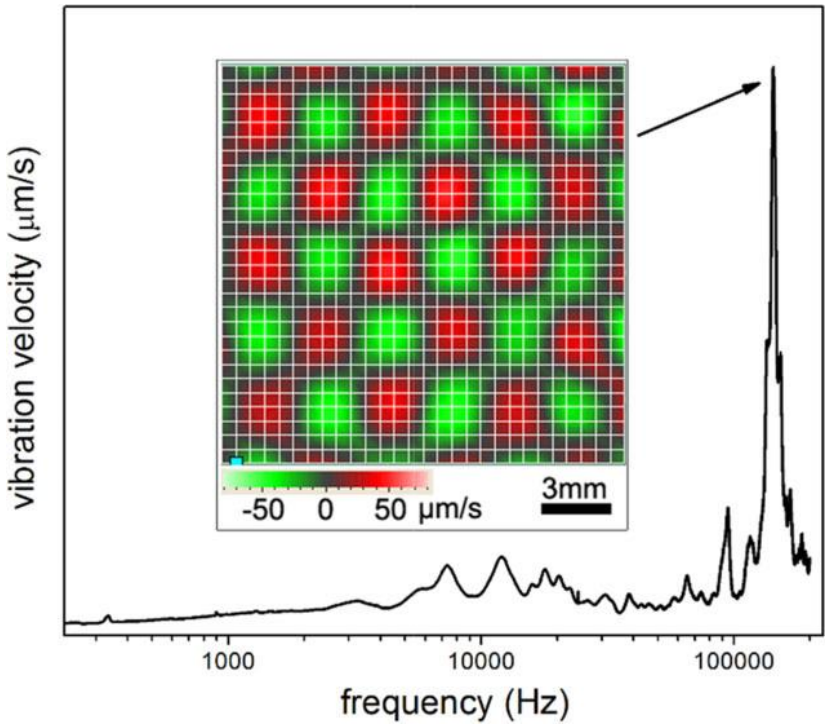

Figure 2-38 Vibration velocity curve for a five-layered device of KNN-LST from 0 to 200 kHz; where inset shows the mode of vibration at resonance frequency [63]

Gao et al also observed an interfacial layer between the ceramic and Ag/Pd inner-electrode by analysing through high-resolution-transmission-electron-microscopy (HRTEM), Figure 2-39. Consequently, they suggested that the direct piezoelectric response was reduced and that the converse piezoelectric was enhanced, due to the interfacial layer. [63]

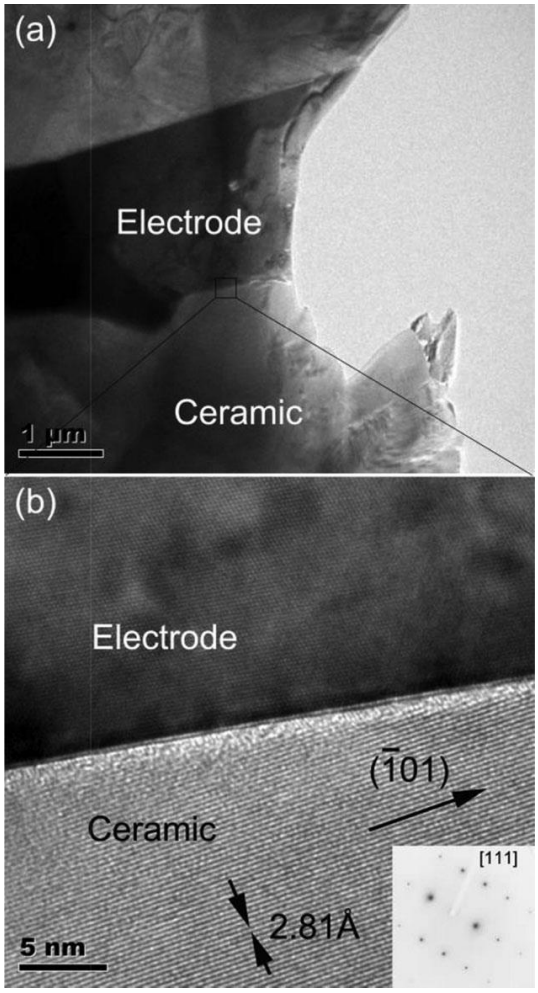

Figure 2-39 HRTEM-image of interface in between of Ag/Pd co-fired electrode and KNNLST ceramic layer, where (a) shows the interfacial lattice image and in (b) the inset showing the SAED pattern of ceramic near the interface [63]

2.4.5.3 KNN-Based Multi-layer in Micro-Speaker

KNN-based multilayers in micro speaker were first fabricated in 2011 by Seo et al which they prepared with 20 layers of CuO doped KNN-50/50.[64] Following on from this earlier work, Gao et al. fabricated a flat panel microspeaker (Figure 2-40) using tape casting and screen printing technology with co-fired Ag/Pd inner electrodes from the formulation of KNNLTS.[65] The dimensions of the micro-speaker were 23x27x0.6 mm^3 which was achieved by using 3-layers of 30 µm thick

KNNLTS. The high average sound pressure level (SPL) attained was 87dB in frequency range of 100Hz – 20kHz at 5 volts and total harmonic distortion (THD) are comparable with PZT, Figure 2-41

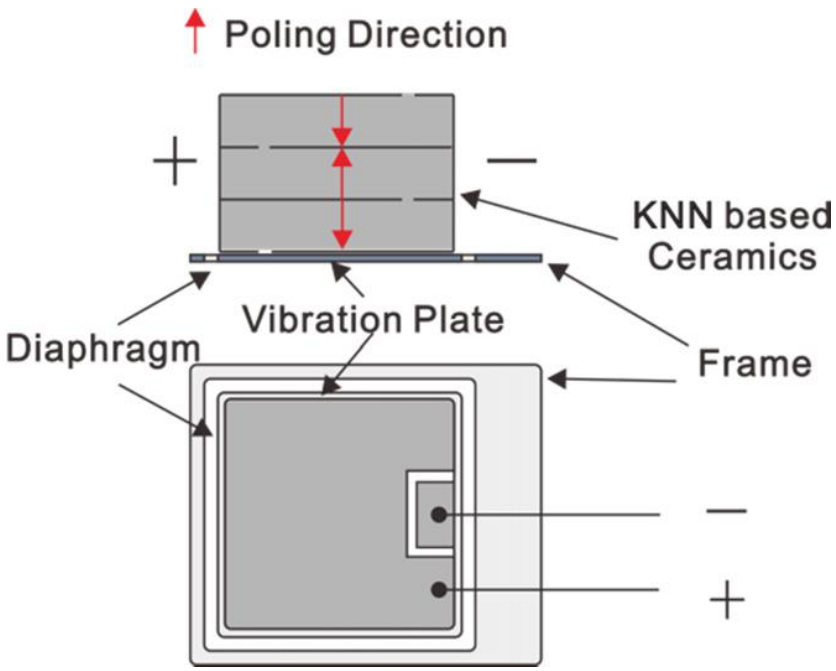

Figure 2-40**.** Prototype of KNN-based piezoelectric flat-panel-micro-speaker[65]

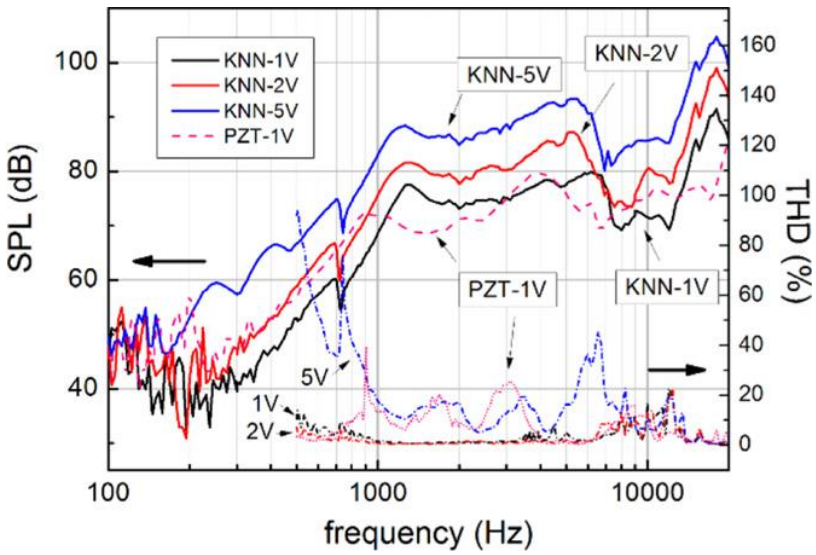

Figure 2-41**.** Comparison between micro speakers made of KNN and PZT-based ceramics under 1Vrms[65]

References

1. David, R.W., *Modern Ceramic Engineering: Properties, Processing and Use in Design*, ed. r. Edition. 2006: CRC.
2. C. K. , K., *DIELECTRIC PHENOMENA IN SOLIDS : With Emphasis on Physical Concepts of Electronic Processes*. 2004, USA: Elsevier Academic Press.
3. Moulson, A.J., & Herbert, J.M.,, *Electroceramics*. Materials, properties, Applications. 2003, England: Wiley.
4. Uchino, K., *Ferroelectric Devices*. 2000, New York, Basel: Marcel Dekker, Inc.
5. University of Cambridge. *Dielectric Materials from: http://www.doitpoms.ac.uk/tlplib/dielectrics/index.php*. 2008 -2009 [cited 2015 27-28 October].
6. Defay, E., *Integration of Ferroelectric and Piezoelectric Thin Films: Concepts and Applications for Microsystems*. 2011, Great Britain and USA: ISTE Ltd and John Wiley & Sons, Inc.
7. Tilley, R.J.D., *Understanding Solids: The Science of Materials*. 2nd ed. 2013, UK: John Wiley and Sons.
8. Wu, J., D. Xiao, and J. Zhu, *Potassium-sodium niobate lead-free piezoelectric materials: past, present, and future of phase boundaries.* Chem Rev, 2015. **115**(7): p. 2559-95.
9. Institution, B.S., *Piezoelectric properties of cetramic materials and components*, in *Part1: Terms and definitions*2002, BSI: BS EN 50324-1:2002, London, UK.

10. Seacor Piezo Ceramics. *Symbols and Terminology Chart from: http://www.seacorpiezo.com/defin_terms/symbol.html*. 2015 [cited 2015 12 to 14 October].

11. Brown, C.S., Kell, R.C, Taylor, R, Thomas, L.A.,, *Piezoekctric Materials, A Review of Progress.* Reprinted From Proc. IEE, 1962. **109**(pt. B, no. 43): p. 99-114.

12. Haertling, G.H., *Ferroelectric Ceramics: History and Technology.* Journal of American Ceramic Society 1999. **82**(04): p. 797-818.

13. Rödel, J.J., Wook Seifert, Klaus T. P. Anton, Eva-Maria Granzow, Torsten Damjanovic, Dragan, *Perspective on the Development of Lead-free Piezoceramics.* Journal of the American Ceramic Society, 2009. **92**(6): p. 1153-1177.

14. Bell, A.J., *Ferroelectrics: The role of ceramic science and engineering.* Journal of the European Ceramic Society, 2008. **28**(7): p. 1307-1317.

15. Donnelly, N.J.S., Thomas R., Randall, Clive A., *Addition of a Sr, K, Nb (SKN) Combination to PZT(53/47) for High Strain Applications.* Journal of the American Ceramic Society, 2007. **90**(2): p. 490-495.

16. ‘‘EU-Directive 2002/96/EC: Waste Electrical and Electronic Equipment (WEEE), O.J.E.U., 46 [L37] 24–38 (2003).

17. 2002/95/EC, E.-D., *Restriction of the Use of Certain Hazardous Substances in Electrical and Electronic Equipment (RoHS)*, in *Off. J. Eur. Union, 46*2003.

18. Zhang, S.X., Ru Shrout, Thomas R., *Lead-free piezoelectric ceramics vs. PZT?* Journal of Electroceramics, 2007. **19**(4): p. 251-257.

19. Takenaka, T.N., H. Hiruma, Y. Yoshii, Y. Matumoto, K., *Lead-free piezoelectric ceramics based on perovskite structures.* Journal of Electroceramics, 2007. **19**(4): p. 259-265.

20. Panda, P.K., *Review: environmental friendly lead-free piezoelectric materials.* Journal of Materials Science, 2009. **44**(19): p. 5049-5062.

21. Aksel, E. and J.L. Jones, *Advances in Lead-Free Piezoelectric Materials for Sensors and Actuators.* Sensors, 2010. **10**(3): p. 1935-1954.

22. Wood, E.A., *Polymorphism in Potassium Niobate, Sodium Niobate, and Other ABO_3 Compounds.* Acta Crystallographica, 1951. **4**(4): p. 353-362.

23. Jaffe, B., Cook, W.R.J. and Jaffe, H., *Piezoelectric Ceramics*. 1971, London and New York: Academic Press.

24. Baker, D.W., et al., *A comprehensive study of the phase diagram of $K_xNa_{1-x}NbO_3$.* Applied Physics Letters, 2009. **95**(9): p. 091903.

25. Stokes, H.T., et al, *Group-theoretical analysis of octahedral tilting in ferroelectric perovskites.* Acta Crystallographica Section B: Structural Science, 2002. **B58**: p. 934 - 938.

26. D. W. Baker, P.A.T., N. Zhang, and A. M. Glazer, *A comprehensive study of the phase diagram of $K_xNa_{1-x}NbO_3$.* Applied Physics Letters, 2009. **95**(091903): p. 1-3.

27. Birol, H., D. Damjanovic, and N. Setter, *Preparation and characterization of $(K_{0.5}Na_{0.5})NbO_3$ ceramics.* Journal of the European Ceramic Society, 2006. **26**(6): p. 861-866.

28. Jaeger R.E, E., L., *Hot Pressing of Potassium-Sodium Niobates.* Journal of the American Ceramic Society, 1962. **45**(5): p. 209-213.

29. LIN, D., Li, Z., Xu, Z., Yao, X.,, *Characterization of KNN Single Crystals by Slow-cooling Technique.* Ferroelectrics, 2009(381:1): p. 1-8.

30. Wang, Y., et al., *High-Temperature Instability of Li- and Ta-Modified (K,Na)NbO_3Piezoceramics.* Journal of the American Ceramic Society, 2008. **91**(6): p. 1962-1970.

31. Lee, Y.-h., et al., *Piezoelectric Properties and Densification Based on Control of Volatile Mass of Potassium and Sodium in ($K_{0.5}Na_{0.5}$)NbO_3Ceramics.* Japanese Journal of Applied Physics, 2008. **47**(6): p. 4620-4622.

32. Lin, D., K.W. Kwok, and H.W.L. Chan, *Dielectric and piezoelectric properties of ($K_{0.5}Na_{0.5}$)NbO_3–Ba($Zr_{0.05}Ti_{0.95}$)O_3 lead-free ceramics.* Applied Physics Letters, 2007. **91**(14): p. 143513.

33. Zhao, Y., et al., *Low-temperature sintering of KNN with excess alkaline elements and the study of its ferroelectric domain structure.* Current Applied Physics, 2013. **13**(9): p. 2082-2086.

34. Tan, C.K.I., et al., *0.94($K_{0.5}Na_{0.5}$)NbO_3–0.06$LiNbO_3$ piezoelectric ceramics prepared from the solid state reaction modified with polyvinylpyrrolidone (PVP) of different molecular weights.* Ceramics International, 2012. **38**(3): p. 2513-2519.

35. Bafandeh, M.R., et al., *Improvement of piezoelectric and ferroelectric properties in (K,Na)NbO_3- based ceramics via microwave sintering.* Journal of Electroceramics, 2014. **33**(1-2): p. 128-133.

36. Wu, J., et al., *New potassium-sodium niobate lead-free piezoceramic: Giant-d_{33} vs. sintering temperature.* Journal of Applied Physics, 2014. **115**(11): p. 114104.

37. Zheng, T., et al., *Giant d_{33} in nonstoichiometric (K,Na)NbO_3-based lead-free ceramics.* Scripta Materialia, 2015. **94**: p. 25-27.

38. Jenko, D., et al., *Electron microscopy studies of potassium sodium niobate ceramics.* Microsc Microanal, 2005. **11**(6): p. 572-80.

39. Kodaira, K., et. al., *Sintering and dielectric properties of $KNbO_3$.* Journal of Materials Science Letters, 1982. **1**(07): p. 277 - 278.

40. Fluckiger, U., and Arend, H,, *On The Preparation Of Pure, Doped And Reduced $KNbO_3$ Single Crystals.* Journal of Crystal Growth, 1978. **43**(04): p. 406 - 416.

41. Deng, H., et al., *Orientation dependence of electrical properties of large-sized sodium potassium niobate lead-free single crystals.* CrystEngComm, 2014. **16**(13): p. 2760.

42. Fisher, J.G., et al., *Structural changes in potassium sodium niobate ceramics sintered in different atmospheres.* Journal of Alloys and Compounds, 2009. **479**(1-2): p. 467-472.

43. Wang, Z., et al., *New Lead-Free $(1-x)(K_{0.5}Na_{0.5})NbO_3$-x(Bi0.5Na0.5)$ZrO_3$Ceramics with High Piezoelectricity.* Journal of the American Ceramic Society, 2014. **97**(3): p. 688-690.

44. Bencan, A., et al., *Compositional and structural study of a $(K_{0.5}Na_{0.5})NbO_3$ single crystal prepared by solid state crystal growth.* Microsc Microanal, 2009. **15**(5): p. 435-40.

45. Ichiki, M., et al., *Electrical properties of piezoelectric sodium-potassium niobate.* Journal of the European Ceramic Society, 2004. **24**(6): p. 1693-1697.

46. Jenko, D., et al., *Electron Microscopy Studies of Potassium Sodium Niobate Ceramics.* Microscopy and Microanalysis, 2005. **11**(06).

47. Fisher, J.G., S.-Y. Choi, and S.-J.L. Kang, *Influence of Sintering Atmosphere on Abnormal Grain Growth Behaviour in Potassium Sodium Niobate Ceramics Sintered at Low Temperature.* Journal of the Korean Ceramic Society, 2011. **48**(6): p. 641-647.

48. *JCPDS No. 00-032-0822. International Centre for Diffraction Data: newton Square, PA*, 1981.

49. *JCPDS No. 01-071-0945. International Center for Diffraction Data: Newton Square, PA.*, 1997.

50. Skidmore, T.A. and S.J. Milne, *Phase development during mixed-oxide processing of a* $[Na_{0.5}K_{0.5}NbO_3]_{1-x}$*–*$[LiTaO_3]$ *x powder.* Journal of Materials Research, 2011. **22**(08): p. 2265-2272.

51. Bomlai, P., et al., *Effect of Calcination Conditions and Excess Alkali Carbonate on the Phase Formation and Particle Morphology of* $Na_{0.5}K_{0.5}NbO_3$*Powders.* Journal of the American Ceramic Society, 2007. **90**(5): p. 1650-1655.

52. Saito, Y., et. al. , *Lead-Free piezoceramics.* Nature, 2004. **432**(7013): p. 84-7.

53. Guo, Y., K.-i. Kakimoto, and H. Ohsato, *Phase transitional behavior and piezoelectric properties of* $(Na_{0.5}K_{0.5})NbO_3$*–*$LiNbO_3$ *ceramics.* Applied Physics Letters, 2004. **85**(18): p. 4121.

54. Guo, Y., K.-i. Kakimoto, and H. Ohsato, $(Na_{0.5}K_{0.5})NbO_3$*–*$LiTaO_3$ *lead-free piezoelectric ceramics.* Materials Letters, 2005. **59**(2-3): p. 241-244.

55. Hollenstein, E., et al., *Piezoelectric properties of Li- and Ta-modified* $(K_{0.5}Na_{0.5})NbO_3$ *ceramics.* Applied Physics Letters, 2005. **87**(18): p. 182905.

56. Jianhua, L., *Characterization of ternary $(Na_{0.5}K_{0.5})_{1-x}$ Li_xNbO_3 lead-free piezoelectric ceramics prepared by molten salt synthesis method.* Journal of Materials Science, 2011. **46**(19): p. 6364-6370.

57. Wang, X., et al., *Giant piezoelectricity in potassium-sodium niobate lead-free ceramics.* J Am Chem Soc, 2014. **136**(7): p. 2905-10.

58. Wang, X., et al., *Large d_{33} in $(K,Na)(Nb,Ta,Sb)O_3$-$(Bi,Na,K)ZrO_3$ lead-free ceramics.* Journal of Materials Chemistry A, 2014. **2**(12): p. 4122.

59. Kim, M.-S., et al., *Lead-free NKN-5LT piezoelectric materials for multilayer ceramic actuator.* Journal of Electroceramics, 2008. **23**(2-4): p. 372-375.

60. Kawada, S., et al., *$(K_{0.5},Na_{0.5})NbO_3$-Based Multilayer Piezoelectric Ceramics with Nickel Inner Electrodes.* Applied Physics Express, 2009. **2**(11): p. 111401.

61. Hiroyuki Hayashi, S.K., et al., *Reliability of Nickel Inner Electrode Lead-Free Multilayer Piezoelectric Ceramics.* Japanese Journal of Applied Physics, 2012. **59**(09LD01).

62. Liu, C., et al., *Base metal Co-fired $(Na,K)NbO_3$ structures with enhanced piezoelectric performance.* Journal of Electroceramics, 2014. **32**(4): p. 301-306.

63. Gao, R., et al., *Investigation on co-fired multilayer KNN-based lead-free piezoceramics.* physica status solidi (a), 2014. **211**(10): p. 2378-2383.

64. Seo, I.-T., et al., *Piezoelectric properties of CuO-added $(Na_{0.5}K_{0.5})NbO_3$ ceramic multilayers.* Journal of the European Ceramic Society, 2012. **32**(5): p. 1085-1090.

65. Gao, R., et al., *A study on (K, Na) NbO_3 based multilayer piezoelectric ceramics micro speaker*. Smart Materials and Structures, 2014. **23**(10): p. 105018.

Chapter 3 Experimental Procedures

The XRD and SEM analysis were initially done to understand the phase assemblage / crystal structure as a function of composition and morphology of the grains with EDX respectively. The defect chemistry of KNN has been investigated under different sintering conditions with the help of LCR, impedance spectroscopy and thermal power analysis. The different kinds of dopants (acceptors: Mn^{2+}, Ti^{4+}, Sn^{4+} in KNN_50/50 ratio; Donor: Sr^{2+} in KNN_50/50 ratio; Ta^{5+} as an isovalent in KNN-51/49 ratio; and co-dopants: Bi^{3+} and Zr^{4+} in KNN_50/50 ratio) have been doped into KNN to upgrade the piezoelectric performance with prototype multilayers of 10 and 16 layers with inner Pt electrodes to demonstrate the potential of 0.942KNN-0.058BNZ+ZrO_2 for the fabrication of multilayer actuators. Their functional properties were obtained through ferroelectric tester, piezoelectric tester (after poling) and precision impedance analyzer. Ceramic tape was casted by conventional tap-casting method and Pt electrodes were printed by screen printing procedure. To fabricate the multilayers, a novel Wet-Multilayer-Method (WMM) was also developed to overcome the issues of delamination during firing of MLCCs.

The general experimental work flow adopted in the project is illustrated in Figure 3-1. Each aspect of the work flow is explained in the following sections:

3.1 Raw Materials Selection and Batch Calculations

All compositions investigated in this study along with the raw materials utilised are shown in

Table 3-1. Carbonates were dried at 300°C (mullite crucible with lid) whereas all other oxides were heated at 900°C (alumina crucible with lid) for 24 hours. Batches varying in size from 10g to 50g of KNN-based compositions were prepared from

dried raw powders in hot condition (~200°C) to avoid the nonstoichiometric conditions caused by moisture, especially in carbonates. Some KNN compositions additionally were fired under different atmospheres but the majority were sintered in air only.

Table 3-1 KNN-based compositions and raw materials used in this study

Formulations	Raw Materials	Supplier / Purity (%)
(1) $K_xNa_{(1-x)}NbO_3$ ($0.49 \leq x \leq 0.51$) (2) $K_{0.5}Na_{0.5}Ti_xNb_{1-x}O_{3-x/2}$, $0.0 \leq x \leq 0.05$ (100xKNN-Ti) (3) $K_{0.5}Na_{0.5}Mn_xNb_{1-x}O_{3-x/2}$, $0.0 \leq x \leq 0.01$ (100xKNN-Mn) (4) $K_{0.5}Na_{0.5}Sn_xNb_{1-x}O_{3-x/2}$, $0.0 \leq x \leq 0.05$ (100xKNN-Sn) (5) $K_{0.51}Na_{0.49}Ta_xNb_{1-x}O_3$, $0.0 \leq x \leq 0.30$ (100xKNN-Ta) (6) $(K_{0.5}Na_{0.5})_{1-x}Sr_xNbO_3$, $0.0 \leq x \leq 0.05$ (Sr-100xKNN) (7) $(1-x)(K_{0.5}Na_{0.5}NbO_3)$-$x(Na_{0.5}Bi_{0.5}ZrO_3)$, $0.0 \leq x \leq 0.06$ (100xKNN-NBZ)	K_2CO_3	Fisher Scientific with 99.5% anhydrous, Fisher Scientific with 99.9% anhydrous (7)
	Na_2CO_3	Aldrich with 99.5% anhydrous, Fisher Scientific with 99.9% anhydrous (7)
	Nb_2O_5	Stanford Materials Corporation with 99.999% , Industrial Grade 99.5% (7)
	TiO_2	Aldrich Chemistry with 99.99%
	MnO_2	Aldrich, 99.9%
	SnO_2	Aldrich, 99.9%
	Ta_2O_5	Stanford Materials Corporation with 99.999% ,
	$SrCO_3$	Aldrich, 99.9%
	Bi_2O_3	Sigma Aldrich with 99.9%

	ZrO_2	Sigma-Aldrich with 99%

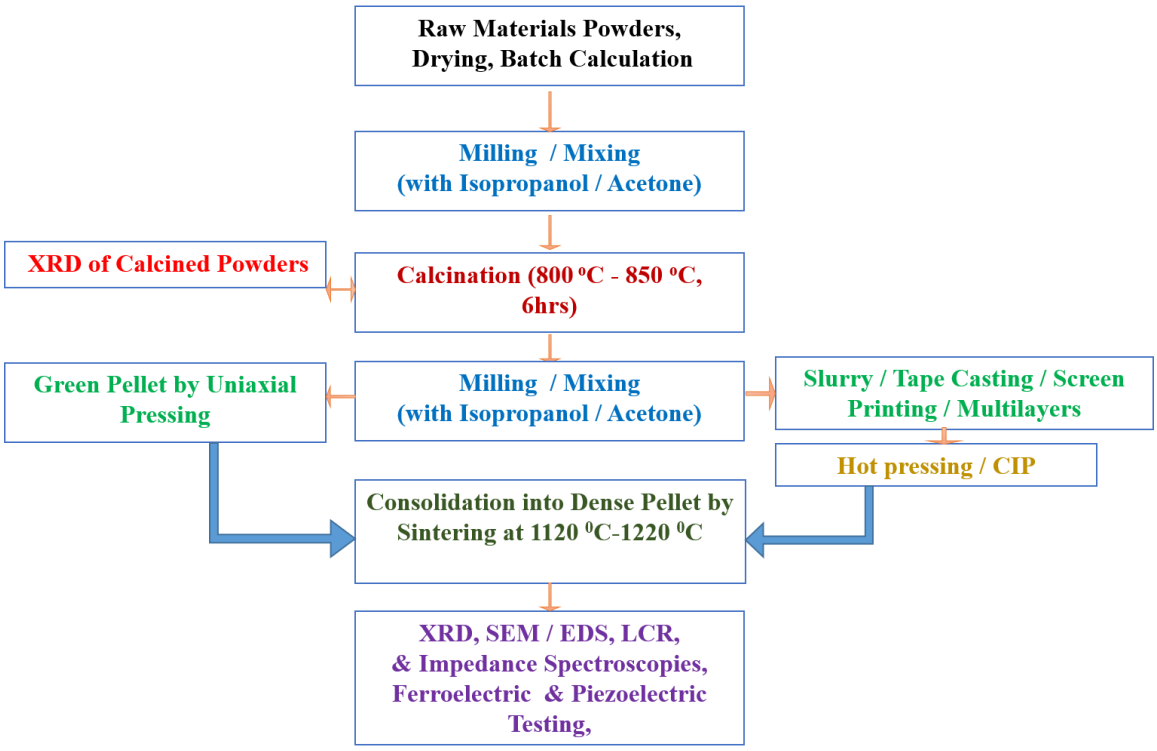

Figure 3-1 Flow diagram of Experimental work of KNN-based ceramics

3.2 Powder Processing and Sintering

KNN-based compositions were attrition milled 1-2h in a 500 ml jar at 300 rpm in isopropanol using 3mm dia. Y_2O_3 stabilised zirconia milling media prior to calcination. After milling, the slurry was washed with further isopropanol, separated from milling media through a sieve and volatiles removed at 80°C for 24 hours in a drying oven. The dried material was sieved through a 150 micron mesh and calcined 6h at 850°C at 3°C/min and 5°C/min, heating and cooling rates respectively. Calcined powders were re-milled prior to pressing a pellet.

Some small batches (i.e. of KNN-NBZ) of 5-10g were also milled in acetone-medium by using agate mortar and pestle to find the optimum MPB composition. These batches were dried in mortar quickly, then collected and calcined in alumina crucibles from 800°C to 1140°C. Generally, lower temperatures (~800°C) were used to avoid Bi^{3+} volatilization.

10mm dia. pellets of KNN-based compositions were pressed uniaxially with 2 ton force and sintered at different temperatures (from 1140°C to 1250°C) in air atmosphere. Only un-doped compounds were sintered in low pO_2 to investigate the semiconducting behaviour of KNN. Densities of pellets were measured using the Archimedes method and compared with X-ray powder density (described in section 3.4). The highest densities (≥ 95 % of theoretical density) of the un-doped KNN pellets obtained under different sintering-conditions (i.e., are shown in Figure 3-2). Nonetheless, other all firing parameters of acceptors, donor, isovalent and co-doped KNN-based; at their respective optimal temperatures, rates and soaking periods are described in detail in Figure 3-3, Figure 3-4, Figure 3-5 and Figure 3-6 respectively.

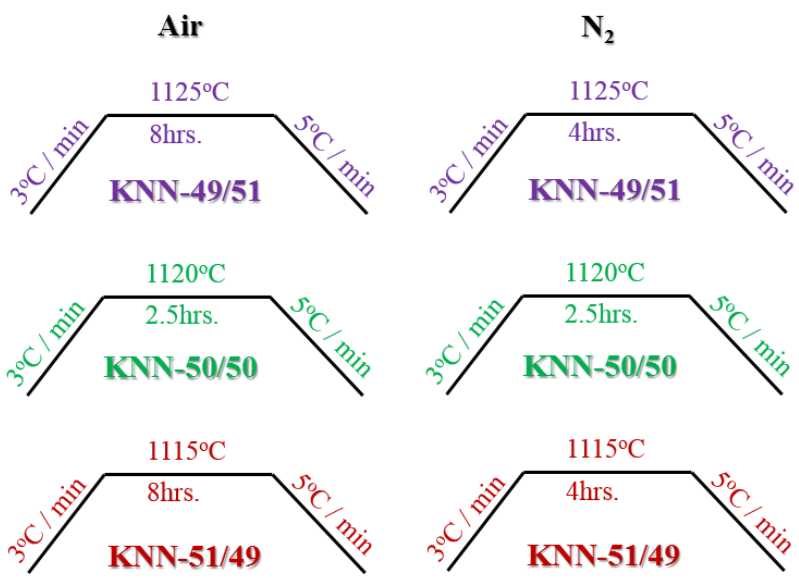

Figure 3-2 Optimum sintering cycles of un-doped KNN

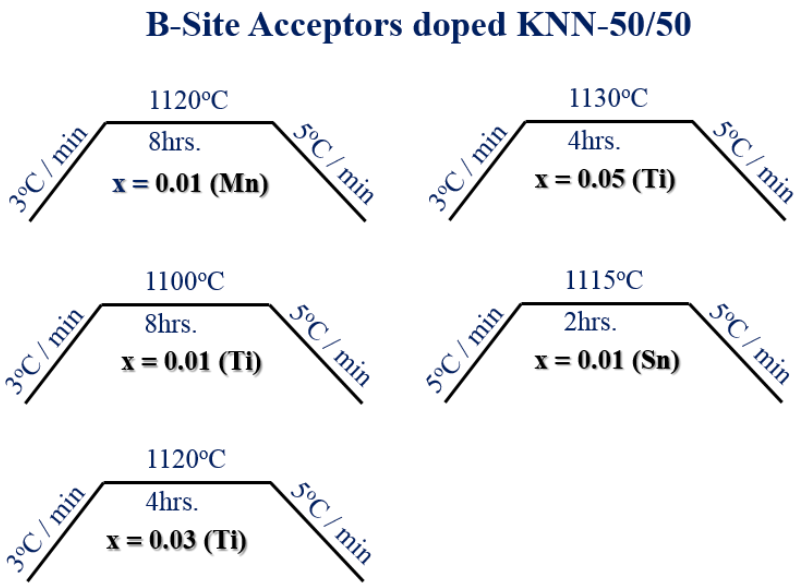

Figure 3-3 Sintering Profiles of Mn^{2+}, Ti^{4+} and Sn^{4+} doped KNN-50/50, at their respective optimum conditions

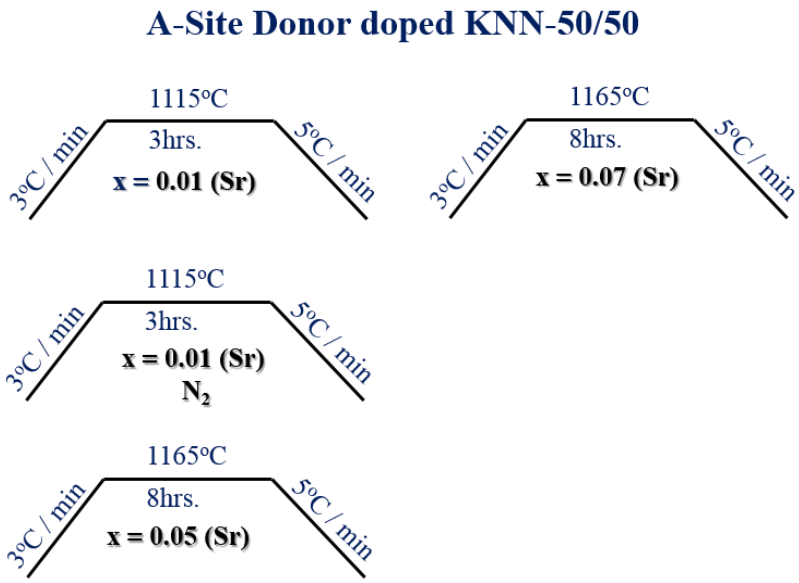

Figure 3-4 Optimum firing cycles of Sr^{2+} doped KNN-50/50

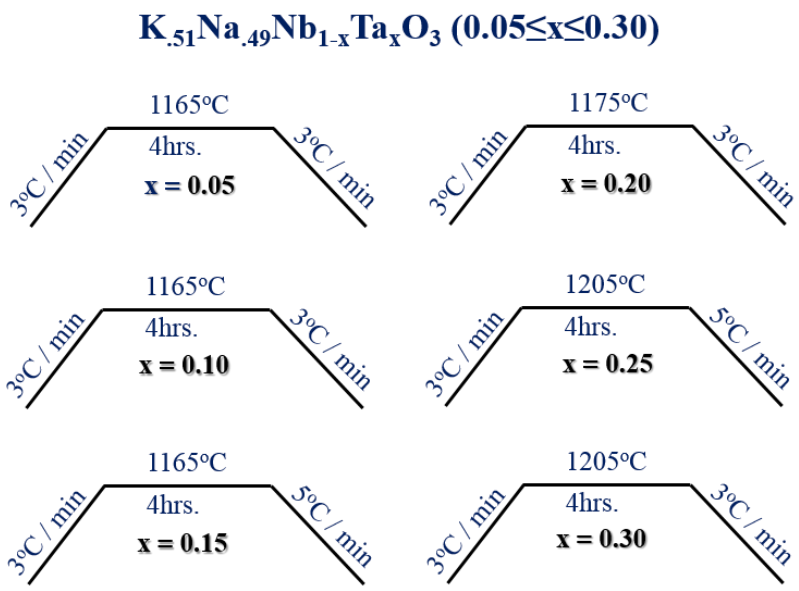

Figure 3-5 Sintering profiles of isovalent (Ta^{5+}) doped KNN-51/49 with respect to the x values

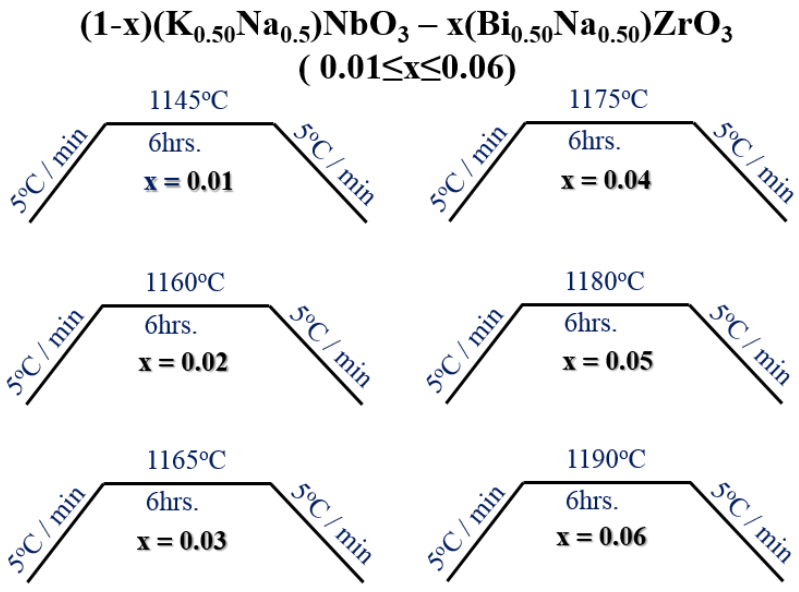

Figure 3-6 Firing cycles of solid solutions of KNN-BNZ with respect to the x values

3.3 Tape Casting and Screen printing

Tape casting and screen printing were used to fabricate multilayers of KNN-based ceramics. The slurry for casting was prepared according to the following formulation: 40g – 50g of calcined ceramic powder; 0.2% of dispersant (Hypermer KD1, Croder); 30% solvent (MEK50%: EtOH50%,Sigma Aldrich); 5% binder (Butvar-B98, Sigma Aldrich); 4% plasticizer (Butylbenzyl phthalate 98%, Sigma Aldrich) and 4% PEG (Polyethylene glycol, Sigma Aldrich) by weight of ceramic powder respectively. The slurry was mixed together using high speed conical mixer. The ceramic slurry was cast onto the polymeric carrier tape through the doctor blade method and the tape dried at room temperature for 12-hours, as shown in Figure 3-7 The dried green tape was cut into square pieces (30 mm × 30 mm) and patterns were made on the tape using Medway-Cutters (Figure 3-8) to facilitae screen printing. After screen printing Pt electrodes (9.2 mm × 7.2 mm), multilayer stacks were prepared using a stack-holder (Figure 3-8b) with alternate layers with short and wide gaps. The stacks were carefully withdrawn from the holder and cut into four samples with the help of marking paper (Figure 3-8c). The samples were then placed in a furnace for organic burn off at 600°C with 2°C/min heating rate and sintered at 1120°C with a heating rate and cooling rate of 3°C/min and 5°C/min, respectively. After sintering, side of samples (normal to the planar dimensions) were polished to reveal the inner electrodes and make an electrical connections. Partial surface electrodes (Ag) were pasted and connected to the inner electrodes after firing. The multilayer actuator design is illustrated further in detail in Figure 3-9.

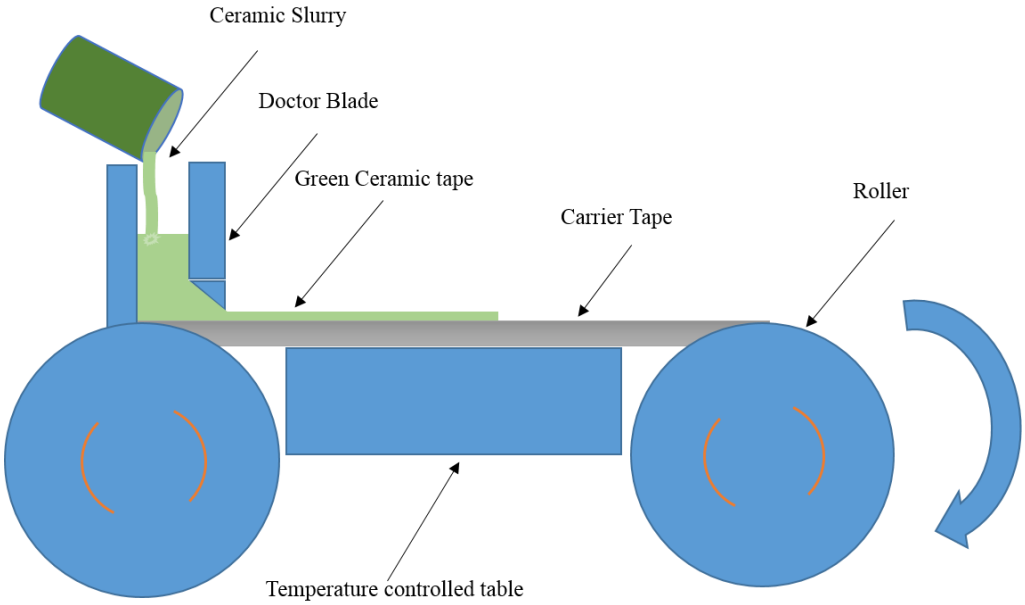

Figure 3-7 Schematic of the tape casting process

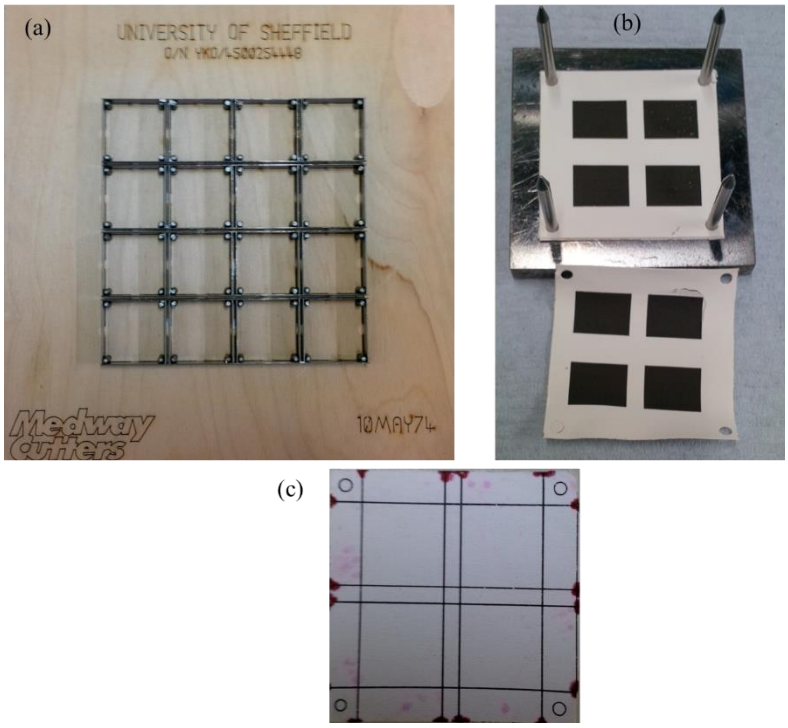

Figure 3-8 (a) Medway Cutters, (b) multilayer stack-holder and (c) marking paper for cutting samples

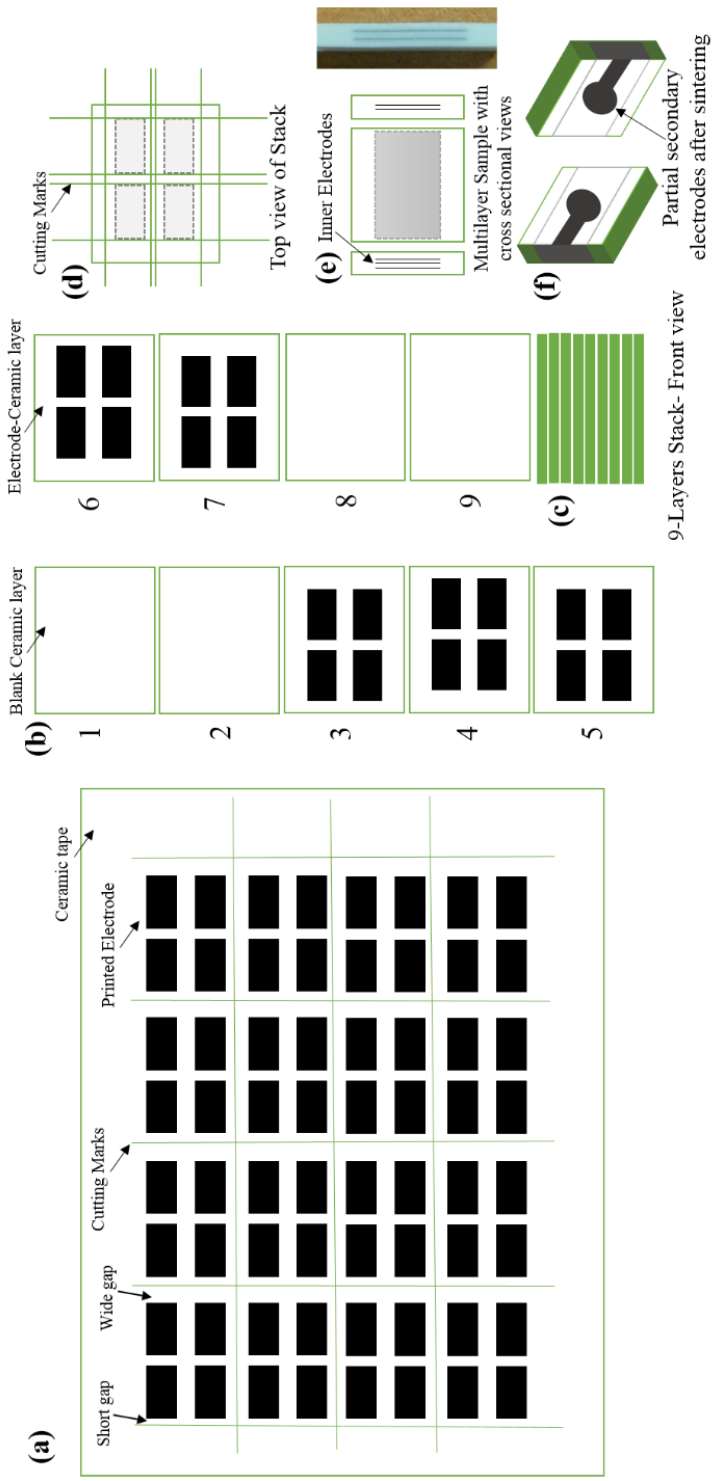

Figure 3-9 Multilayer actuator design: (a) screen printing of inner electrode, (b) stacking procedure, (c) stacking view, (d) sample cutting, (e) cross-sectional inner electrode views with real sample and (f) partial secondary electrode

3.4 XRD Analysis

XRD was used to obtain the phase assemblage and to determine the changes in crystal structure as a function of composition. The phase assemblage and structure were matched and verified using the ICDD-PDF-4^{+} database. XRD traces of calcined powders, sintered pellets and crushed sintered pellets were obtained using a Siemens D500 and Bruker-D2-Phaser diffractometers at 2θ range of 05° – 80°, speed 1°/min, step size .05° using CuKα radiation (λ = 1.5406Å). A schematic of the principles of operation of XRD is shown in Figure 3-10. To calibrate peak positions and to calculate the lattice parameters, Si powder (99% pure, -325 mesh size, Aldrich) was mixed with KNN crushed pellets and calculations were performed using WinX^{Pow} (v2.10). A scan range of 2θ = 05° - 80° with step size 0.02 at 0.1°/min were selected for more precise analysis. The X-ray powder density was also calculated from the obtained lattice parameters.

KNN based powder (calcined powder and crushed pellets) was placed in an Al or polymeric sample holder and levelled with glass slide. If a solid pellet was being studied, it was mounted with the help of putty. Note that the putty was placed completely beneath the pellet to avoid unwanted contributions to the XRD pattern and the surface of the pellet was level with the top edge of the sample holder.

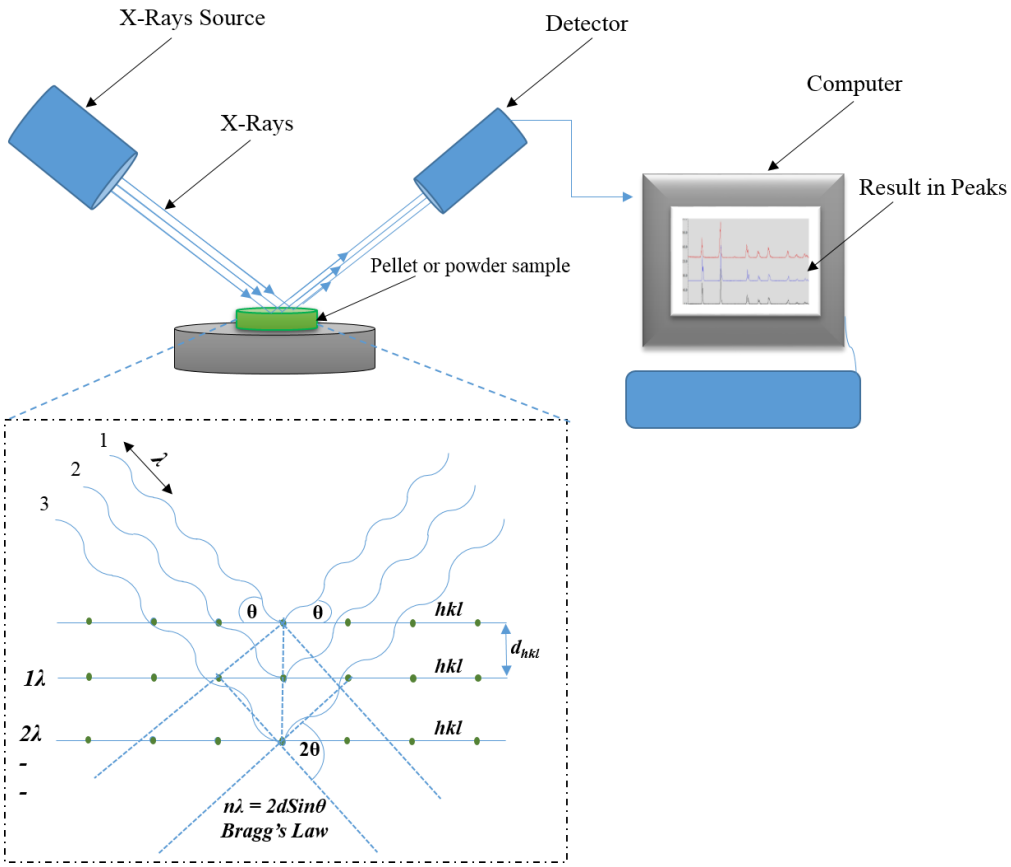

Figure 3-10 Schematic showing the principles of X-ray diffraction.

3.5 LCR (L= Inductance, C= Capacitance and R= Resistance) measurements

The dielectric properties were measured using an LCR meter (Model 4284A, Hewlett Packard). Primary electrodes of Au were pasted on both flat surfaces of the pellet and fired at 800°C. Au electroded pellets were then connected between Pt secondary electrodes to form a capacitor. Samples were placed in a non-inductively wound tube furnace, with extra thermocouples near the pellet for accurate temperature measurements. The LCR meter was connected to a computer through a CP-IB interface and data were collected by software, as schematically illustrated in Figure 3-11. Capacitance and tanδ were measured every 60 seconds in a total of 800 scans, from room temperature to 600°C at 1KHz, 10KHz, 100KHz, 250KHz and 1MHz.

Data were sorted and exported to MS-Excel with capacitance values converted to relative permittivity according equation 3.1,

$$\varepsilon_r = \frac{C}{\varepsilon_0} \cdot \frac{t}{A}, \qquad 3.1$$

where, C = capacitance (F), ε_0 = permittivity of free space (8.85419×10^{-12}F-m^{-1}), t = thickness of pellet without electrode (m) and A = area of the flat surface of the pellet (m^2)

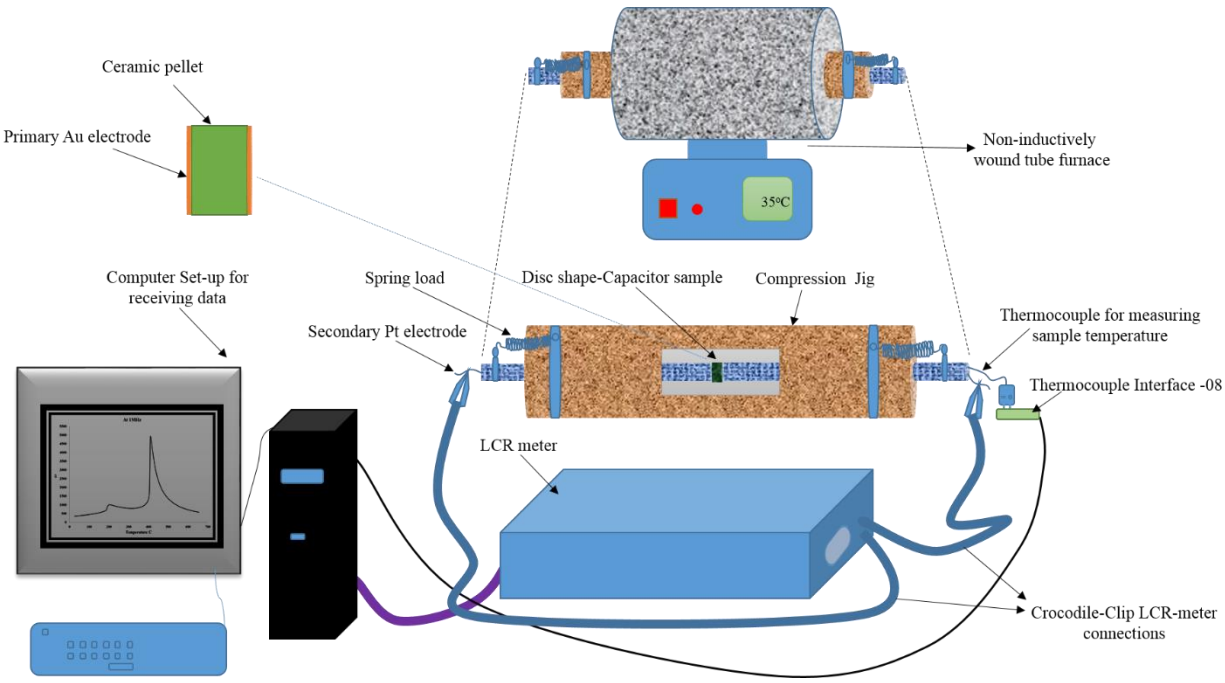

Figure 3-11 Schematic showing the experimental set up for measuring dielectric properties as a function of temperature.

3.6 Impedance Spectroscopy

Impedance has two components; resistive (capacitive) and reactive (inductive). Both can be measured through applying an AC voltage across a sample and standard resistor in series after which the in and out phase components through the sample can

be determined. Dividing the phase components of voltage by the magnitude of the current gives the resistive and reactive components utilised in impedance spectroscopy (IS). IS measurements are commonly performed as a function of frequency over a range of temperatures.[1] The sample and furnace requirement for impedance spectroscopy were the same as discussed in section 3.5. Data were collected using a Solartron SI 1260 impedance/gain-phase analyser operating from room temperature to 600°C and from 10 mHz to 1MHz at 100 mV. The data were corrected using a sample geometry factor and analysed in Z-View software.

From IS theory, insulating regions (Grain Boundary G_b / surface layer) may be differentiated from more semiconducting regions (Grain: G). In this study, semiconduction was induced in the sample either by chemical doping or through oxygen loss when samples are fired under reducing conditions. Each region can be characterised as a single parallel RC element, as shown in Figure 3-12.

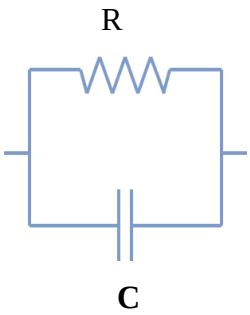

Figure 3-12 Single parallel RC element representing part of the electrical microstructure of a ceramic.

In many electroceramics R_{gb} is >> R_b (e.g. R_b= 20kΩ and R_{gb} = 1MΩ) and each RC element produces an arc in Z* and M* (or a Debye peak in Z" and M'' spectroscopic plots), however, if Z* (and Z" spectra) are dominated by large R, the response is from grain boundaries and if M* (and M'' spectra) are dominated by small C the

response is from bulk grains. In other words, low frequency arcs correspond to the $R_{gb}C_{gb}$ response and high frequency arcs correspond to the R_bC_b response.[2]

3.7 Thermo-Power

Thermopower measurements (Figure 3-13) were performed on 20 mm bar samples to calculate the Seebeck coefficient and to determine the type (*p*- or *n*-type) of semiconduction of KNN sintered in air and in low pO_2. Samples were placed in a ProboStat™. A (NorECs AS) cell (Figure 3-13) was connected to a digital voltmeter (KEITHLEY 182), and the cell retracted a few cm from the centre of the hot zone of a tube furnace to establish a thermal gradient. The voltage (ΔV) was measured using different temperature gradients (ΔT).

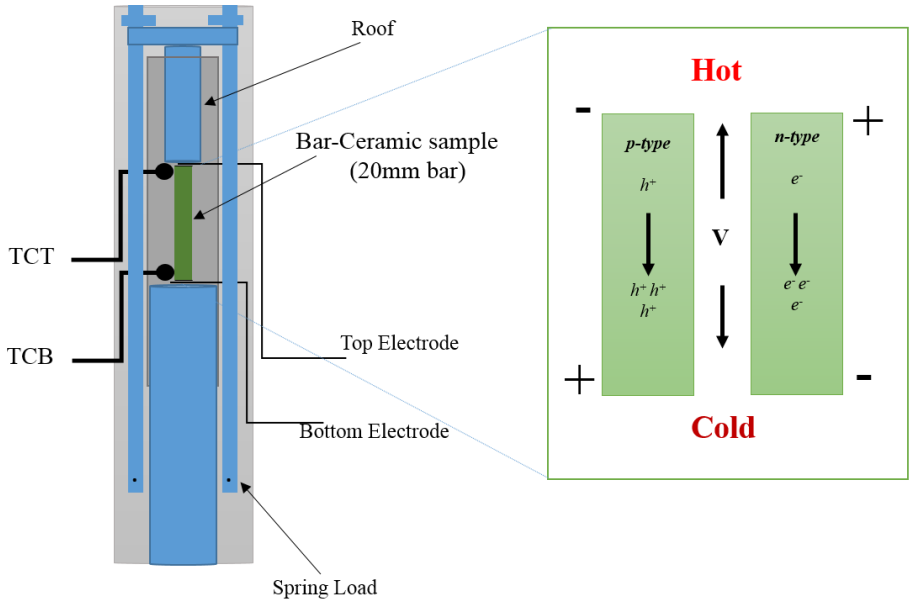

Figure 3-13 Experimental set-up for Seebeck measurement used to determine p-type and n-type semiconduction.

3.9 Ferroelectric Testing

Polarization versus electric field (P-E) loops (Figure 3-14) were obtained using a ferroelectric tester composed of an RT66A signal generator (Radiant Technology,

USA) linked to a high voltage interface (HVI), power box (PB) and a high voltage amplifier (HVA, Trek). Electroded pellets (see section 3.5) were placed in silicone oil between Cu electrodes, as shown in Figure 3-14. The maximum applied field in air sintered pellet was 50 kV/cm and in N_2 sintered pellet 60 kV/cm. The samples of multilayer composition (KNN-BNZ) were tested by using an aix-ACCT TF2000FE-HV ferroelectric test unit (aix-ACCT Inc., Germany), at 'Christian Doppler Laboratory on Advanced Ferroic Oxides', Sheffield Hallam University, Sheffield, UK. Similarly, the sample was put into silicone oil (i.e., good insulator for high voltages) holder coupled with a laser beam interferometer (for recording the displacements in micrometres), where 40 kV/cm field was applied at fixed frequency of 1Hz to collect the data of P-E and S-E at room temperature.

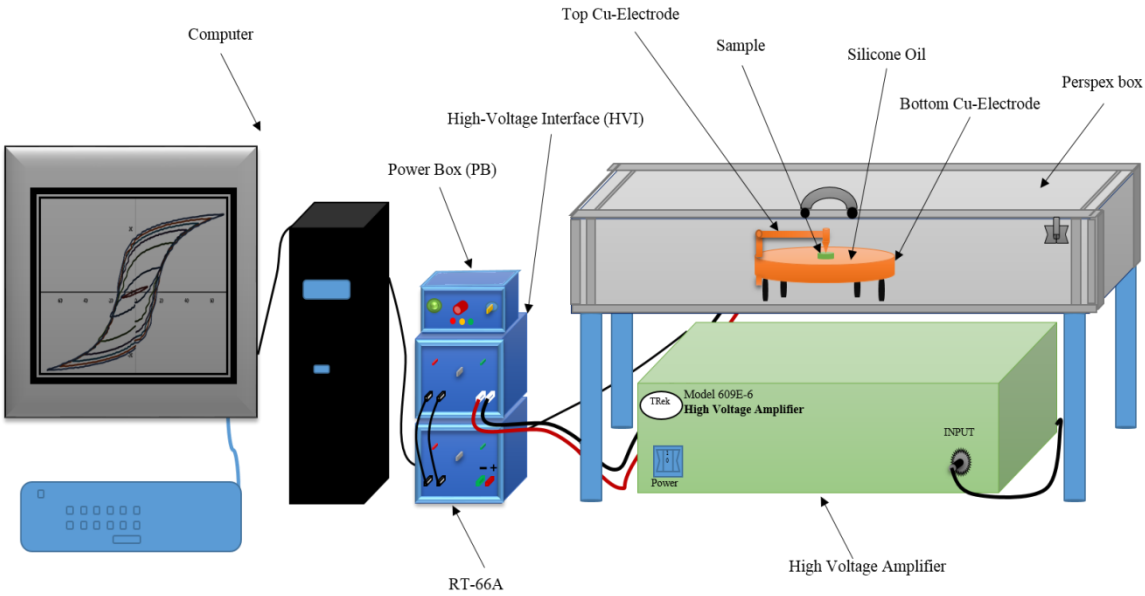

Figure 3-14 Schematic illustration of ferroelectric testing equipment.

3.10 Poling and Piezoelectric Testing

Poling of the electroded thin disc samples was carried out by using a high voltage power supply (Model PS350 / 5000V – 25W, SRS: Stanford Research Systems, Inc.) at 40kV/cm and at 100°C with a 20 minute holding time, followed by cooling to

room temperature under the applied voltage. After poling, d_{33} values were measured by a Piezometer (Piezotest PM300, PiezoMeterSystem), operating at a frequency of 110Hz and at dynamic force of 0.25N.

Poled samples were also tested in the resonant frequency range (Agilent 4295A precision Impedance Analyser) to obtain the piezoelectric electromechanical coupling factor (k_p).[3] The initial frequency range was set as 4 to 10^7Hz over which 800 data points were selected. Long range frequency data was swept in log format and short range in linear. This data was saved in csv. format and analysed in Z-view software. From a narrow range maximum and minimum frequencies of impedance, a k_p factor was calculated according to the procedures described by the British Standard Institution, 2002a. [4]

3.11 Scanning Electron Microscopy (SEM) and Energy Dispersive Spectroscopy (EDS)

Sintered pellets were ground and polished using SiC papers (800 mesh, 1200 mesh) and 6, 3, 1 µm diamond paste respectively then cleaned by acetone and thermally etched for 30 minutes at 10% less than their respective sintering temperatures. To electrically ground the samples, they were mounted on Al stubs with Ag paste, and coated in C. Secondary electron images (20 kV) and EDS analysis were performed on a JEOL SEM Model6400, Tokyo, Japan operating at 20kV with a working distance of ~17.5 mm. Milled powder samples were mounted on Al stubs with double sided carbon tape and Au sputtered to prevent charging.

References

1. Irvine John T. S., S.D.C., West A. R., , *Electroceramics: Characterisation by impedance sepctroscopy.* Advanced Materials, 1990. **2**: p. 132-138.
2. Sinclair, D.C., F. D. Morrison, and A. R. West., *"Applications Of Combined Impedance And Electric Modulus Spectroscopy To Characterise Electroceramics."* Int. Ceram. , 2000. **2**: p. 33-34.
3. Jaffe, B., Cook, W.R.J. and Jaffe, H., *Piezoelectric Ceramics*. 1971, London and New York: Academic Press.
4. Institution, B.S., *Piezoelectric properties of ceramic materials and components*, in *Methods of measurement-Low power*BS EN 50324-2:2002, BSI: London.

Chapter 4 Results and Discussions: Semiconductor behaviour of $K_xNa_{(1-x)}NbO_3$ ($0.49 \leq x \leq 0.51$) as a function of $P(O_2)$

Summary

Potassium Sodium Niobate (KNN) is one of the leading candidates to replace PZT but there are many fundamental science and materials processing issues to be understood before it can be used commercially, including the influence of non-stoichiometry and processing atmosphere on the conduction mechanisms. Consequently, KNN pellets with different K/Na ratios were sintered to 95% relative density in air and N_2 using a conventional mixed oxide route. Oxygen vacancies ($V_O^{\bullet\bullet}$) played a major role in the semi-conduction mechanism in low $P(O_2)$ for all compositions, and impedance spectroscopy and thermo-power data confirmed KNN to be n-type in low $P(O_2)$ in contradiction to previous reports of p-type behaviour.

4.1 Introduction

Piezoelectric ceramics are an important class of functional materials but the majority are based on $Pb(Zr,Ti)O_3$ (PZT). According to European environmental legislation, Pb is toxic and not environmentally friendly. The main contenders for lead-free piezoelectrics are based on $K_{0.5}Na_{0.5}NbO_3$ (KNN) and $Na_{0.5}Bi_{0.5}TiO_3$. The former is advantageous as it is compatible with cheap Ni-based internal electrodes and it is therefore feasible to manufacture low cost KNN multilayer devices provided that properties do not deteriorate in the reducing conditions required to suppress the formation of NiO [1]. One further advantage is that KNN-based ceramics are bio-compatible and thus may be used within the human body for micromotor and sensing applications. [2-4]

Despite its potential importance, there are only a few studies of KNN processed under reducing conditions. Fisher *et al.* (2009) sintered KNN under a range of $P(O_2)$ and noted that the polymorphic transition temperatures ($T_{O\text{-}T}$ & $T_{T\text{-}C}$) decreased as a function of decreasing $P(O_2)$ with similar phenomena reported by Glaister *et al* (1960), DeVries (1960), Hardtl *et al* (1972) and Lee *et al.* (2007) for $BaTiO_3$[5-8]. In each case, the decrease in Curie temperature was attributed to the loss of lattice oxygen with the formation of oxygen vacancies. Nb^{5+} is a d^0 cation and can therefore accommodate the electrons associated with the oxygen loss and consequently KNN has the potential to be an n-type semiconductor in inert and reducing conditions, as described by the defect equation:

$$O_O^x \rightarrow \tfrac{1}{2}O_2\,(g) + V_O^{\bullet\bullet} + 2e' \quad \ldots\ldots\ldots\ldots (1)$$

Kobayashi *et al.* (2012) reported that B-site substituted Li works as an acceptor and consequently reduced KNN-LiF had much higher resistivity than air sintered ceramics which would support this premise [9]. However, many other authors have

claimed KNN exhibits p-type behaviour induced by volatilisation of alkali oxides [5] during processing.[10, 11] This facilitates the uptake of oxygen into the lattice via the oxygen vacancies formed after the volatilisation of the alkali oxides, according to the equation

$$\frac{1}{2}O_{2\,(g)} + V_O^{\bullet\bullet} \rightarrow O_O^{x} + 2h^{\bullet} \quad \ldots\ldots\ldots\ldots (2)$$

If KNN is to replace PZT, dopant strategies are required which can modify its properties in a manner similar to that adopted for 'hard' and 'soft' piezoelectrics. The controversy in the scientific literature over whether KNN exhibits *p* or *n*-type behaviour has for a number of years inhibited research into the development of such dopant strategies. The aim of this paper therefore, is to establish unambiguously the semiconductor behaviour of KNN ceramics as a prelude to modifying its properties via appropriate dopant strategies.

4.2 XRD

XRD traces of crushed KNN pellets calcined/sintered in air and N_2 are shown in Figure 4-1. All major peaks are indexed according to an orthorhombic KNN structure (ICDD card No. 00-032-0822) with a minor peak attributed to a tetragonal tungsten bronze (TTB) structured phase ($K_3Nb_{5.4}O_{15}$, ICDD card No 04-010-8978), present in air but not in N_2 sintered samples. $K_3Nb_{5.4}O_{15}$ has been reported by several workers and to date there are no known processing conditions that completely eliminate this phase. After calibrating and correcting the traces of KNN-50/50_ Air by using an internal Si standard, the lattice parameters, cell volume (V_{cell}) and theoretical density (ρ_{th}) were obtained as a = 5.6510(3) Å, b = 3.9436(11) Å, c = 5.6726(21) Å, V_{cell} = 126.42(6) Å^3 and ρ_{th} = 4.51 g/cm^3, respectively.

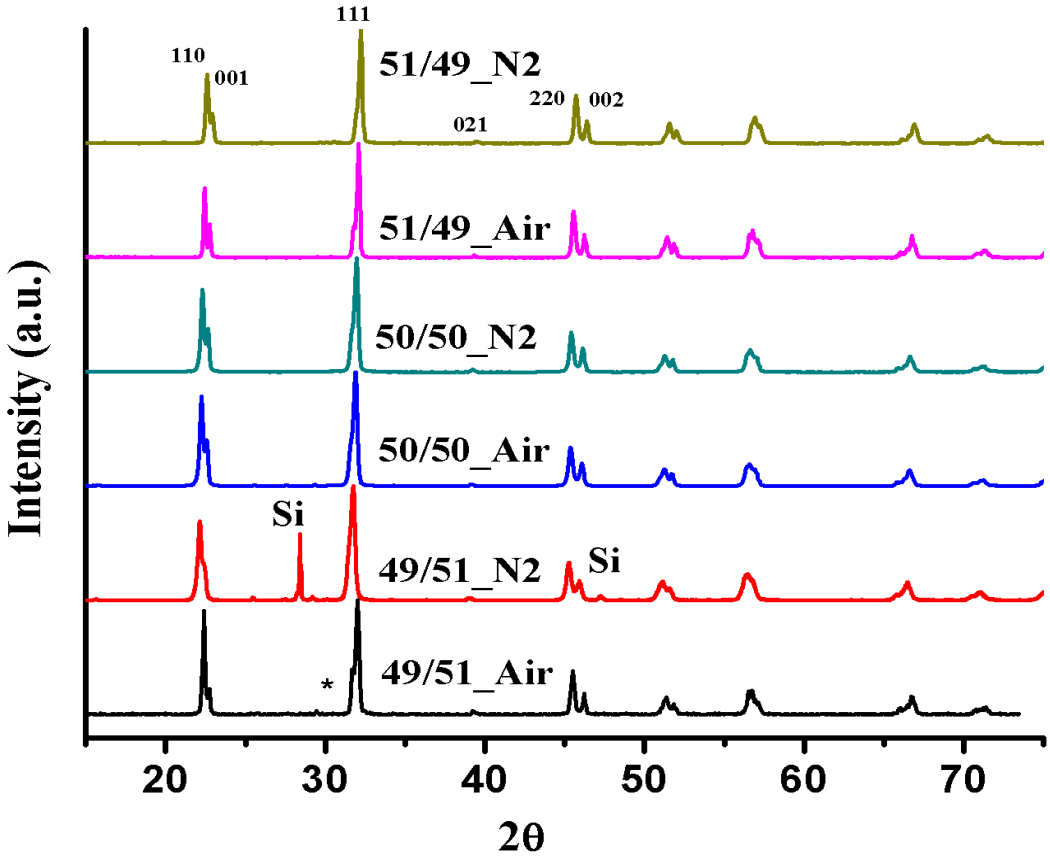

Figure 4-1[4] XRD patterns from sintered KNN samples. * denotes a peak associated with a tetragonal tungsten bronze phase.

4.3 SEM

SEM images of fracture surfaces of air and N_2 sintered KNN compositions are consistent with a relative density > 95 %. The grains of KNN are cubic in morphology as commonly reported by other researchers [12]. In Na-rich samples, a fine grain size was observed (1-3μm) as shown in Figure 4-2, despite this composition (KNN-49/51) being sintered at slightly higher temperature than the others. From the SEM images it appears that Na plays a role of grain-refiner. In polished and thermally etched samples of air sintered KNN-50/50, some large grains are observed which give rise to slightly different EDS spectra than the small grained

[4] Si peak shown in 49/51_N_2 is of internal Si standard used in the sample

matrix, Figure 4-3. It is assumed these larger grains correspond to the TTB phase, recorded in the XRD patterns in Figure 4-1.

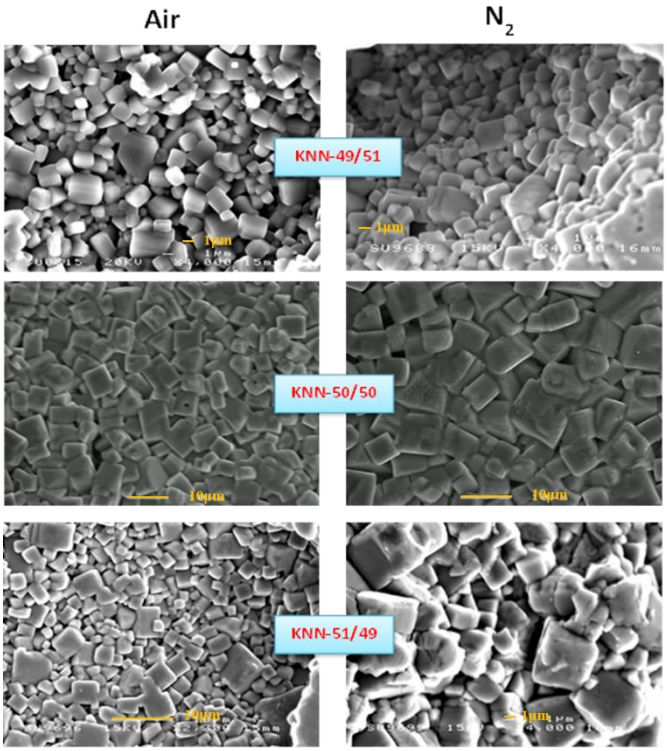

Figure 4-2 SEM images of fracture surfaces of N_2 and air sintered KNN compositions.

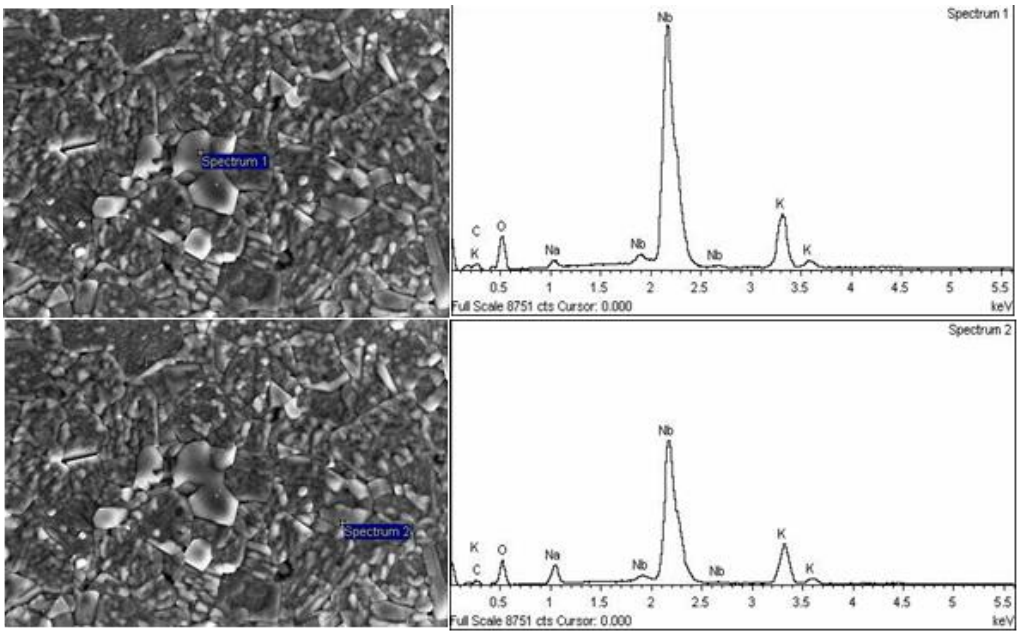

Figure 4-3 EDS spectra of air sintered KNN-50/50.

4.4 Dielectric Properties

Relative permittivity and tanδ vs. temperature relationship obtained at 1 MHz for KNN ceramics sintered in air and N_2 are shown in Figure 4-4. In each sample, two peaks are visible and the transition temperatures T_{O-T} & T_{T-C} are given in the expanded insets. Compared to KNN-51/49, the polymorphic transitions of other compositions are lower in air sintered samples whereas a similar trend is also observed for N_2 sintered ceramics where KNN-50/50 shows the lowest values in both transitions. In the case of the 50/50 ceramics, sintering in low $P(O_2)$ atmosphere, such as N_2, results in a decrease of T_{O-T} & T_{T-C} by ~ 11 and 18 °C, respectively, similar behaviour was also noted in 49/51 and 51/49. In contrast, T_C decreased accordingly, but T_{O-T} transition temperature slightly increased for 49/51 upon sintering in N_2. The decrease in T_C for all compositions may relate to the formation of V_O during sintering in N_2 as discussed by Fisher (2009) for KNN-50/50 [6] and by DeVries (1960) and Lee *et al.* (2007) for $BaTiO_3$. tan δ at room temperature is slightly higher in air/N_2 processed KNN-49/51 and air processed 51/49 formulations as compared to KNN-50/50 (i.e. 0.035-0.04).

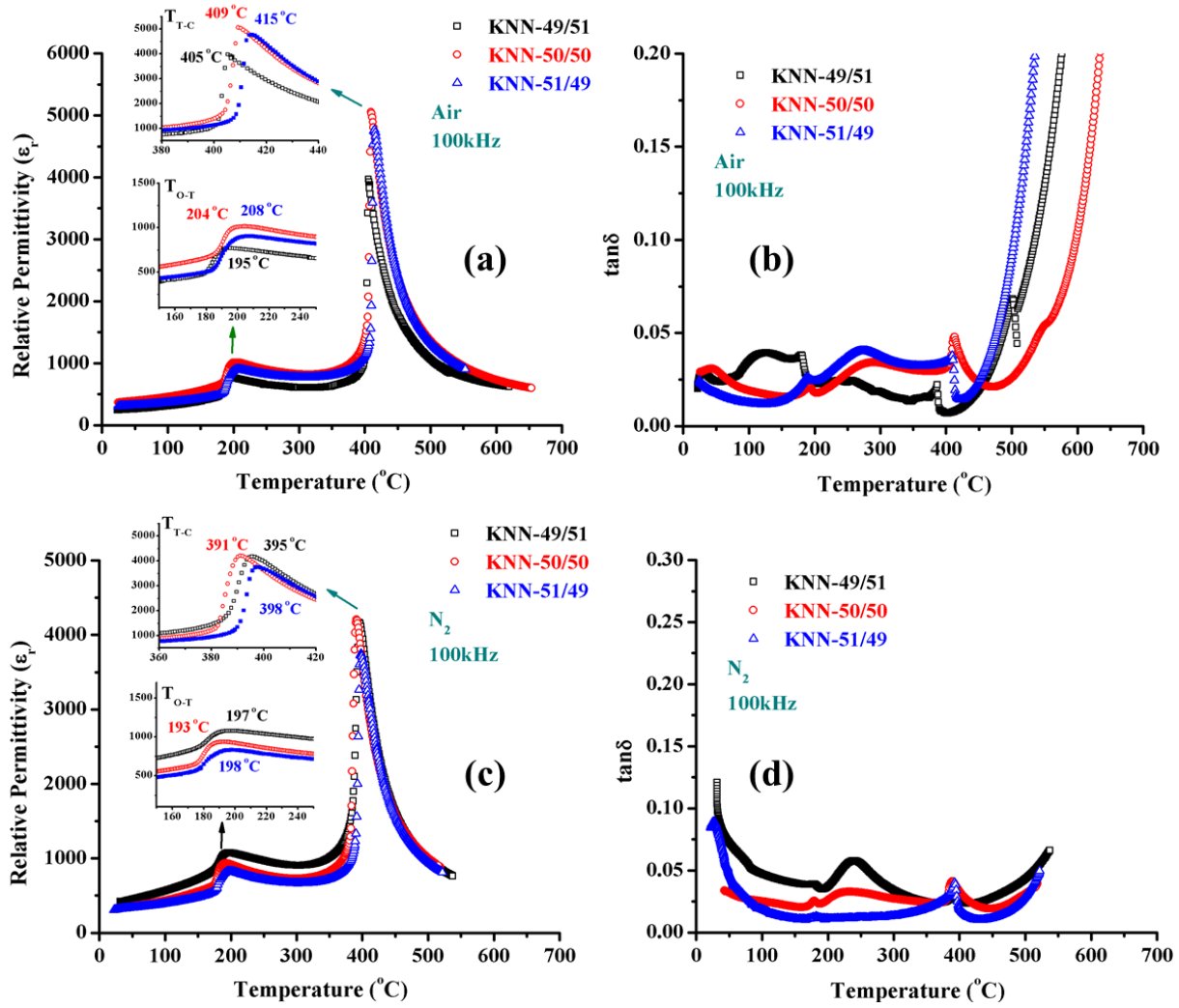

Figure 4-4 (a & c) Temperature dependence of ε_r at 100 kHz of air and N_2 sintered KNN and (b & d) the temperature dependence of tanδ at 100 kHz of air and N_2 sintered KNN, and all transition temperatures are shown in the zoomed insets.

4.4 Impedance Spectroscopy in Air/N_2

Figure 4-5, Figure 4-6, Figure 4-7 and Figure 4-8 show combined spectroscopic plots of M'' and Z'' and complex Z^* plots of air/N_2 sintered KNN within the frequency range from 0.1 Hz to 1 MHz. All KNN samples except one (Figure 4-5 c-d), exhibit single semicircles with single Debye peaks of combined Z'' and M'' spectroscopic plots as a bulk response (R_bC_b) which indicate that these ceramics have a

homogenous electrical microstructure. In contrast, electrical inhomogeneity was seen in N_2 sintered 49/51 (Na-rich) composition as shown in Figure 4-5(c) & (d) where a grain boundary resistance is dominant in the Z'' spectrum with the M'' spectrum showing a high frequency incline, indicating that the bulk (grain) response is much more conductive in this sample. This is in agreement with the higher dielectric loss observed for this sample in Figure 4-4 (d). The Z^* plot shows a single semicircle which corresponds to the more resistive grain boundary response in this sample. [13] Interestingly this response converted into the bulk (grain) when this sample was annealed in ambient air at 650ºC temperature for one day and again in N_2 for one day; as in Figure 4-6 (a-d), although the bulk (grain) response becomes more conductive in N_2 but still looks dominant because the magnitude of M'' is similar in both air/N_2 annealing, Figure 4-6. Consequently, it is proposed that this inhomogeneity is not associated with any cation compositional change but with oxygen vacancies. In comparison, air annealed samples of 49/51_originally sintered in N_2 (Figure 4-6 a-b) are more resistive than purely air sintered sample (Figure 4-5 a-b), for the same temperature.

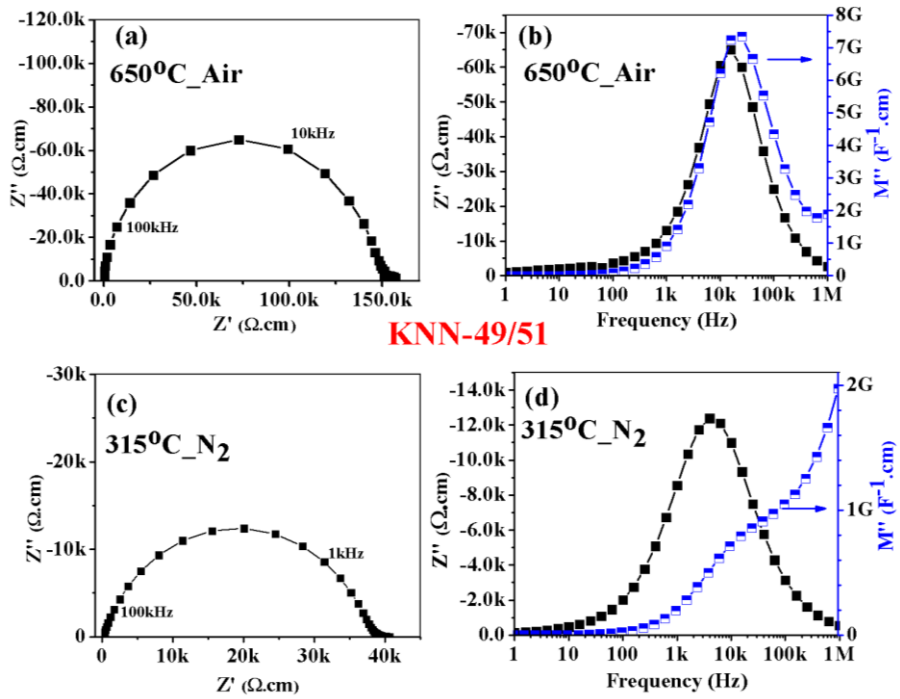

Figure 4-5 Complex impedance plot (Z*) and combined spectroscopic plot of M″ and Z″, of (a-d) KNN-49/51_Air_N_2, respectively over the frequency range 0.1 Hz to 1 MHz.

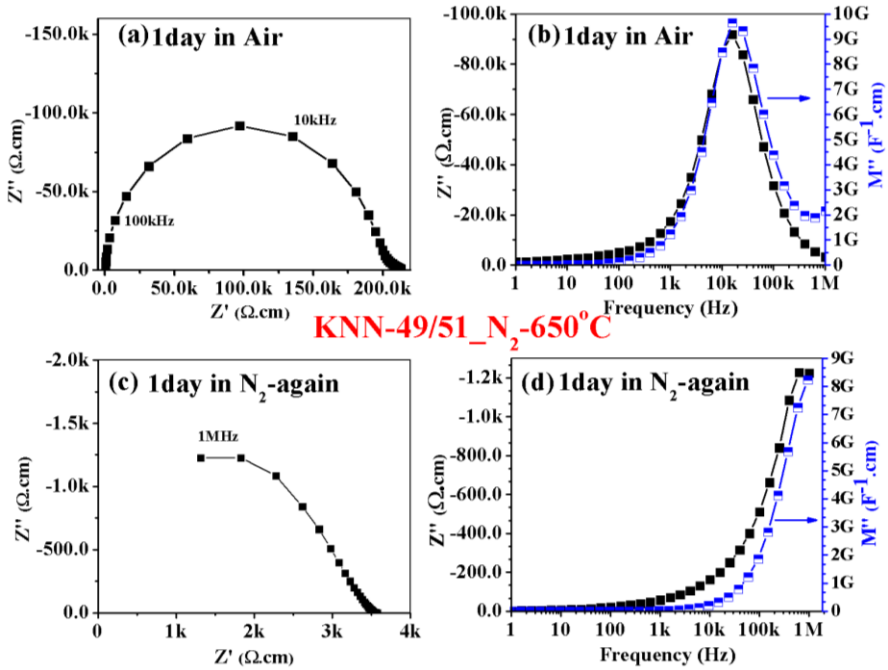

Figure 4-6 Bulk response after annealing in air/N_2 of KNN-49/51_N_2 sintered sample at 650°C.

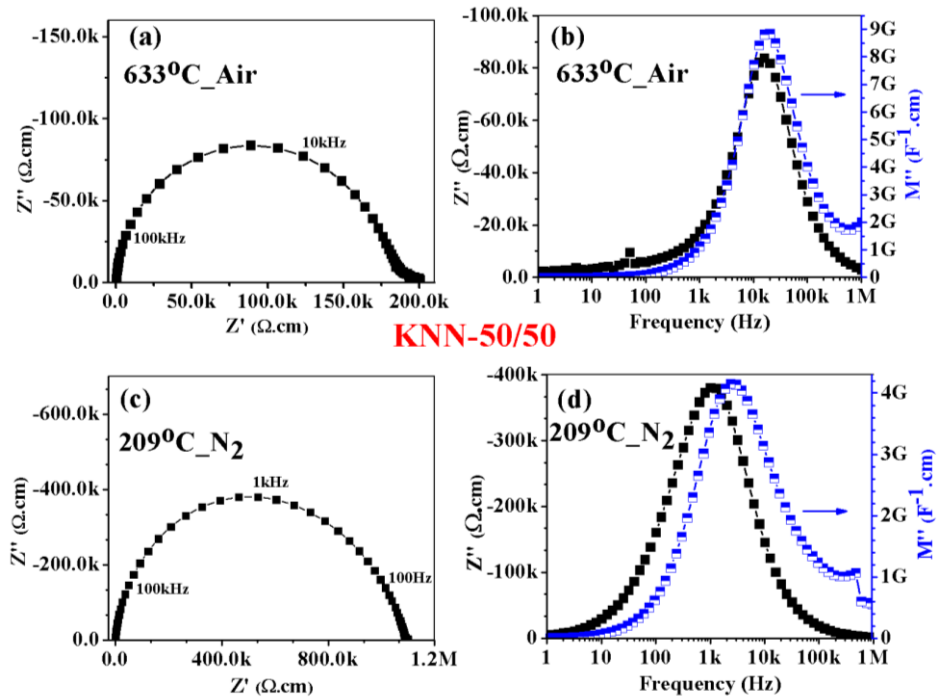

Figure 4-7 Complex impedance plot (Z^*) and combined plot of M'' and Z'', of (a-d) KNN-50/50_Air_N_2, respectively over the frequency range 0.1 Hz to 1 MHz.

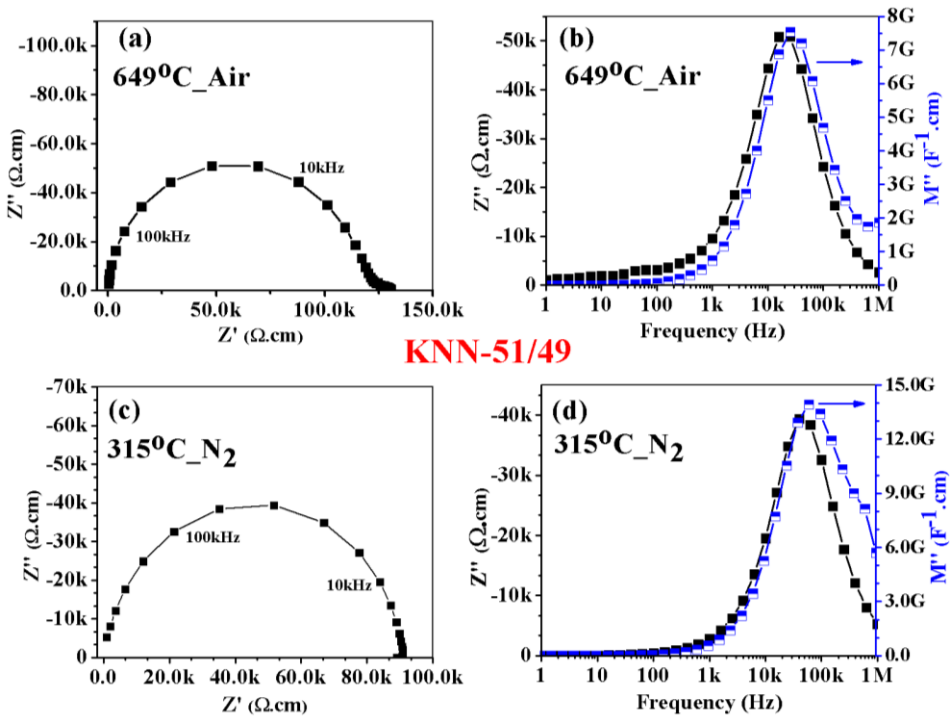

Figure 4-8 Complex impedance plot (Z^*) and combined spectroscopic plot of M'' and Z'', of (a-d) KNN-51/49_Air_N_2, respectively over the frequency range 0.1 Hz to 1 MHz.

Figure 4-9 shows an Arrhenius plot of bulk conductivity vs. temperature for both air and N_2 sintered pellets, where the data were taken from the low frequency intercept of the Z^* plot. As discussed above the conductivity of air sintered samples is lower and the activation energy for conduction is slightly higher than for the N_2 sintered samples.

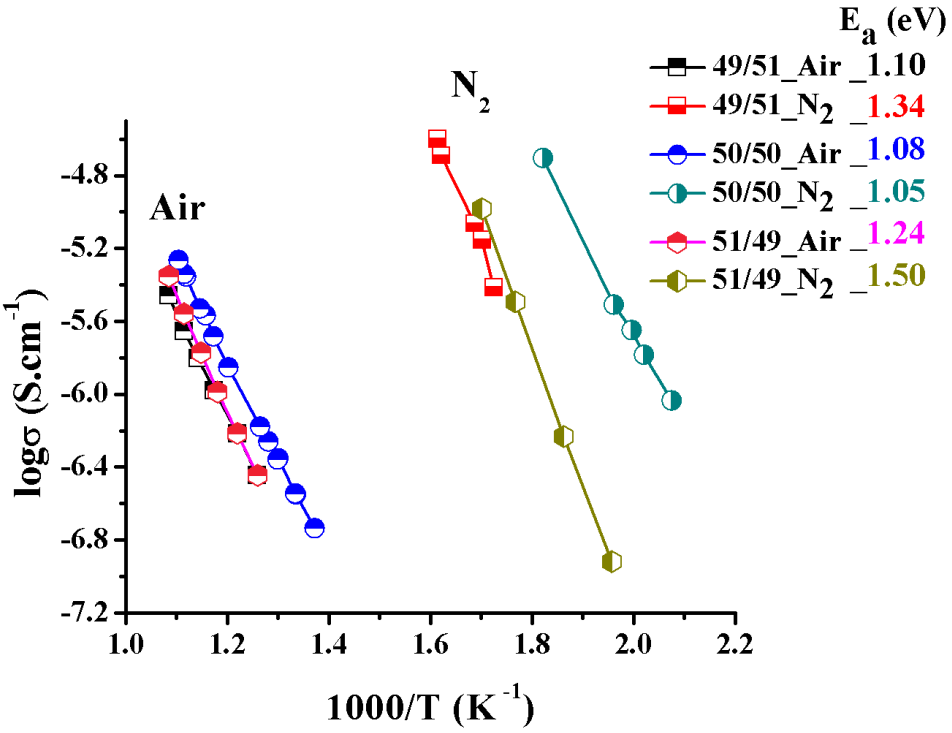

Figure 4-9 Arrhenius plots of various air and N_2 sintered KNN from Impedance Spectroscopy data, inset with activation energy of each ratio.

4.5 p-type and n-type behaviour

Seebeck coefficient (S) is a measure of the potential difference between hot and cold points of a sample, usually a semiconductor. If electrons diffuse from the hot to cold side then a negative S is observed. If holes diffuse from the hot to the cold side then S is positive [14]. This technique therefore, allows comparatively easy differentiation of *p* and *n* type behaviour. S was measured for KNN samples sintered in air and inert conditions. Negative voltages were observed for all samples fired in N_2

irrespective of composition confirming them to be n-type but in contrast positive coefficients and therefore p-type behaviour was observed for all air sintered samples, as shown in Figure 4-10(a-e), where Figure 4-10 (a-b) are plotted from heating data of bar samples and Figure 10 (c-e) from furnace-cooling data of samples. It is interesting to note that the average transition temperature T_{T-C} can also be observed from the S data. Lowest S values were observed at T_{T-C}, which is highly influenced by polymorphic transitions, and this observation is in good agreement with Lee et al. (2009) in their investigation of the phase transitions in $BaTiO_3$ [15]. Here, cooling data show a clear trend if we compare Figure 4-10 (c) and (e) which are from the air sintered samples KNN-50/50 and KNN-51/49, respectively, with the latter composition having the higher Curie temperature. Though these are average temperatures and thus not exactly the same as from LCR measurements (Figure 4-4), lower S values are observed at the transition temperatures. Heating cycles of air fired samples showed consistent data but N_2 sintered samples showed changes in the Seebeck coefficients depending on the number of cycles albeit always n-type. This may be because the thermopower measurements were carried out in air and it is assumed that holding at elevated temperatures affect the concentration of oxygen vacancies in low $p(O_2)$ samples. To test this hypothesis, KNN-50/50-N_2 was heated and cooled down three times in air, with the Seebeck data collected and plotted in Figure 4-10(d). In result, the n-type behaviour associated with sintering in N_2 gradually changes to p-type as the number of heating/cooling cycles increases in air.

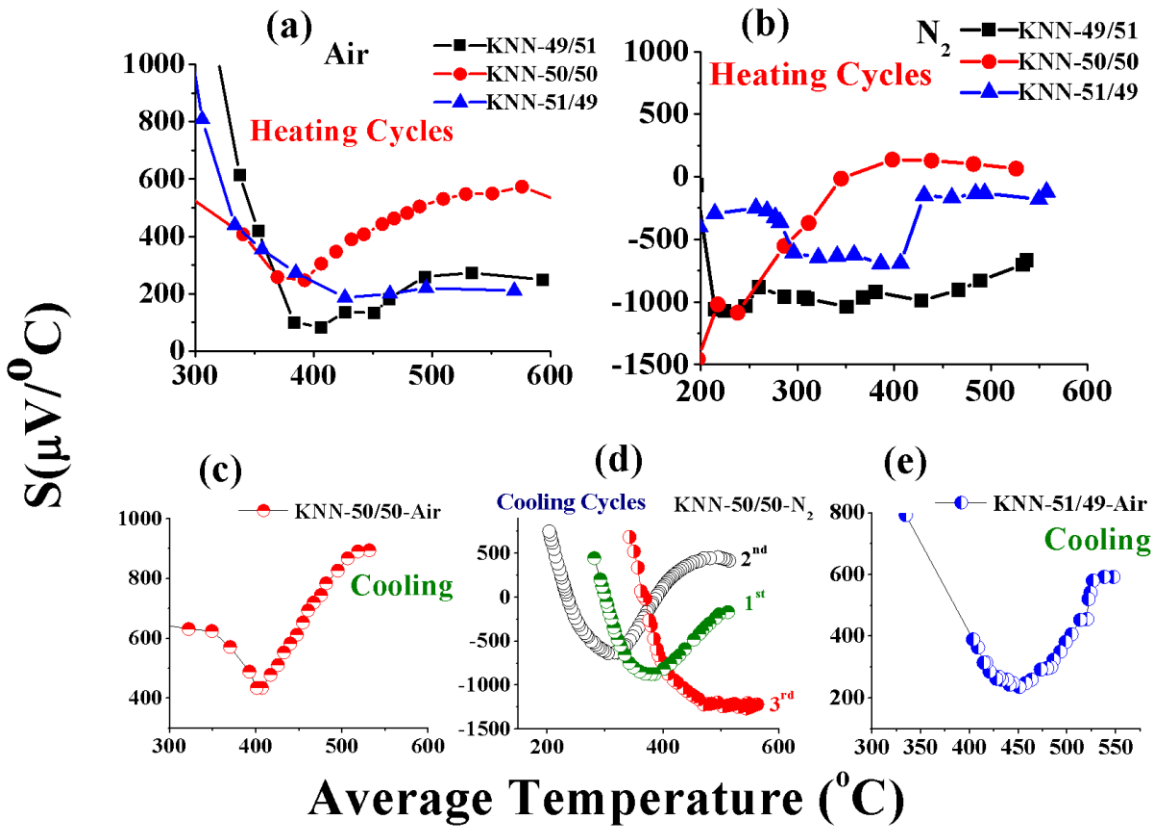

Figure 4-10, p-type vs. n-type behaviour of KNN 50/50 in the form of (top) positive Seebeck coefficient and (bottom) negative Seebeck vs. average temperatures range 300 to 550 ^{0}C, obtained on cooling.

4.6 Functional Properties

4.6.1 Ferroelectric and Piezoelectric

Figure 4-11 shows the polarisation vs. field loops for air and N_2 sintered samples with piezoelectric properties tabulated in Figure 4-12. The remanent polarisation (P_r) is higher in air-sintered samples except for KNN49/51 for which N_2 sintering gives higher P_r and P_{sat}, consistent with enhanced piezoelectric properties, Figure 4-12. In K-rich samples, there is only a slight difference between P_r and the saturation polarisation (P_{sat}) which suggests the leakage current for both compositions is low, consistent with the impedance spectroscopy data. In all samples, the coercive field

(E_c) is higher in N_2 which suggests that N_2 increases the degree of difficulty of polarisation reversal, consistent with the premise that $Nb_{Nb}^{/}$-$V_O^{\bullet\bullet}$-$Nb_{Nb}^{/}$ defect dipoles are present within the samples that pin domains. The preliminary piezoelectric data are shown in Figure 4-12. As expected, d_{33} and k_p values of KNN are higher in K-rich samples with respect to other compositions; this is most probably due to the grain size increase (Figure 4-2) in K-rich samples, in result non-180° domains switching happened easier in large grains, as same phenomenon was reported in the case of PZT.[16, 17]

Many researchers have used CuO and/or MnO dopants in air processed KNN 50/50 and their results showed Cu^{2+} and Mn^{2+} substitute for Nb^{5+} as an acceptor ($Mn/Cu^{///}_{Nb}$). In this case, $V_O^{\bullet\bullet}$ are created to maintain electro-neutrality as in defect equation (1). [18-23] These vacancies and acceptor dopants are considered to create defect dipoles ($Mn/Cu^{///}_{Nb}$ - $V_O^{\bullet\bullet}$) providing a restoring-force that results in harder KNN ferroelectric and piezoelectric properties. The addition of CuO and MnO also results in an increase in conductivity consistent with the formation of V_O.

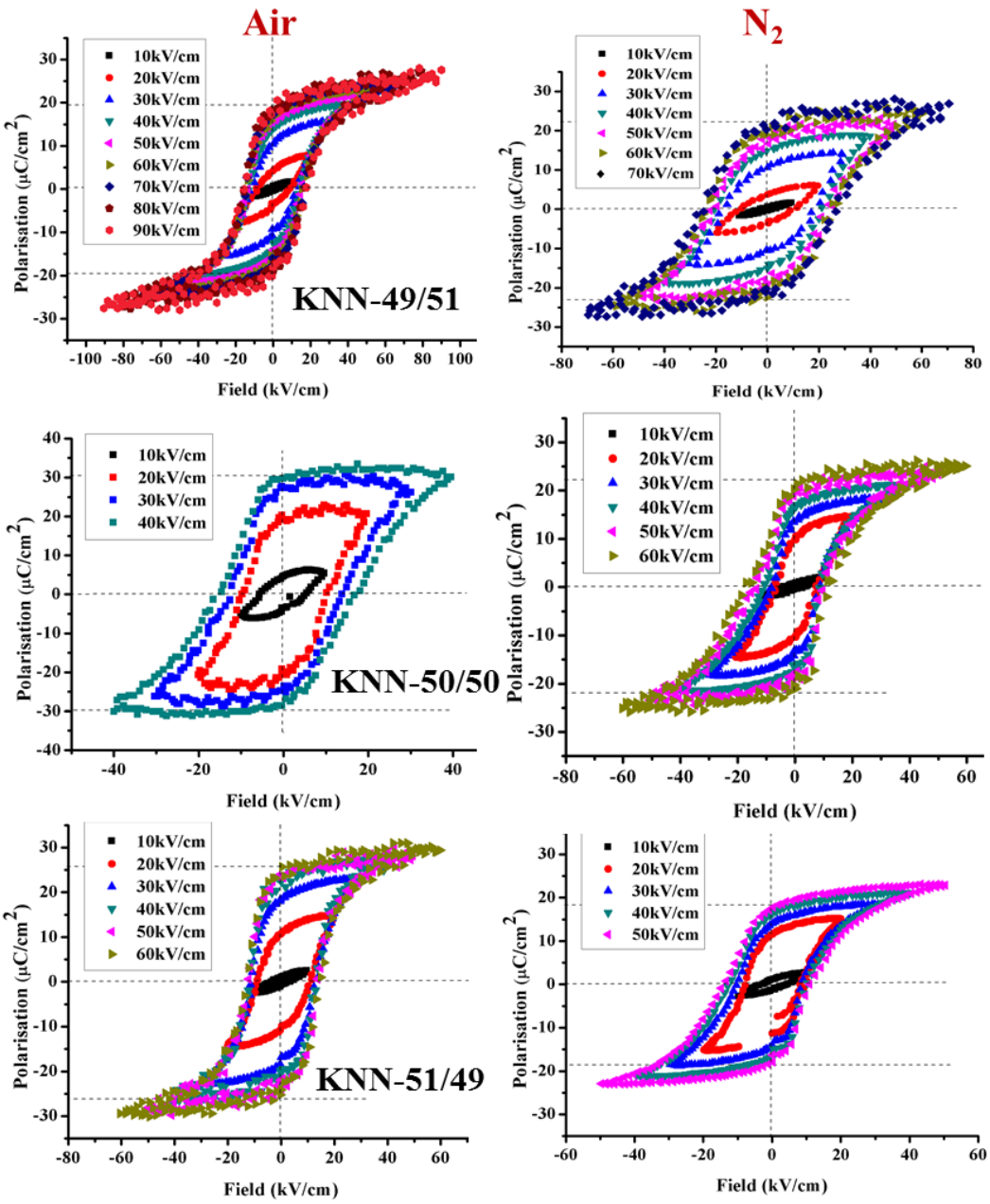

Figure 4-11 P-E hysteresis loops of air and N_2 sintered KNN samples.

Table 2 Ferroelectric key values from Figure 4-11

Sample Name	P_r (μC/cm^2)	P_{sat} (μC/cm^2)	E_c (kV/cm)	Max. Applied Field (kV/cm)
KNN-49/51 Air	19	26	18	90
KNN-49/51 N2	20	27	26	70
KNN-50/50 Air	29	30	17	40
KNN-50/50 N_2	21	25	18	60
KNN-51/49 Air	25	29	12	60
KNN-51/49 N_2	18	23	13	50

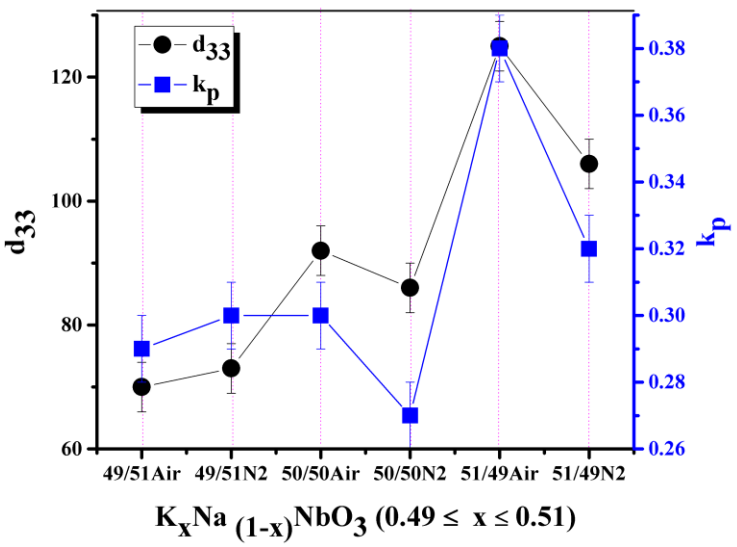

Figure 4-12 Piezoelectric properties of KNN compositions.

4.7 Conclusions

Dense KNN pellets sintered in air and N_2 were fabricated by the conventional mixed oxide route. XRD revealed the structure in all cases to be orthorhombic with Bmm2 symmetry in all ratios. Some weak TTB structured second phase peaks were observed in air but not N_2 sintered samples. Impedance spectroscopy and thermo-power data confirmed KNN was n-type under reducing condition but p-type when fired in air. Conductivities increased in low P (O_2) conditions as a result of oxygen vacancies or free electrons. Higher remanent polarisation and piezoelectric coefficients were observed in air-sintered with respect to N_2-sintered samples.

References

1. Kawada, S., et al., *$(K_{0.5},Na_{0.5})NbO_3$-Based Multilayer Piezoelectric Ceramics with Nickel Inner Electrodes.* Applied Physics Express, 2009. **2**(11): p. 111401.
2. Nilsson K., e.a., *Biocompatible material for implants*, U.S. Patent, Editor 2003, St. Jude Medical AB, Jarfalla (SE): Sweden.
3. Wang Q., J.Y., Wu Zhang, et. al., *Manufacture and Cytotoxicity of a Lead-free Piezoelectric ceramics as a bone substitute.* International Journal of Oral Science, 2009. **1**(2): p. 99-104.
4. Jalalian A., G.A.M., *Biocompatible ferroelectric $(Na,K)NbO_3$ nanofibers.* Applied Physics Letters, 2012. **100**(1).
5. Fisher, J.G. and S.-J.L. Kang, *Microstructural changes in $(K_{0.5}Na_{0.5})NbO_3$ ceramics sintered in various atmospheres.* Journal of the European Ceramic Society, 2009. **29**(12): p. 2581-2588.

6. Fisher, J.G., et al., *Structural changes in potassium sodium niobate ceramics sintered in different atmospheres.* Journal of Alloys and Compounds, 2009. **479**(1-2): p. 467-472.

7. K.H. Hardtl , R.W., *Lowering the Curie temperature in reduced $BaTiO_3$.* Solid State Communications, 1972. **10**: p. 153-157.

8. Glaister R M, K.H.F., *An Investigation of the Cubic-Hexagonal Transition in Barium Titanate.* Proceedings of Physical Society, 1960. **76**(5).

9. Kobayashi, K., et al., *A Route Forwards to Narrow the Performance Gap between PZT and Lead-Free Piezoelectric Ceramic with Low Oxygen Partial Pressure Processed $(Na_{0.5}K_{0.5})NbO_3$.* Journal of the American Ceramic Society, 2012. **95**(9): p. 2928-2933.

10. Tsai, C.-C., et al., *Influence of A-site deficiency on oxygen-vacancy-related dielectric relaxation, electrical and temperature stability properties of CuO-doped NKN-based piezoelectric ceramics.* Ceramics International, 2013. **39**: p. S165-S170.

11. Wang, K. and J.-F. Li, *$(K, Na)NbO_3$-based lead-free piezoceramics: Phase transition, sintering and property enhancement.* Journal of Advanced Ceramics, 2012. **1**(1): p. 24-37.

12. Eriksson, M., et al., *Ferroelectric Domain Structures and Electrical Properties of Fine-Grained Lead-Free Sodium Potassium Niobate Ceramics.* Journal of the American Ceramic Society, 2011. **94**(10): p. 3391-3396.

13. Irvine John T. S., S.D.C., West A. R., , *Electroceramics: Characterisation by impedance sepctroscopy.* Advanced Materials, 1990. **2**: p. 132-138.

14. Kasap, S.O., *Thermoelectric effects in Metals: Thermocouples*, 1997-2001: The department of Electrical Engineering, University of Saskatchewan Canada. p. 01-11.

15. Lee, S., et al., *Thermopower in highly reduced n-type ferroelectric and related perovskite oxides and the role of heterogeneous nonstoichiometry.* Physical Review B, 2009. **79**(13).

16. Xu, F., et al., *Domain wall motion and its contribution to the dielectric and piezoelectric properties of lead zirconate titanate films.* Journal of Applied Physics, 2001. **89**(2): p. 1336.

17. Randall, C.A., et al.,, *Intrinsic and Extrinsic Size Effects in Fine-Grained Morphotropic-Phase-Boundary Lead Zirconate Titanate Ceramics.* Jounal of American Ceramic Society, 1998. **81**(3): p. 677-88.

18. Ebru Mensur Alkoy, A.B.Y., *Electrical properties and impedance spectroscopy of pure and copper-oxide-added potassium sodium niobate ceramics.* IEEE Transactions on Ultrasonics Ferroelectrics and Frequency Control, 2012. **59**(10): p. 2121-2128.

19. Li, E., et al., *Enhancement of Q(m), by co-doping of Li and Cu to potassium sodium niobate lead-free ceramics.* IEEE Transactions on Ultrasonics Ferroelectrics and Frequency Control, 2008. **55**(5): p. 980-987.

20. Körbel, S. and C. Elsässer, *Ab initio and atomistic study of ferroelectricity in copper-doped potassium niobate.* Physical Review B, 2011. **84**(1).

21. Eichel, R.d.-A., et al., *Interactions of defect complexes and domain walls in CuO-doped ferroelectric (K,Na)NbO_3.* Applied Physics Letters, 2013. **102**(24): p. 242908.

22. Alkoy, E.M. and M. Papila, *Microstructural features and electrical properties of copper oxide added potassium sodium niobate ceramics.* Ceramics International, 2010. **36**(6): p. 1921-1927.

23. Azough, F., et al., *Microstructure and piezoelectric properties of CuO added (K, Na, Li)NbO_3 lead-free piezoelectric ceramics.* Journal of the European Ceramic Society, 2011. **31**(4): p. 569-576.

Chapter 5 Results and Discussions: Effect of acceptor, donor, isovalent and co-doping in potassium sodium niobate based ceramics

Summary

B-site doping with Mn^{2+}($Mn_{Nb}^{\prime\prime\prime}$) and Ti^{4+} ($Ti_{Nb}^{\prime}$) dopants prevented KNN from achieving a high relative density while Sn^{4+} was not soluble in the structure as evidenced by second phase peaks in XRD traces. However, SnO_2 was an effective sintering aid in KNN-50/50. A-site doping with Sr^{2+} up to 1 mol% initially improved density but higher sintering temperatures were required for compositions with > 1 mol% Sr. All Sr-doped compositions showed an increase in conductivity, manifested as high values of tanδ and non-saturated hysteresis (1%-Sr). Isovalent doping of Ta^{5+} (Ta_{Nb}^{x}) marginally improved d_{33} at low concentrations but overall no singly doped system showed a significant enhancement in piezoelectricity and most resulted in deterioration. In contrast, stoichiometric co-doping with Bi^{3+} (A-site) and Zr^{4+} (B-site) in KNN-50/50, according to the solid solution, KNN-NBZ, resulted a significant enhancement of d_{33}=315pC/N and k_p =0.45.

5.1 Introduction

This chapter explores a range of acceptor, donor, isovalent and co-doping strategies to in an attempt to improve the properties of potassium sodium niobate (KNN). Previous workers have suggested a number of possible dopants, e.g., Mn^{2+} in KNN was shown to decrease leakage current by Rafiq et al.[1] but most authors have focussed on co-doping. Li and Ta/Sb co-doping results in a significant enhancement of piezoactivity [2-16], with Ta generally giving a lower d_{33} than Sb- doped ceramics. Optimisation appears to be based around lowering the T-O transition

temperature which presumably facilitates greater movement of non-180° domain walls. [17, 18]. More recently, co-doped compositions based on (1-x)$(K_{0.50}Na_{0.5})NbO_3$ – x$(Bi_{0.50}Na_{0.50})ZrO_3$ (KNN-BNZ) have been initiated through Wang et al., [19]. For $0.01 \leq x \geq 0.06$, there is a significant enhancement of d_{33} (>300 pC/N) based on the development of a reputed MPB between rhombohedral (R) and T phases. This chapter explores a range of aliovalent and isovalent dopants culminating in an investigation and optimisation of the co-doped composition, KNN-BNZ.

5.2 Characterisation

5.2.1 XRD of doped KNN compositions

The XRD traces from KNN-50/50 doped on the B-site with Mn^{2+}, Ti^{4+} and Sn^{4+} are shown in Figure 5-1 and Figure 5-2. The XRD traces from KNN-50/50 doped with 1% Mn and 1% Ti both look similar, but the shape of 2θ=45° {220} and {002} peaks shows a slight difference, Figure 5-1. In both cases the intensity of the 2θ=32° {111}is lower [19] than that of undoped KNN. Increasing the concentration of Ti to 5% Ti emphasised the structural change observed at 1% Ti. There are few studies on singly Mn acceptor dopant in KNN. Peaks shifting towards higher 2θ is evidence of shrinkage in lattice volume, which took place for Mn^{2+} [1] and Ti^{4+} acceptor dopants as compared to undoped KNN peak (shown in Figure 5-4; 2θ=45-46°). Conversely, Lin et al. reported that XRD peaks shifted towards lower 2θ (i.e., expansion in the lattice volume) in the case of Mn^{4+} doped KNN. [19]

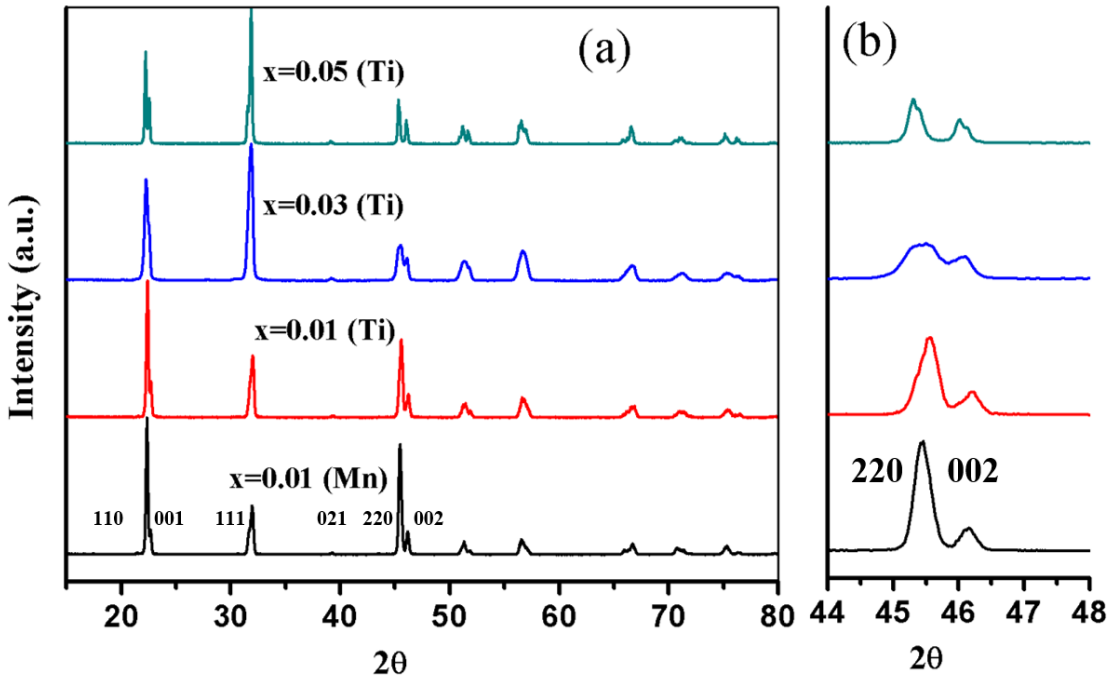

Figure 5-1 (a) Single phase XRD patterns of Mn and Ti doped KNN-50/50, (b) zoomed peaks at 2θ ~ 45-46

For KNN-50/50 doped with Sn^{4+}, secondary peaks of SnO_2 are visible in Figure 5-2. Moreover, within the resolution limits of in-house XRD, there was no discernible change in the trace of the major KNN peaks, confirming that Sn does not enter into solid solution with KNN. Su, S et al. 2010 [20], incorporated SnO_2 with CuO co-doping in KNN and concluded that Sn^{4+} was not soluble after 1mol%. Their XRD traces also depicted secondary peak positions similar to those in this study. Akca, E, et al. 2014 [21] also reported insolubility issues for Sn^{4+} in KNN with secondary peaks visible in their XRD data. The reasons behind the insolubility of Sn^{4+} issues in KNN is unclear, since Sn^{4+} (0.69 Å) has a similar ionic radius to Nb^{5+} (0.68 Å).[22] However, Sn^{4+} is more covalently bonded to O than Nb^{5+} which may influence its solubility.[23, 24]

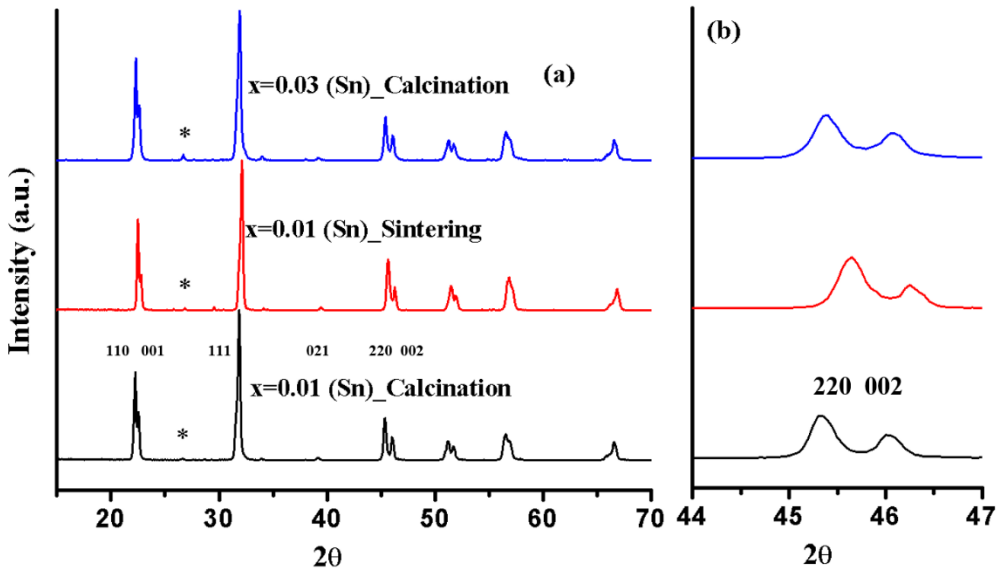

Figure 5-2 XRD patterns of Sn doped KNN-50/50, (b) zoomed peak at 2θ ~45-46

For KNN-50/50 doped with Sr^{2+} on the A-site, the XRD traces revealed broadening of the {111} peaks as a function of x with respect to undoped KNN-50/50 when fired in both air and N_2, Figure 5-3 and Figure 5-4, indicating that Sr^{2+} was incorporated within the KNN lattice.

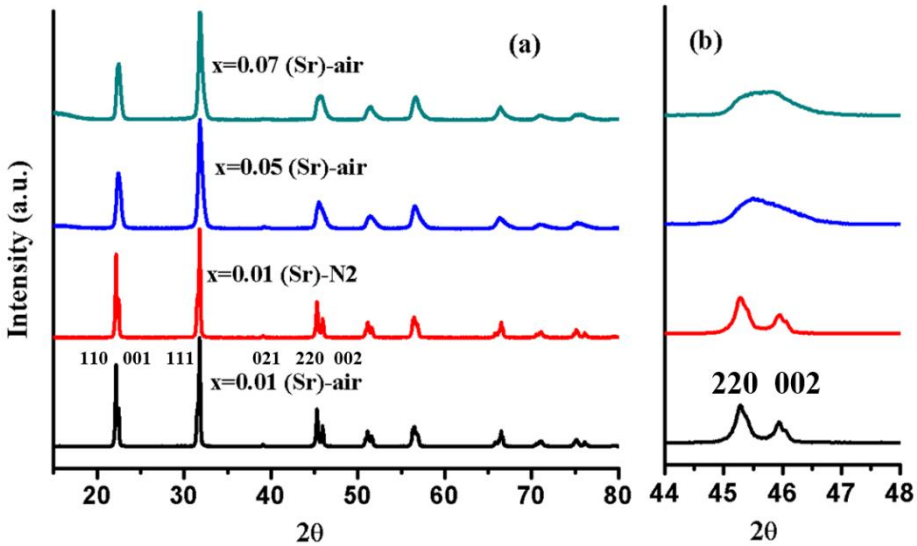

Figure 5-3 X-ray diffraction data of Sr doped KNN-50/50, (b) zoomed peak at 2θ ~ 45-46

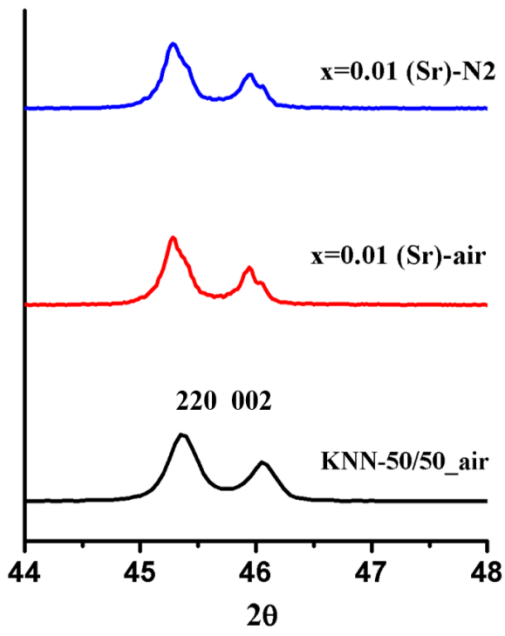

Figure 5-4 Zoomed peak at 2θ ~ 45-46, in comparision the peak shape of 1%Sr_air/N_2 with KNN_50/50_air

Figure 5-5 shows the XRD patterns from isovalent doped compositions $K_{.51}Na_{.49}Nb_{1-x}Ta_xO_3$ ($0.05 \leq x \leq 0.30$). All isovalent doped compositions were single phase within the detection limits of in-house diffractometers. This composition exhibited an O-T transition at x = 0.3 as illustrated by splitting of the 2θ ~ 45°, {220} and {002} peaks zoomed in Figure 5-5(b).

The XRD result of sintered samples of co-doped KNN-BNZ are shown in Figure 5-6. All traces showed single phase perovskite in the range of 2θ=15° to 80°. A transition from a room temperature O to T structure occurs at ~x=0.05. It is reported that for values of x≥0.05, an MPB is present between R and T phase. [25] However, a possible alternative explanation is that the stoichiometric substitution of BNZ into KNN results in a 'pinch point' at which the T_{R-O} and T_{O-T} transitions become coincident, in a similar way to Zr-doping in $BaTiO_3$.[26-29] One aspect of the definition of an MPB is that it is temperature independent but most authors report changes in structure and a permittivity peak at around 100°C in these compositions,

suggesting that the phase boundary is temperature dependent and thus not a true MPB. [30, 31]

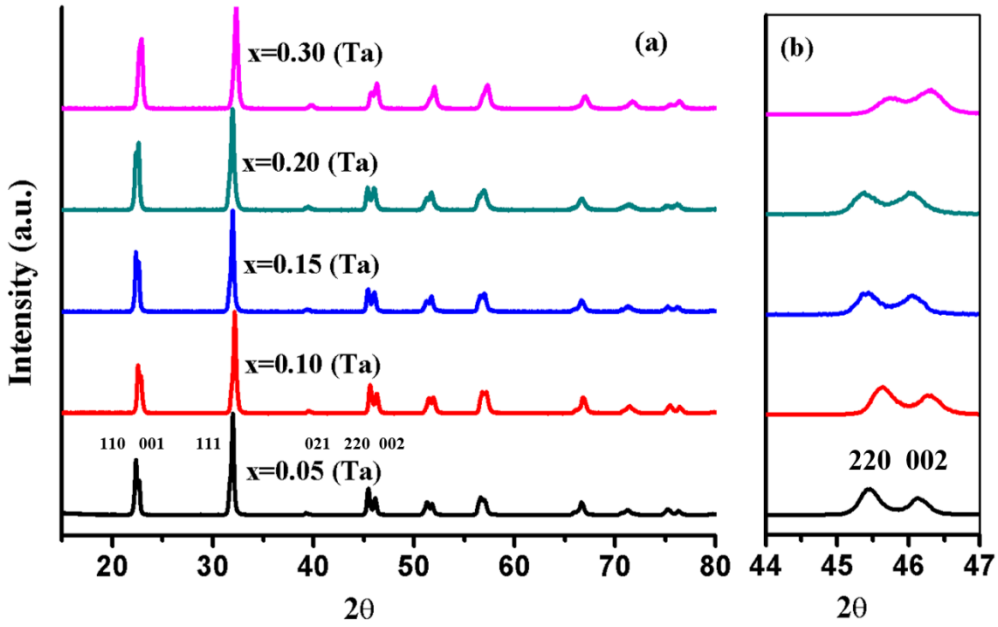

Figure 5-5 Single phase XRD patterns of Ta doped KNN-51/49, (b) zoomed peak at 2θ ~ 45-46

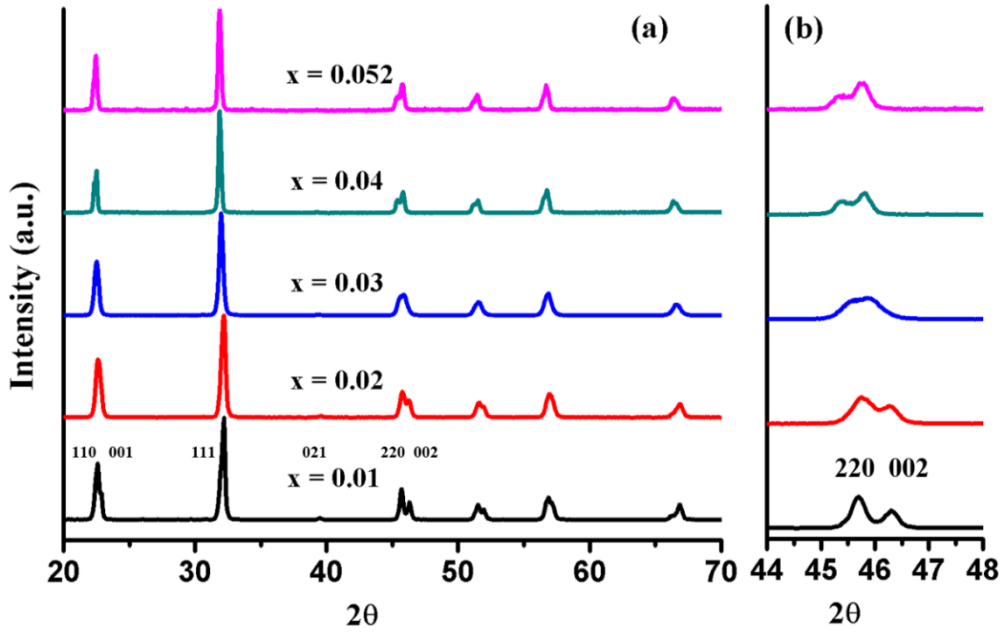

Figure 5-6 Single phase XRD patterns of KNN-50/50-BNZ, (b) zoomed peak at 2θ ~ 45-46

5.2.2 Scanning Electron Microscopy of doped compositions

In comparison to un-doped KNN, the grain morphology of KNN-NBZ remained similar all compositions of KNN, Figure 5-7, with all compositions revealing densely packed arrangement of grains consistent with a relative density >95% of theoretical. Figure 5-7(e) (x=0.05.2) shows some evidence of liquid phase sintering with higher Bi concentration with many grains appearing fused but overall the average grain size is smaller for doped with respect to undoped compositions.

SEM images from Ta-doped KNN-51/49 are shown in Figure 5-8. The grains are densely merged together perhaps through liquid phase sintering for low Ta concentrations but for x = ≥ 0.20 a cuboid grain morphology was observed implying that the more refractory Ta_2O_5 with respect to Nb_2O_5 was favouring a solid rather than liquid state reaction. (Figure 5-8). It is worth noting that intragranular cubic pores (~1µm) are observed in x = 0.15 and 0.2, bottom part of Figure 5-8.

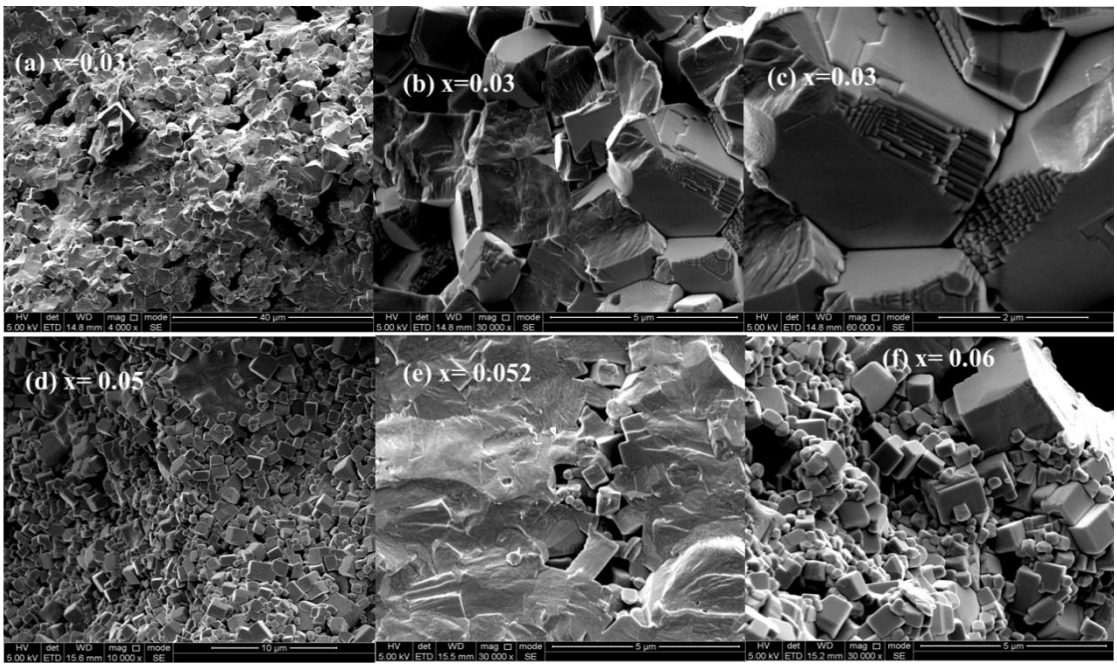

Figure 5-7 Fracture surface images of KNN-NBZ taken by SEM, (a-c) x=0.03 & (d-f) x=0.05, x=0.052 and x=0.06 respectively; at different magnification for grain morphology

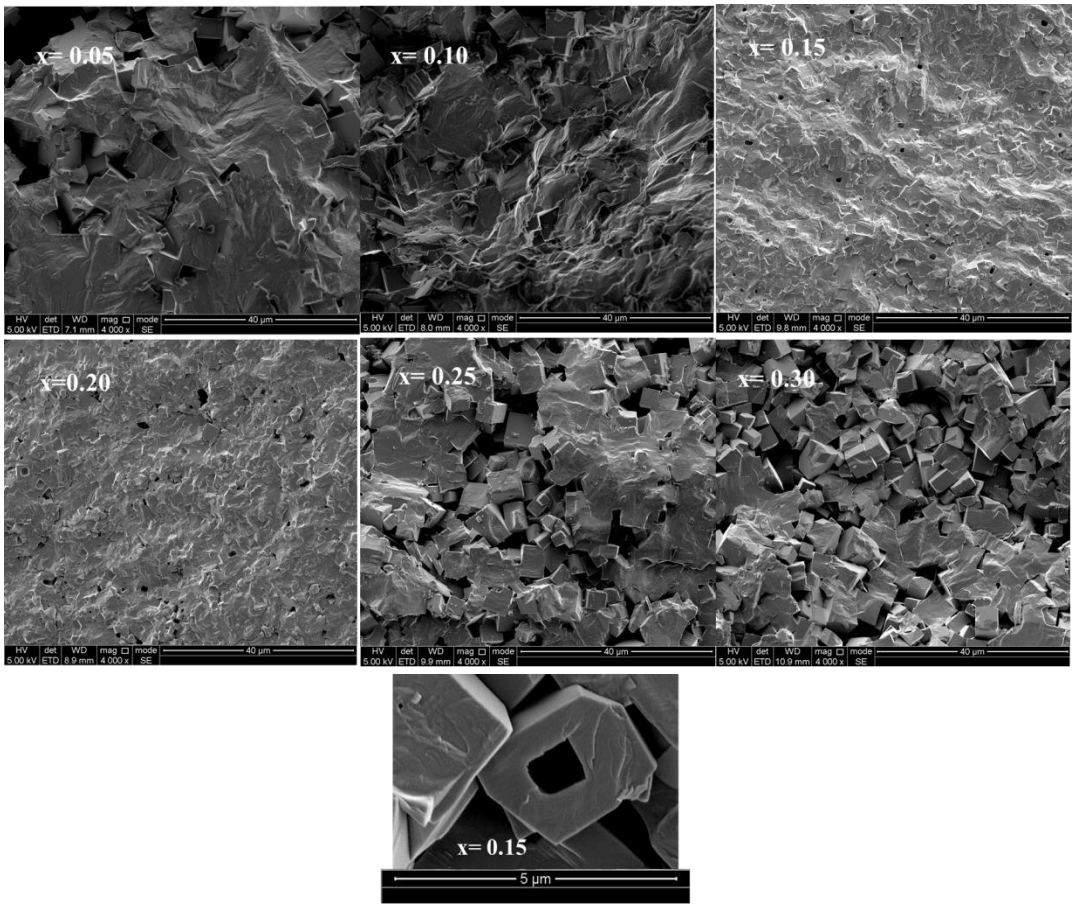

Figure 5-8 SEM images of Ta_doped KNN-51/49. A single is grain shown in the bottom image.

5.2.3 Dielectric Properties

5.2.3.1 Acceptor dopants: Mn^{2+}, Ti^{4+} and Sn^{4+}

The temperature dependence of relative permittivity and tanδ of 1 mole% Mn doped KNN-50/50 are shown in Figure 5-9 (a-b) as a function of temperature and frequency. Two transitions, i.e., T_{O-T} and T_{T-C} are clearly presented, though both transitions are shifted towards lower temperature compared to undoped KNN-50/50 sintered in air. The ε_r and tanδ at room temperature of 1%Mn doped KNN-50/50 were 380 and 0.05, respectively, at 100 kHz. However, at lower frequency the dielectric losses increased dramatically with increasing the temperature. The most likely cause of the loss relates to V_O formed according to the defect equation:

$$Mn_{Nb}''' \equiv 3/2V_O^{\bullet\bullet}$$

At high frequency (1MHz) tanδ is suppressed with acceptor Mn^{2+} dopant. At these frequencies the loss mechanism relating to V_O may clamp out, resulting a decrease in the overall dielectric loss. There are number of potential loss mechanisms relating to V_O such as rotation of defect dipoles and movement of space charge. It is not known which mechanism dominates in this study.

The dielectric properties of Ti doped KNN-50/50 are shown in Figure 5-9(c-d). For low concentrations, 1%, the T_{T-C} temperature decreases with little change in T_{O-T}. However, for high concentrations, T_{T-C} phase transition temperatures increased and T_{O-T} decreased compared to the undoped and 1% Ti doped compositions and the phase transitions become broader. The peak in permittivity at around room temperature in 3% and 5% Ti doped KNN, may relate to the observation of minor changes to the shape of some XRD peaks (at {220} and {002} planes) (Figure 5-1).

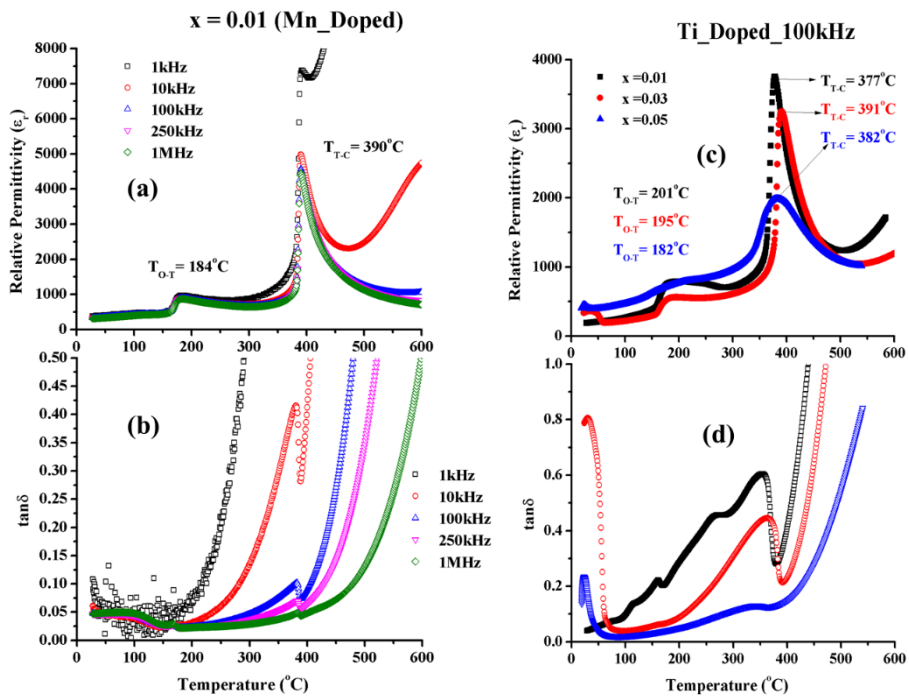

Figure 5-9 (a) ε_r versus temperature of Mn doped KNN and (b) tanδ; (c) ε_r versus temperature of Ti doped KNN compositions and its (d) tanδ,

The dielectric properties of Sn^{4+} doped KNN are shown in Figure 5-10 (a-b). Unsurprisingly, there was no effect on dielectric properties with respect to undoped compositions since there was no evidence that Sn^{4+} enters the KNN lattice.

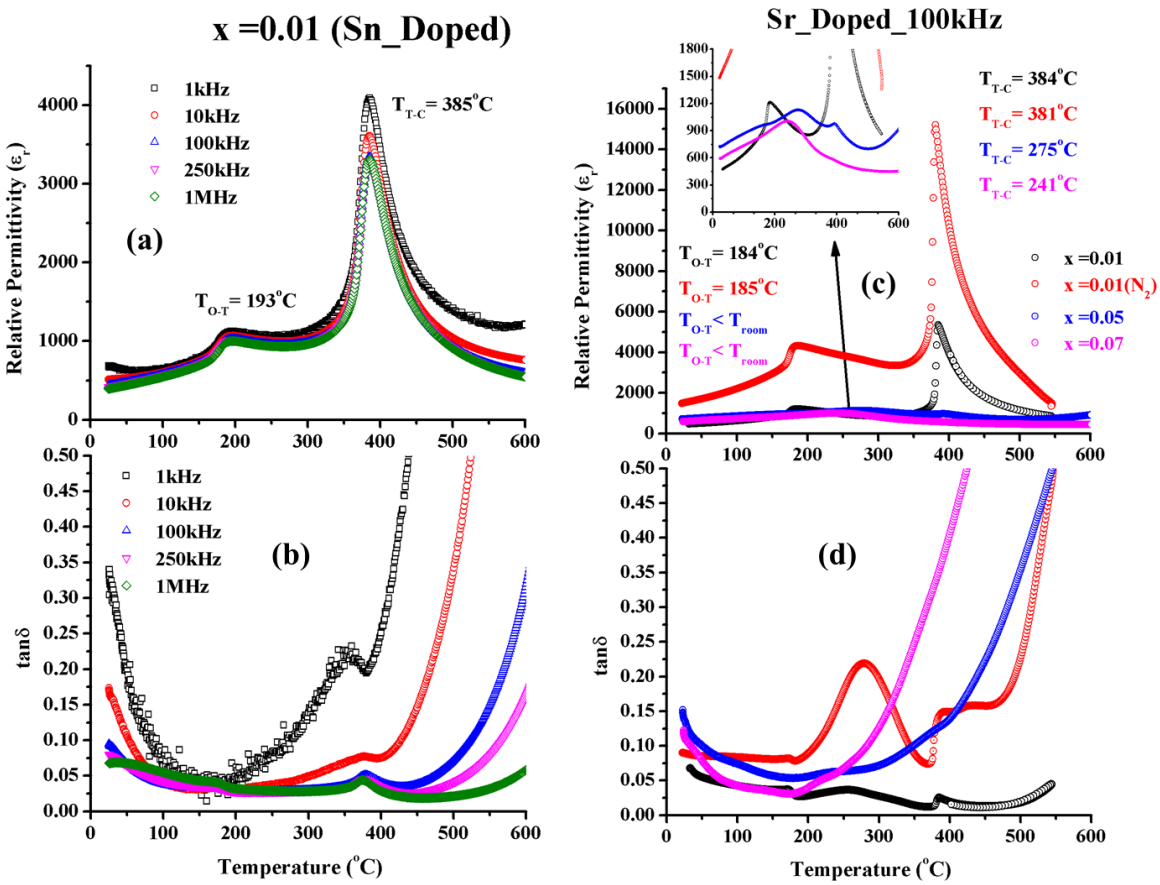

Figure 5-10 (a) ε_r verses temperature of Sn doped KNN and its (b) tanδ; (c) ε_r verses temperature of Sr doped KNN compositions and its (d) tanδ.

5.2.3.2 Donor Dopant (Sr^{2+})

Dielectric properties of Sr donor dopant (A-site) in KNN-50/50 are presented in Figure 5-10 (c-d). 1% Sr doped KNN-50/50 compositions were sintered in both air and N_2 to compare the behaviour with undoped in Chapter 4 and acceptor doped compositions in the previous sections. However for undoped KNN sintered in N_2, the transition temperature decreased in agreement with 1% Sr doped KNN (N_2). N_2 sintered Sr^{2+} KNN becomes more conductive as compared to undoped KNN,

presumably because Sr^{2+} donates extra electrons ($h^{\bullet}$) and low pO_2 creates $V_O^{\bullet\bullet}$. It is proposed that the increase in conductivity contributes to the larger permittivity for N_2 sintered KNN-1Sr. T_{T-C} with acceptor (Mn^{2+}) and donor (Sr^{2+}) in air are 390°C and 384°C, respectively, which suggests that disruption of ferroelectric order to reduce T_{T-C} is greater for A-site Sr^{2+} doping in comparison to B-site Mn^{2+}.

At higher Sr concentrations, x = 0.05 and 0.07, the phase transitions broaden in temperature (inset of Figure 5-10 c), consistent with broadening of peaks in the XRD traces (Figure 5-3). In addition, the dielectric loss increased with samples becoming more conductive, resulting in an inability to pole ceramics for piezoelectric measurements.

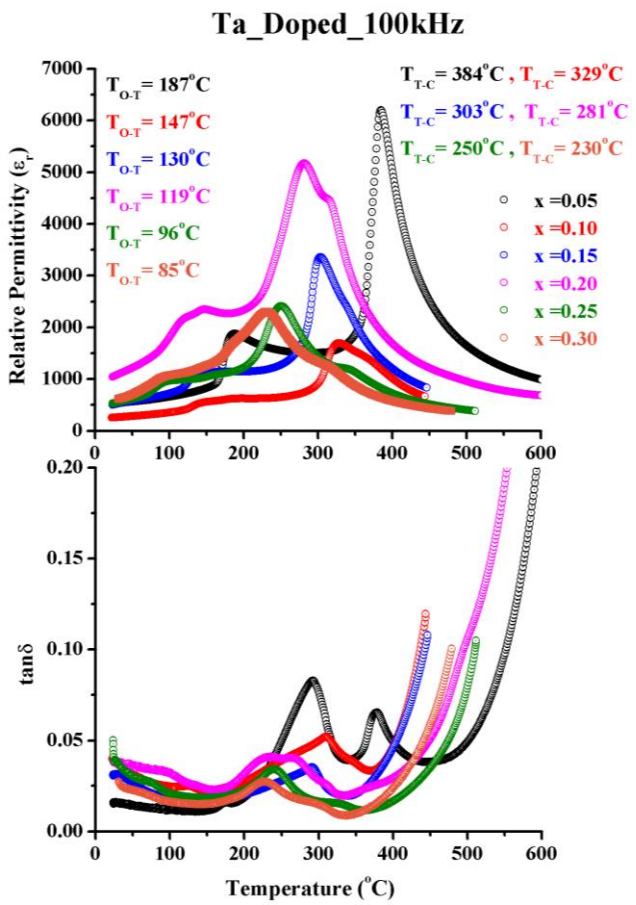

Figure 5-11 Comparison of ε_r and its tanδ verses temperature of different Ta doped KNN-51/49 compounds at 100 kHz

5.2.3.3 Iso-valent (Ta^{5+} doped)

Figure 5-11 illustrates dielectric properties of $K_{0.51}Na_{0.49}Ta_xNb_{1-x}O_3$ for x= 0.05, 0.10, 0.15, 0.20, 0.25 and 0.30) or $K_{0.51}$NNT at 100 kHz, and measured up to 600°C. For compositions with x > 0.05, the dielectric data reveal two peaks at the T_{T-C} and T_{T-O} transition temperatures. These double peaks are considered to arise from two ferroelectric phases, one KNN and other KNT rich with respect to the base composition. There are no extra peaks in XRD of Ta-doped KNN compositions (Figure 5-5) but Ta^{5+} and Nb^{5+} have the same ionic radius and differ only in mass, hence it likely that the XRD peaks overlap for KNT and KNN based compositions with substitution occurring according to the defect equation.

$$Ta_2O_5 \rightarrow 2Ta_{Nb}^{X} + 5O_{O}^{X}$$

Despite the presence of two peaks, the T_{T-O} and T_{T-C} transition still decrease systematically with increasing x which precludes immiscibility and favours the argument that the compositions are chemically inhomogeneous as a result of incomplete inter-diffusion of the Ta and Nb species. Effectively, the presence of two phases is kinetically driven rather than thermodynamic as in the case of immiscible systems. This conclusion is further supported by broadening of the peaks which suggests that the Ta and Nb rich regions themselves have a distribution of Curie temperatures consistent with inhomogeneity.

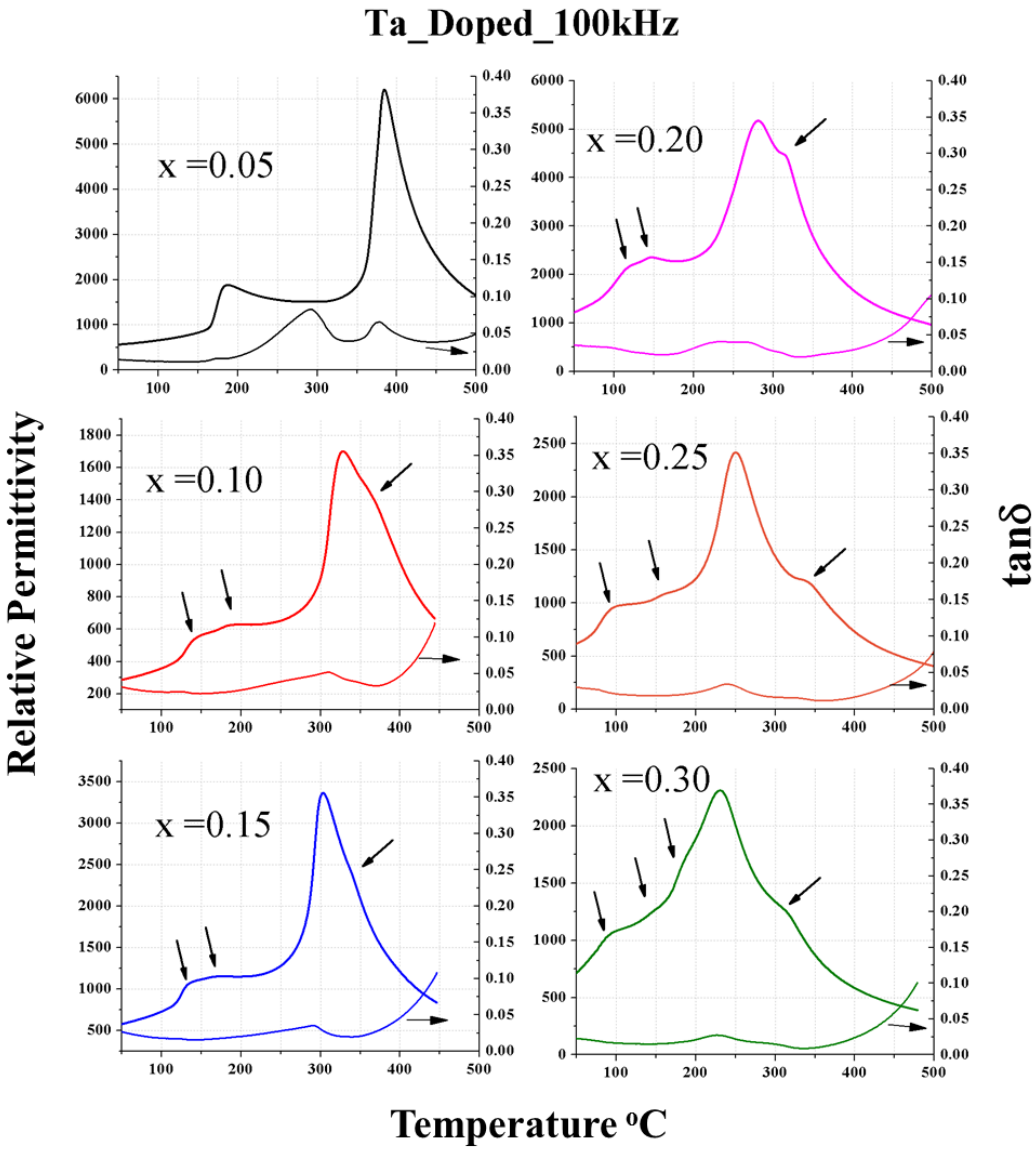

Figure 5-12 ε_r and tanδ versus temperature of different Ta doped KNN-51/49 compositions at 100 kHz from 50°C to 500°C illustrating the behaviour in T_C.

5.2.3.4 Stoichiometric co-doping of donor (Bi^{3+}) and acceptor (Zr^{4+}) KNN-BNZ

Bi^{3+} (A-site) and Zr^{4+} (B-site) play a major role in the development of piezoelectricity and dielectric properties in the KNN based ceramics [25, 32-35]. Although the combination of Bi^{3+} and Zr^{4+} constitutes stoichiometric doping, the compositions are best described by considering them as part of the (1-x)KNN – xBNZ solid solution where $0.01 \leq x \leq 0.06$. BNZ is considered to promote the low

temperature T_{R-O} transition to room temperature whilst simultaneously the T_{O-T} decreases, along with a slight but not dramatic decrease in T_{T-C}. However, the so called RT MPB is not stable above room temperature and the piezoelectric properties decline alarmingly above 80 – 100°C. [36]

The properties of these compounds are presented here as part of the doping section to illustrate that the co-doping strategy is by far the most successful in optimising KNN but a detailed study of their capability to form multilayers and the optimisation of composition for this technology is discussed in the following chapter.

The dielectric data for KNN-BNZ compositions is presented in Figure 5-13 (a-b) at 100 kHz as a function of temperature, along with the requisite Curie temperatures. T_{T-C} and T_{O-T} in un-doped KNN-50/50 are 409°C and 204°C[5], while for BNZ doped KNN, the temperatures are illustrated in Figure 5-13(a). The RT ε_r is increased to ≥ 1600 for compositions with x=0.06 and it has been suggested that ceramics with x ≥0.06 may be used for high temperature capacitor applications up to 250 ºC [37, 38]. The precise composition of the purported MPB is open to debate. x = 0.06 has no visible T_{O-T} transition but maximum properties are achieved at lower values of x. The best estimate of the composition of the so-called MPB therefore is $0.05 \leq x \leq 0.06$. Tanδ (Figure 5-13b) is <0.05 in all compounds up to the Curie point.

[5] Temperature values got from previous chapter of this study

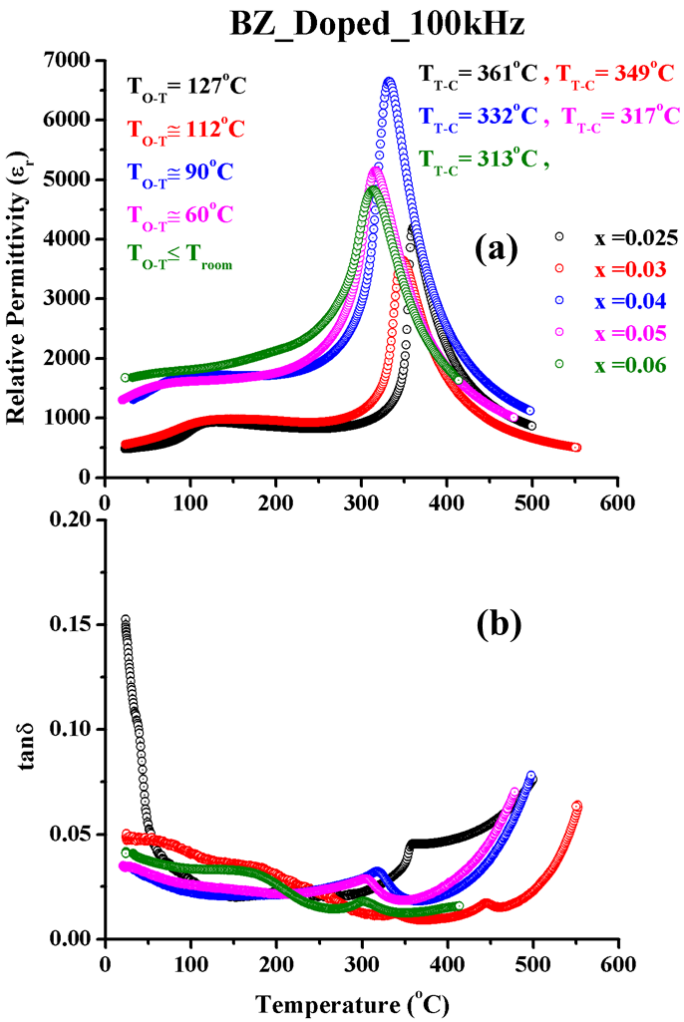

Figure 5-13 Comparison of (a) ε_r and (b) tanδ versus temperature of different KNN-50/50_BNZ compounds at 100 kHz.

5.2.4 Functional Properties of Doped KNN

5.2.4.1 Ferroelectric Properties

Hysteresis loops of Sr donor doped KNN sintered in air are plotted in Figure 5-14. The loops remain unsaturated and remanent polarisation (P_r) and coercive field (E_c) increase with increasing applied field. Moreover, the maximum value of polarisation occurs away from saturation polarisation (P_S) and Pr, suggesting that there is a strong contribution from conductivity to the hysteresis loop in which regions of space

charge reverse under the alternating field and contribute to the total polarisation, in addition to the well documented ferroelectric switching expected for these compositions. The origin of conductivity is complex but likely relates to the Sr^{2+} substituting onto the A-site which donates an electron according to the equation,

$$Sr_A^{\bullet} \equiv e'$$

Figure 5-15 (a-f) illustrates the hysteresis loops for Ta doped KNN-51/49 compositions with $0.05 \leq x \leq 0.3$. They all exhibit symmetrical loops, but as the Ta concentration increases, P_r decreases for the same applied field. E_c broadly remains the same for all formulations (10kV/cm). Figure 5-16 (b) is extracted from (a) where P_r and E_c versus composition are plotted. Undoped KNN has the maximum peak values of remanent polarisation and coercive field but then decreases at 15% and slightly increases up till 30%. These anomalous changes are principally because not all samples saturate at 40kV/cm.

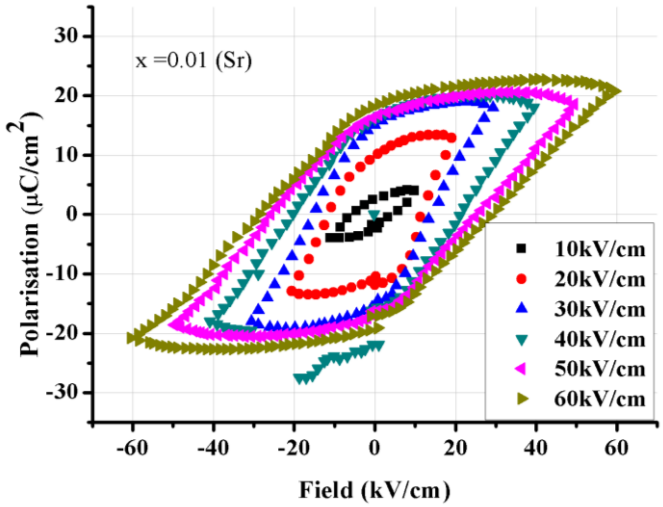

Figure 5-14 Ferroelectric loops of 1%_Sr (A-site) doped KNN_50/50**,** at T_{room} and 6Hz frequency.

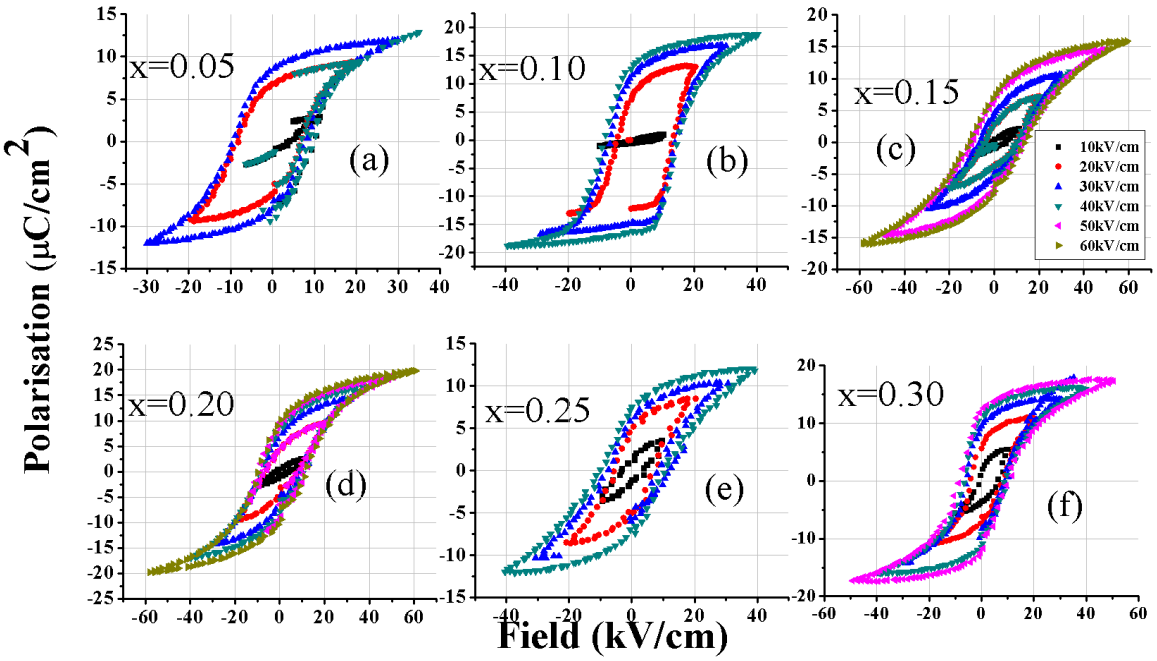

Figure 5-15 Ferroelectric hysteresis loops of Ta^{5+} (Nb^{5+}-site) doped KNN_51/49, where (a), (b), (c), (d), (e) and (f) are $0.05 \leq x \leq 0.3$ respectively.

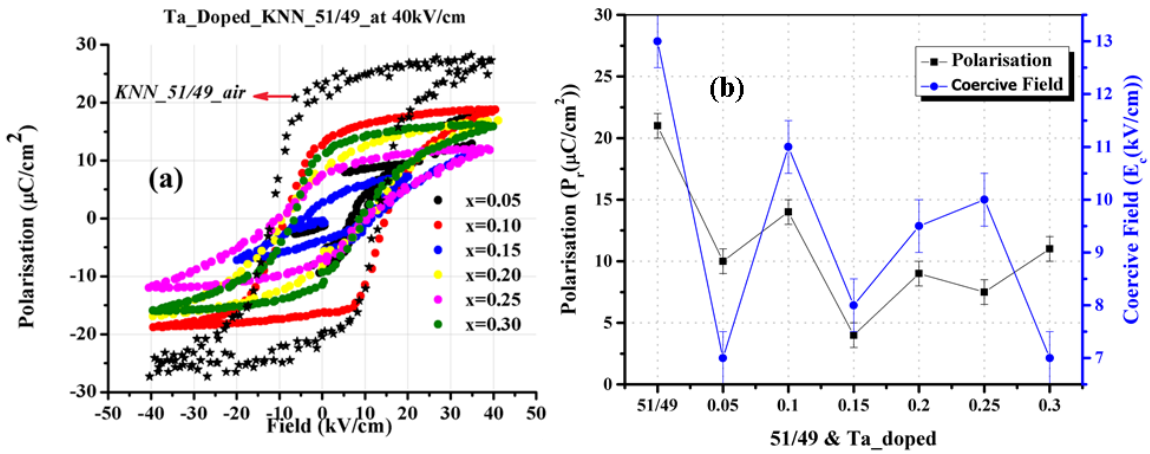

Figure 5-16 (a) PE loops of Ta-doped KNN_51/49 (at T_{room} and 6Hz frequency), compared with KNN_51/49_air loop at 40kV/cm; (b) P_r and E_C versus composition.

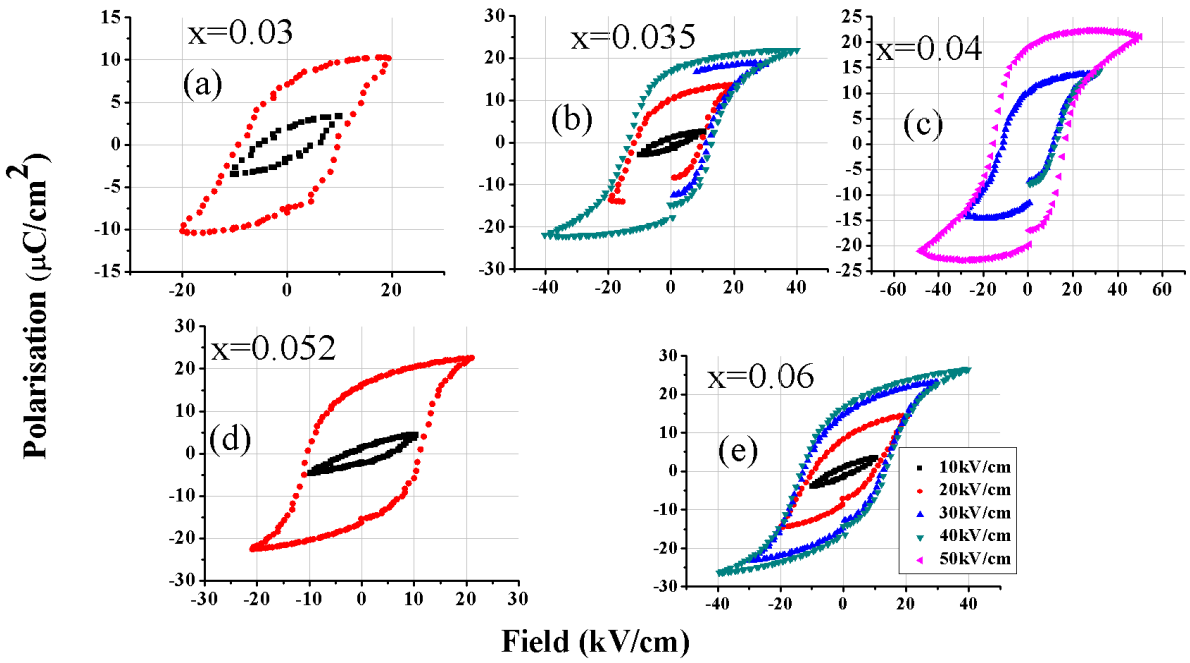

Figure 5-17 Polarisation versus electric field hysteresis loops of (1-x) (KNN-50/50) – x(BNZ-50/50), electric field representation bullet point values given in (e) commonly for all.

Figure 5-17 (a-e) shows the hysteresis loops for KNN-BNZ as a function of composition. Most noteworthy is that ceramics with x = 0.52 saturate at the lowest field (20kV/cm), hence it is suggested that the so called MPB resides between 0.052 ≤ x ≤0.06 and has only a narrow compositional range. This conclusion broadly agrees with XRD and LCR data (Figure 5-6 and Figure 5-13, respectively). As phase transitions 'pinch' together around room temperature as a function of BNZ concentration, ferroelectric switching becomes easier. Easier switching is often associated with the proximity of a phase transition to room temperature, when the energy well for the reversal of polarisation is at its most shallow.

5.2.4.2 Piezoelectric Properties

Overall, single aliovalent dopants on either the B-site (Mn^{2+}, Ti^{4+}, Sn^{4+}) or the A-site (Sr^{2+}) did not enhance the piezoelectric properties of KNN. d_{33} of Mn^{2+}, Ti^{4+} and Sr^{2+}

was no more than 60pC/N and for 1%-Sn^{4+} 95pC/N at the electric field of 40kV/cm. d_{33} values for Ta doped KNN are presented in Figure 5-18. These data are consistent with their respective PE loops (Figure 5-15a-f) with compositions showing in some cases marginally higher values than undoped KNN (10%Ta reveals a maximum value of 135pC/N). However, the dielectric data unambiguously illustrates that these compositions are heterogeneous. Hence the real trends in d_{33} may be obscured until further studies are carried out on compositions which have undergone either longer sintering times or multiple calcinations to homogenize the B-site ion distribution.

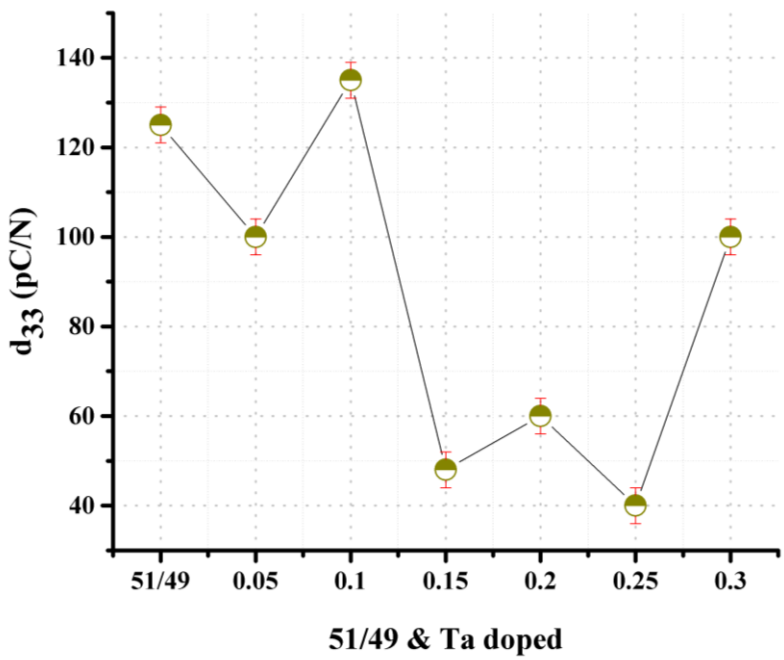

Figure 5-18 d_{33} values of Ta doped KNN in comparison with KNN-51/49 at 40kV/cm

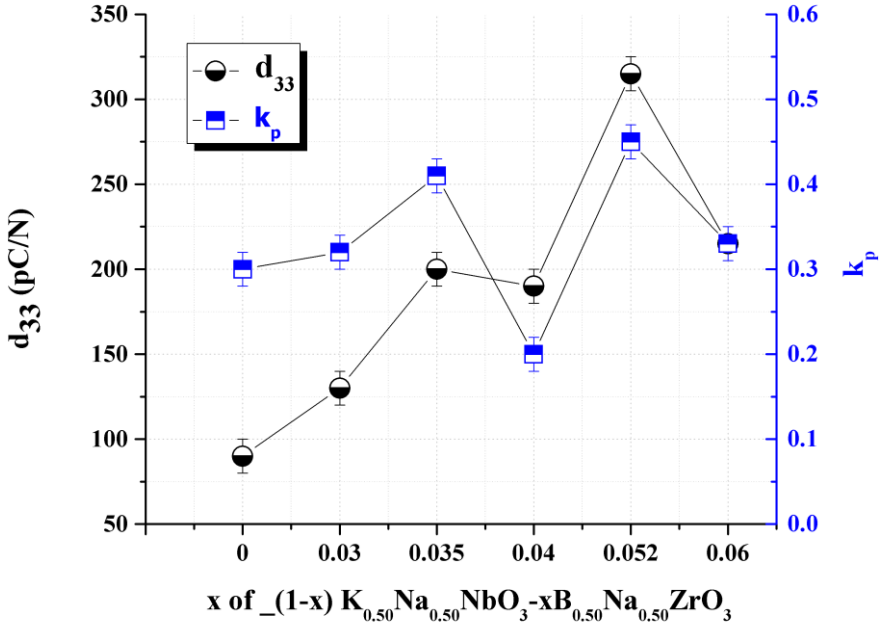

Figure 5-19 Piezoelectric coefficient and coupling factor versus addition of BNZ in KNN-50/50

In stark contrast to singly doped KNN, KNN-BNZ compositions revealed a huge enhancement in piezoelectric activity with an optimum of d_{33}=315pC/N and k_p =0.45 for compositions with x = 0.052 (Figure 5-19). d_{33} and k_p decreased markedly for x = 0.06 to 215pC/N and 0.33, respectively, illustrating the potential difficulties of maintaining high values of d_{33} for large scale batch production.

5.3 Conclusions

Overall, the use of single dopant species, either aliovalent or isovalent has little positive impact on the dielectric, piezoelectric or ferroelectric properties of KNN. The solubility of single aliovalent dopants is generally low and for both donor and acceptor dopants the result is an increase in conductivity/reduction in density leading to difficulties of poling or lossy PE loops. For isovalent dopants such as Ta, the only positive potential impact is a broadening of the Curie maxima leading to suggestions

that these compositions may have practical applications in temperature stable capacitors, although the cost of Ta may prove prohibitive.

Stoichiometric co-doped compositions with Bi^{3+} and Zr^{4+}, in agreement with other authors, show great promise for applications, with improvement in the d_{33} and square hysteresis loops generated over a range of compositions indicating clear trends relating to the structural changes proposed in these compositions. The stark contrast between singly doped and co-doped compositions have thus prompted further work on the latter and these will be subject of the following chapter in which the possibility of illustrating their commercial potential is explored through the fabrication of prototype multilayer actuators.

References

1. Rafiq, M.A., et al, *Defects and charge transport in Mn-doped $K_{0.5}Na_{0.5}NbO_3$ ceramics.* Phys.Chem.Chem.Phys., 2015. **17**: p. 24403-24411.
2. Guo, Y., K.-i. Kakimoto, and H. Ohsato, *Phase transitional behavior and piezoelectric properties of $(Na_{0.5}K_{0.5})NbO_3$–$LiNbO_3$ ceramics.* Applied Physics Letters, 2004. **85**(18): p. 4121.
3. Guo, Y., K.-i. Kakimoto, and H. Ohsato, *(Na0.5K0.5)NbO3–LiTaO3 lead-free piezoelectric ceramics.* Materials Letters, 2005. **59**(2-3): p. 241-244.
4. Hollenstein, E., et al., *Piezoelectric properties of Li- and Ta-modified $(K_{0.5}Na_{0.5})NbO_3$ ceramics.* Applied Physics Letters, 2005. **87**(18): p. 182905.
5. Jiang, X.P., et al., *Li-modified sodium potassium tantalum niobate lead-free piezoelectric ceramics.* Journal of Inorganic Materials, 2007. **22**(3): p. 465-468.

6. Hollenstein, E., D. Damjanovic, and N. Setter, *Temperature stability of the piezoelectric properties of Li-modified KNN ceramics.* Journal of the European Ceramic Society, 2007. **27**(13-15): p. 4093-4097.

7. Lopez-Juarez, R., et al., *Piezoelectric properties of Li-Ta co-doped potassium-sodium niobate ceramics prepared by spark plasma and conventional sintering.* Journal of Alloys and Compounds, 2011. **509**(9): p. 3837-3842.

8. Rubio-Marcos, F., et al., *Control of the Crystalline Structure and Piezoelectric Properties of* $(K,Na,Li)(Nb,Ta,Sb)O_3$ *Ceramics through Transition Metal Oxide Doping.* Applied Physics Express, 2011. **4**(10): p. 101501.

9. Skidmore, T.A.M., S. J., *Phase development during mixed-oxide processing of a* $[Na_{0.5}K_{0.5}NbO_3]_{1-x}-[LiTaO_3]_x$ *powder.* Journal of Materials Research, 2011. **22**(08): p. 2265-2272.

10. Wang, H.Q., et al., *Sol-gel derived (Li, Ta, Sb) modified sodium potassium niobate ceramics: Processing and piezoelectric properties.* Journal of Alloys and Compounds, 2011. **509**(3): p. 936-941.

11. Zhang, L., et al., *Normal sintering and electric properties of* $(K,Na,Li)(Nb,Sb)O_3$ *lead-free piezoelectric ceramics.* Journal of Electroceramics, 2011. **26**(1-4): p. 105-111.

12. Du, J., et al., *Piezoelectric properties and time stability of lead-free* $(Na_{0.52}K_{0.44}Li_{0.04})Nb_{1-x-y}Sb_xTa_yO_3$ *ceramics.* Ceramics International, 2012.

13. Du, J., et al., *Effects of* $CaAl_2O_4$ *on the electrical properties and temperature stability of* $(Na_{0.53}K_{0.404}Li_{0.066})Nb_{0.92}Sb_{0.08}O_3$ *ceramics.* Journal of Alloys and Compounds, 2012. **541**: p. 454-457.

14. Li, Y., et al., *Microstructures and electrical properties of $KNbO_3$ doped (Li,Ta,Sb) modified (K,Na)NbO_3 lead-free ceramics by two-step sintering.* Materials Letters, 2012. **89**: p. 70-73.

15. Wang, K., et al., *Temperature-Insensitive (K,Na)NbO_3-Based Lead-Free Piezoactuator Ceramics.* Advanced Functional Materials, 2013. **23**(33): p. 4079-4086.

16. Gio, P.D. and N.D. Phong, *Effects of LiF on the Structure and Electrical Properties of ($Na_{0.52}$ $K_{0.435}$ $Li_{0.045}$) $Nb_{0.87}$ $Sb_{0.08}$ $Ta_{0.05}$ O_3Lead-Free Piezoelectric Ceramics Sintered at Low Temperatures.* Journal of Materials Science and Chemical Engineering, 2015. **03**(11): p. 13-20.

17. Zhang, Q., et al., *Domain wall excitations and their contributions to the weak-signal response of doped lead zirconate titanate ceramics.* Journal of applied physics, 1988. **64**(11): p. 6445-6451.

18. Reaney, I.M.a.D., D.,, *Crystal structure and domain-wall contributions to the piezoelectric properties of strontium bismuth titanate ceramics.* Journal of Applied Physics, 1996. **80**(07): p. 4223-4225.

19. Lin, D., et al., *Influence of MnO_2 doping on the dielectric and piezoelectric properties and domain structure in ($K_{0.5}Na_{0.5}$)NbO_3 single crystals.* Jounal of American Ceramic Society, 2010. **93**(4): p. 941-944.

20. Su, S., et al., *Sintering, microstructure and piezoelectric properties of CuO and SnO_2 co-modified sodium potassium niobate ceramics.* Materials Research Bulletin, 2010. **45**(2): p. 124-128.

21. Akça, E. and H. Yılmaz, *Sintering behavior and electrical properties of $K_4CuNb_8O_{23}$ modified $K_{0.5}Na_{0.5}NbO_3$ ceramics with SnO_2, ZnO or Yb_2O_3 doping.* Ceramics International, 2015. **41**(3): p. 3659-3667.

22. Shannon, R.D., *Revised Effective Ionic Radii and Systematic Studies of Interatomie Distances in Halides and Chalcogenides.* Acta Crystallographica Section A, 1976. **32**(5): p. 751-767.

23. Barret, R.L., *Electronegativity Chart.* Journal of Chemical Education, 1962. **39**(5): p. 251.

24. Ibchem. *Covalent Bond: http://ibchem.com/IB/ibnotes/04.2.htm*. 2016 [cited 2016 27/09/2016].

25. Wang, Z., et al., *New Lead-Free* $(1-x)(K_{0.5}Na_{0.5})NbO_3$-$x(Bi_{0.5}Na_{0.5})ZrO_3$*Ceramics with High Piezoelectricity.* Journal of the American Ceramic Society, 2014. **97**(3): p. 688-690.

26. Tuller, Y.A.H.L., *Improved Electromechanical Response in Rhombohedral* $BaTiO_3$. Journal of Electroceramics, 2004. **13**: p. 463-469.

27. D., H.A.S., *Diffuse Ferroelectric Phase Transitions in* $Ba(Ti_{1-y}Zr_y)O_3$ *Ceramics.* Journal of the American Ceramic Society 1982. **65**(11): p. 539-544.

28. Rehrig, P.W., et al., *Piezoelectric properties of zirconium-doped barium titanate single crystals grown by templated grain growth.* Journal of Applied Physics, 1999. **86**(3): p. 1657.

29. R.C., K., & N.J., Hellicar,, *Structural transitions in barium titanate-zirconate transducer materials.* Acta Acustica united with Acustica, 1956. **6**(2): p. 235-245.

30. Jaffe, B., Cook, W. R. & Jaffe, H, *Piezoelectric Ceramics*. 1971, New York: Academic.

31. Saito, Y., et. al. , *Lead-Free piezoceramics.* Nature, 2004. **432**(7013): p. 84-7.

32. Wang, X., et al., *Large d_{33} in (K,Na)(Nb,Ta,Sb)O_3-(Bi,Na,K)ZrO_3 lead-free ceramics.* Journal of Materials Chemistry A, 2014. **2**(12): p. 4122.

33. Zheng, T., et al., *Giant d_{33} in nonstoichiometric (K,Na)NbO_3-based lead-free ceramics.* Scripta Materialia, 2015. **94**: p. 25-27.

34. Wang, X., et al., *Giant piezoelectricity in potassium-sodium niobate lead-free ceramics.* J Am Chem Soc, 2014. **136**(7): p. 2905-10.

35. Cheng, X., et al., *Giant d_{33} in (K,Na)(Nb,Sb)O_3-(Bi,Na,K, Li)ZrO_3 based lead-free piezoelectrics with high Tc.* Applied Physics Letters, 2013. **103**(5): p. 052906.

36. Wang, D., Hussain, F, Khesro, A, et al., *Composition and temperature dependence of piezoelectricity in (1-x)($K_{1-y}Na_y$)NbO_3-x($Bi_{1/2}Na_{1/2}$)ZrO_3 lead-free ceramics.* American Ceramic Society, 2016.

37. Dittmer, R., et al., *A High-Temperature-Capacitor Dielectric Based on $K_{0.5}Na_{0.5}NbO_3$-Modified $Bi_{1/2}Na_{1/2}TiO_3$-$Bi_{1/2}K_{1/2}TiO_3$.* Journal of the American Ceramic Society, 2012. **95**(11): p. 3519-3524.

38. Raengthon, N., et al., *$BaTiO_3$-Bi($Zn_{1/2}Ti_{1/2}$)O_3-$BiScO_3$Ceramics for High-Temperature Capacitor Applications.* Journal of the American Ceramic Society, 2012. **95**(11): p. 3554-3561.

Chapter 6 Results and Discussion: Fabrication of Lead-Free Multilayer Actuators

Summary

The replacement of PZT with a PbO-free alternative is the subject of intense investigation worldwide. Currently, PZT is ubiquitous and features in a wide variety of applications, such as Energy Harvesters, multilayer actuators, dynamic body sensor, parking aid devices (PAD), transducer, micro distance precision devices for camera lens focusing, non-destructive ultra sound testing and spark igniters on gas appliances. [1] In this chapter, a cheap reliable methodology for the fabrication of multilayers of KNN-BNZ + ZrO_2 is presented without the need for vacuuming and/or cold isostatic pressing of the tape. For this investigation, commercial grade Nb_2O_5 and ZrO_2 were also used to demonstrate the scalability of the process with 10 and 16-layer multilayers fabricated. Pt was used as the internal electrode but for commercial fabrication, it is anticipated that Ag-Pd and potentially Cu inks could be utilised. The thickness per active layer was 193µm and 102µm for the 10 and 16 layer actuators, respectively. Effective d_{33}, effective d_{33}*, bi-polar strain (S_{max}), max displacement, ε_r and tanδ are 2500pC/N, 4604 pm/V, 0.17% (bulk), 2.2µm, 1812 and 2% at 1kHz (multilayer), respectively. Where effective d_{33} or d_{33}* is total output of all layers together. The ultimate target materials for potential substitution with KNN-BNZ are PZT-4 and PZT-8.

6.1 Introduction

Piezoelectric actuators are used in many applications. Mostly they are based on PZT, the lead content of which is considered toxic and not environmentally friendly particularly in the end of use phase. Consequently, replacement piezoelectric compositions are sought, a leading candidate of which is potassium sodium niobate (KNN). KNN has the added potential of being safe for deployment as internal medical devices, expanding its potential range of piezoelectric applications to biosensors and internal motors/pumps.

The main issues of KNN processing was discussed in the literature review, specifically that K_2O and Na_2O are highly volatile [2-9]. However, PbO is also volatile,[10] nonetheless PZT is a versatile piezoelectric used commercially, hence it is reasonable to expect this limitation to be overcome in production by adopting similar methodologies to those developed for PZT. The volatility of PbO is known to be sensitive to the incorporation of specific dopants (SrO) and to the Zr:Ti ratio[11-13]. In KNN based compounds, doping with more stable, less volatile species such as ZrO_2 is considered to inhibit volatilisation.[14, 15] Moreover, forming solid solutions with $(Na_{1/2}Bi_{1/2})ZrO_3$ (NBZ) have been shown in previous chapters to enhance the piezoelectric properties. Therefore, from both a processing and properties perspective NBZ with excess ZrO_2 are useful substituents/dopants in KNN. To demonstrate that control of final properties in multilayers could be achieved using low cost raw materials, industrial grade Nb_2O_3 (99.5%) and ZrO_2 (99.0%) were utilised in the fabrication process of some actuators. It is noted that this chapter is the first demonstration to the candidate's knowledge of the use of KNN-BNZ in the fabrication of multilayer actuators.

6.2 Fabrication of multilayers

Multilayering is a viable [15-23], and sustainable technology to optimise properties for many types of functional ceramics and the reader is referred to previous chapters for a detailed explanation of the process. Typically, multilayers are created by stacking and cutting the samples, vacuuming in plastic bag, hot pressing and/or cold-isostatic pressing (CIP) to adhere the layers prior to firing. In this study, a simple methodology was developed which is heretofore referred to as the wet-method-multilayers (WMM) method which is low cost and simple. The method was developed primarily to resolve issues of delamination which dogged early attempts at multilayering using conventional processing.

6.2.1 Wet Method Multilayers (WMM)

In the WMM method, a small quantity of tape-cast solvent was brushed onto each layer which could then be laminated by applying a gentle manual pressure. This procedure resolved problems of delamination, typically encountered by more conventional lamination methods. Typically, 10 to 16 layers were pressed together with screen printed Pt electrodes in between. From each stack, four samples were cut with extra green tape then pressed onto the sides of the laminated sample to further minimise delamination.

The disadvantage of standard method is that air between layers of ceramic and electrode may become trapped and cannot be evacuated. During cold isostatic pressing, these air bubbles burst and the liquid of the CIP floods between the layers. If hot pressing is used, it dries the volatiles unevenly and deforms the structure. It is proposed that the WMM method can be modified for potential commercial use with a fine spray mist of the solvent passed over each layer prior to gentle pressure being applied with a rubber pad. The optimized ingredients of recipe of slurry for WMM

were ceramic 40g of powder, 10% of binder butvar, 5% of each PEG & BBP plasticizers and 50% of isopropanol as a solvent.

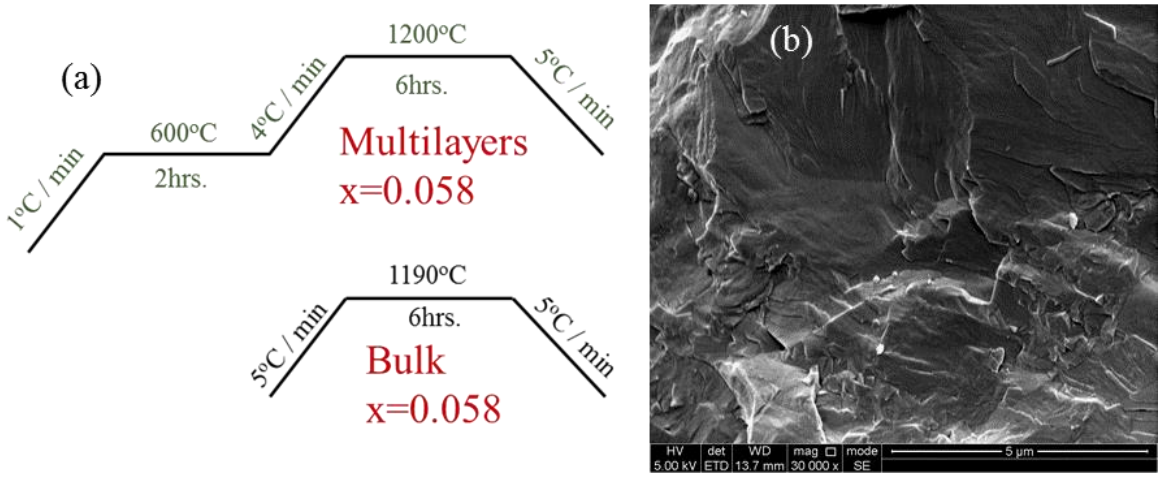

Figure 6-1 (a) Heat treatment and sintering profile of MLCC and bulk, and SEM image of bulk, of (0.942KNN-0.058BNZ) +ZrO_2.

The advantage of isopropanol over other solvents (MEK 50% : EtOH 50%) which was used in undoped KNN on trials was that, it evaporated more slowly. But the drawback of isopropanol containing tape was that it needed to be dried at higher temperature (40°C).

6.3 Characterisation of functional Ceramics

6.3.1 SEM, Optical Microscopy and photography

A SE image of the fracture surface of a bulk pellet is shown in Figure 6-1b Grain boundaries and morphology of grains could not be identified even at 30000X magnification, while its relative density was 98% measured by Archimedes' principle. The high density and large grain size suggests a liquid phase sintering mechanism but more evidence is required for this to be proved conclusively. Polyvar Met optical microscope with, Carl Zeiss digital camera and Axiovision software was

used to take the photos of MLA samples (0.942KNN-0.058BNZ) at 5X magnification, Figure 6-2 (a-b). Samples were cut through the centre so that all internal Pt electrodes could be observed. The 10 layers are well adhered with a dense ceramic monolithic layer in between, after heat treatment and sintering (Figure 6-1). After firing, the average thickness of a single layer of ceramic of 10-layers stack sample is 193µm approximately double the thickness of the 16_layer sample (102µm).

The greater thickness of the 10 layer sample is because 2 tape cast ceramic layers per electrode layer were utilised whereas the 16 layer sample has only one. The latter was used to minimize the potential of short circuiting during the application of high fields during poling and strain-field measurements. Figure 6-2(c) shows a 5-layer sample of KNN_51/49 were two electrodes out of 5-layers are clearly visible at one end of the multilayer.

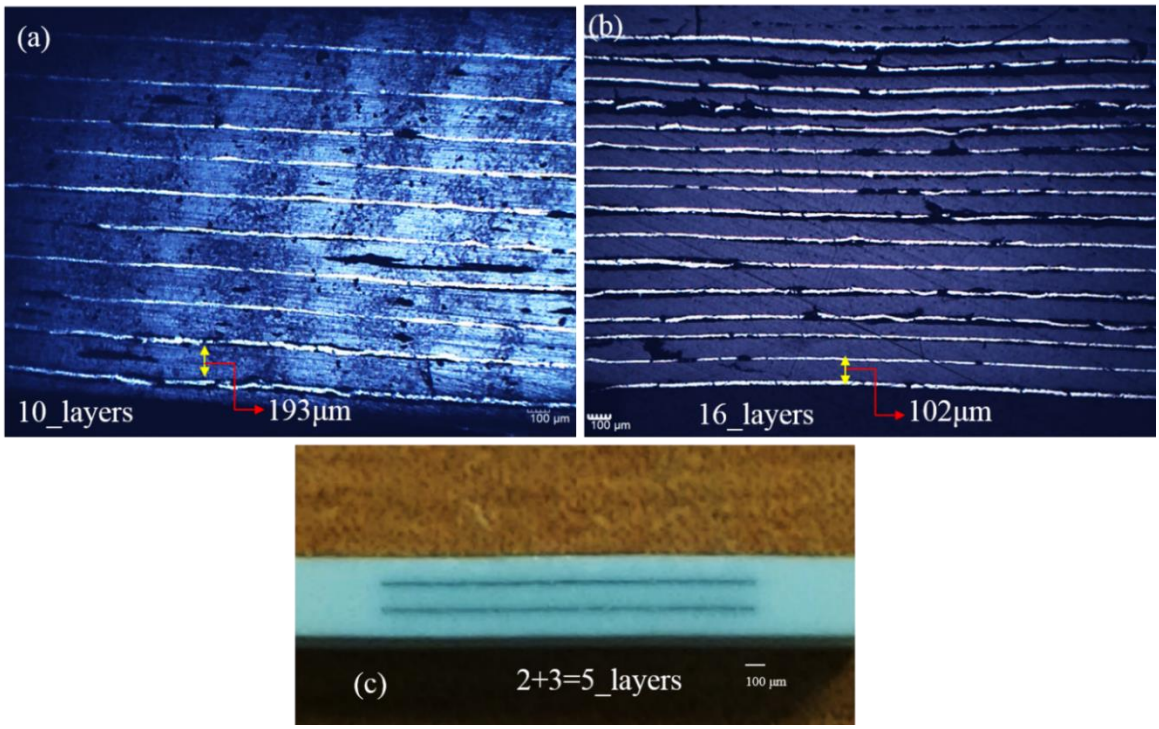

Figure 6-2 Optical Microscopic viewing cross-sectional images of middle-sectioned sample to show all inner electrodes of (a) 10_layers & 16_layers MLA

(0.942KNN_50/50-0.58BNZ); (c) Optical photograph of 5_layers KNN_51/49 showing two alternate layers of inner electrode of one side cross section

6.3.2 Relative permittivity and tanδ

ε_r and tanδ were studied for compositions with 0.06≥x≥0.05 (Figure 6-3) and compared at 100kHz with key formulations also fabricated using commercial grade raw materials of Nb_2O_5 and ZrO_2 to minimize the cost and to improve the overall properties of KNN with BNZ. More details concerning the dielectric loss of KNN-BNZ compounds were given in chapter 5. Here, the aim was to select the optimum compound to fabricate an MLA or potentially in the future an energy harvester to improve reproducibility. In general, the higher the concentration of ZrO_2 the lower the dielectric loss. [24]

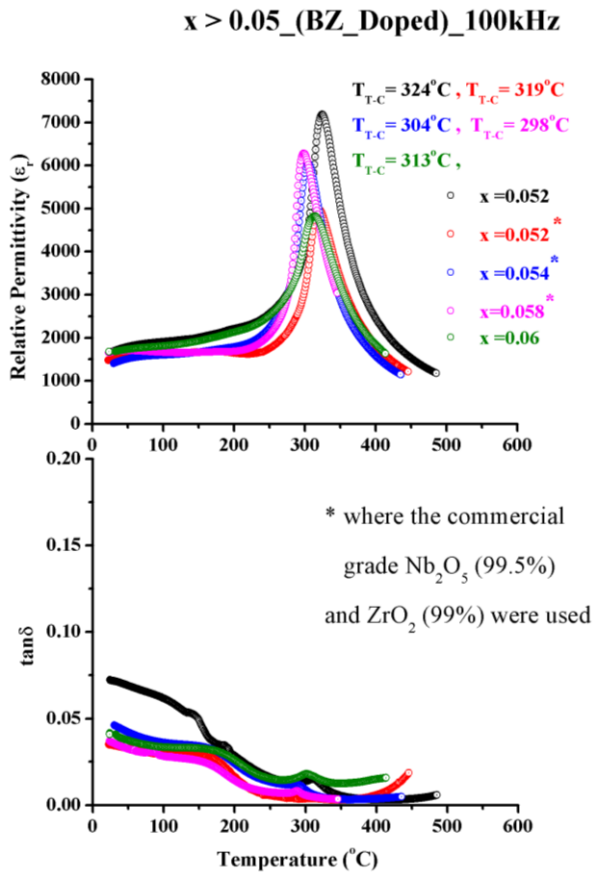

Figure 6-3 Relative permittivity vs. tanδ loss of BNZ doped KNN-50/50 where (0.05 ≤ x ≤ 0.06), compared with commercial grade raw materials.

The exact composition and temperature of the so called MPB in KNN-BNZ varied with processing even if different Na/K ratios were utilised, as discussed in a previous study [25], hence a KNN-50/50-0.058BNZ+ZrO_2 was selected in which the T_{O-T} transition was below RT for multilayering, as this gave the most reproducible properties despite d_{33} being the highest for x=0.052 (d_{33}=315pC/N) processed using analytical grade raw materials.

Consequently, compositions with x=0.058 were optimised from commercial grade raw materials since at > x=0.06 ceramics begin to exhibit strong relaxations as discussed by Wang, Z., et al., 2014.[26] There is some variation in T_C for the compositions illustrated in Figure 6-3 with x=0.058 the lowest. The variation in loss and permittivity as a function frequency is given in Figure 6-4.

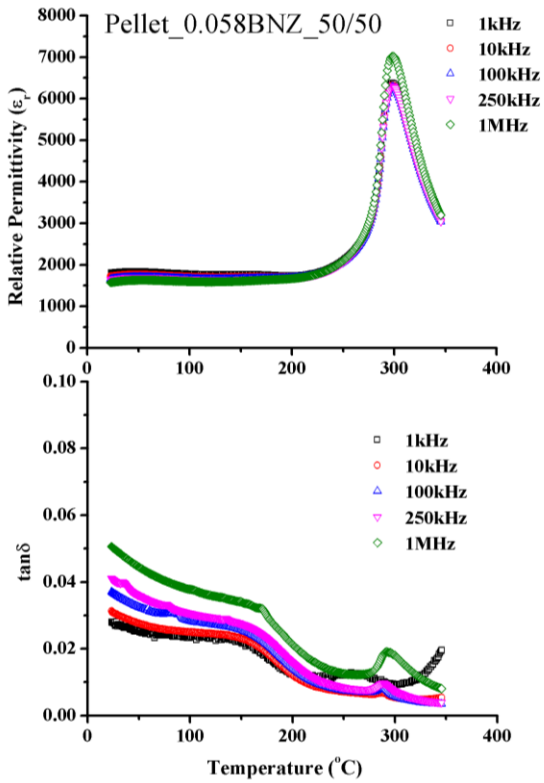

Figure 6-4 Pellet sample made of commercial grade raw materials of 0.942KNN-0.058BNZ formulation showing relative permittivity and tanδ loss at frequency of 1kHz-1MHz

T_{T-C} (298°C) for x = 0.058 is comparable with data reported by other authors [1, 27, 28] and similar to PZT-4D (320°C) [29]. Table 6-1 compares T_C and ε_r at RT for x = 0.058 with other commercial ceramics. Interestingly, the dielectric losses decreased to 1% with increasing temperature, superior to PZT.[30]

The LCR data of multilayer ceramics of 0.942KNN-0.058BNZ with 10 Pt-inner electrodes were also recorded (Figure 6-5-a-c). The dielectric of both the bulk (Figure 6-4) and of the MLA are similar in terms of T_C temperature, ε_r and tanδ. However, there is a slope of increasing capacitance with increasing temperature from RT in MLA compared to pellet data. There was also a difference in sintering temperatures of bulk (1190°C) and multilayers (1200°C) (Figure 6-1).

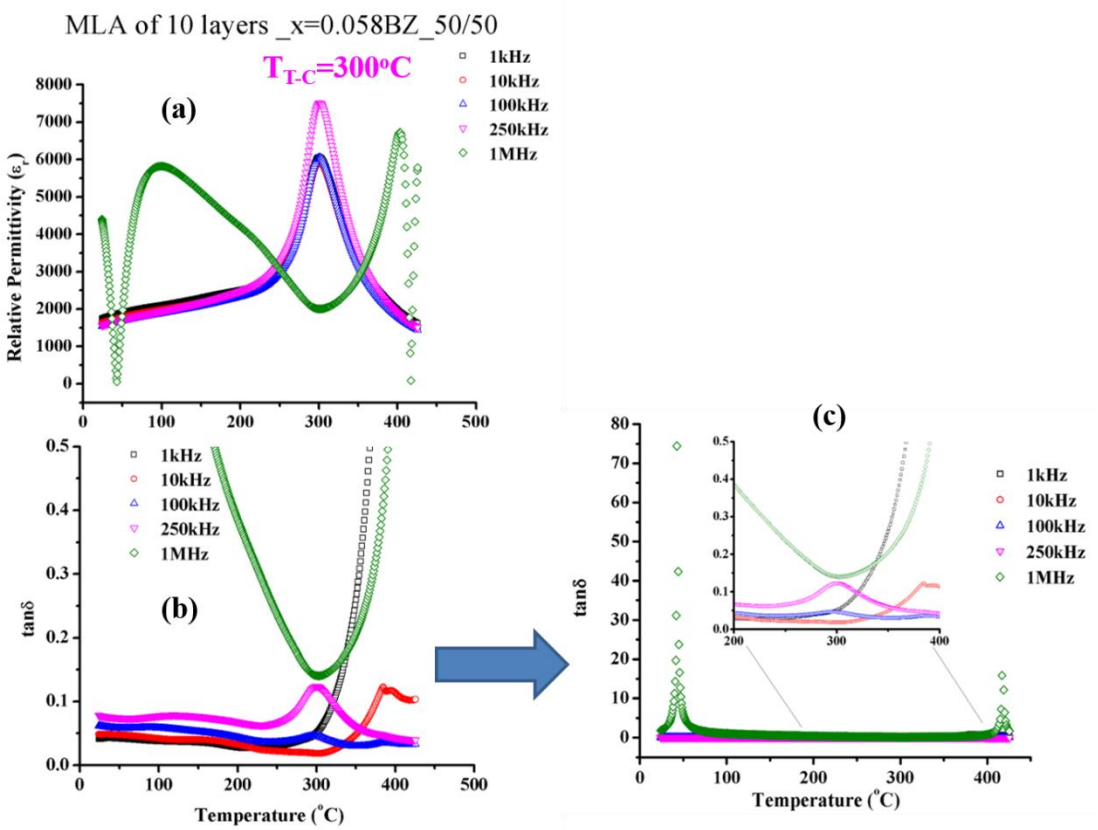

Figure 6-5 MLA of 10-layers made of commercial grade raw materials of 0.942KNN-0.058BNZ formulation showing (a) relative permittivity, (b) tanδ loss & tanδ loss of 1MHz.

It is noted that there is some evidence of resonance modes becoming active in the LCR data presented in Figure 6-5. Whilst this phenomenon is interesting, it has not been the subject of further investigation in this thesis.

6.3.3 Ferroelectric properties of bulk vs. multilayers

Strain-voltage, strain-field and polarisation-field loops of bulk pellets of x=0.058 + ZrO_2 (0.76 wt %-age of total ZrO_2) are shown in Figure 6-6(a-c), respectively. As discussed previously, ZrO_2 was added to decrease the volatilisation of alkali ions and therefore the dielectric loss of compositions. Although this is an empirical observation, it is speculated that, in addition, Zr^{4+} acts as an acceptor dopant in KNN. Equivalent acceptor doping with Mn and Fe classically controls the dielectric loss in PMN-PT and PZT based ceramics respectively [31, 32].

The pellet saturated at an applied electric field of 40kV/cm at room temperature (RT) and 1Hz. All loops are symmetrical and show evidence of ferroelectric/piezoelectric behaviour [33]. S_{max}, S_{neg}, P_s, P_r, and E_c are 1.1μm (0.17%), - 0.5μm (0.075%), 26μC/cm^2, 17μC/cm^2 and 14.5kV/cm, respectively at 40kV/cm. In general, relaxors do not show negative strain (S_{neg}) and this phenomenon is characteristic of piezoelectric ceramics. Both negative and positive strain can be utilised to harvest electrical energy through vibration with the positive mode most effective because it gives rise to greater deflection. The deflection is typically dominated by extrinsic effects which relate to the number and switching behaviour of 90° domains walls. 180° are known as ferroelectric domain walls whilst non-180° as the

ferroelastic/ferroelectric domain walls [12, 34]. There has been significant study based on the Rayleigh Law on the behaviour of domain walls under applied field in PZT and PbO-free compositions and it is generally accepted that irreversible displacement of non-180° domains is lower in tetragonal compared with rhombohedral compositions [35]

Bulk ceramics are effectively a single thick layer and have limited applications in energy harvesting and related applications. Instead, multilayers are widely used to enhance the properties, performance and reduce the overall cost. [36]

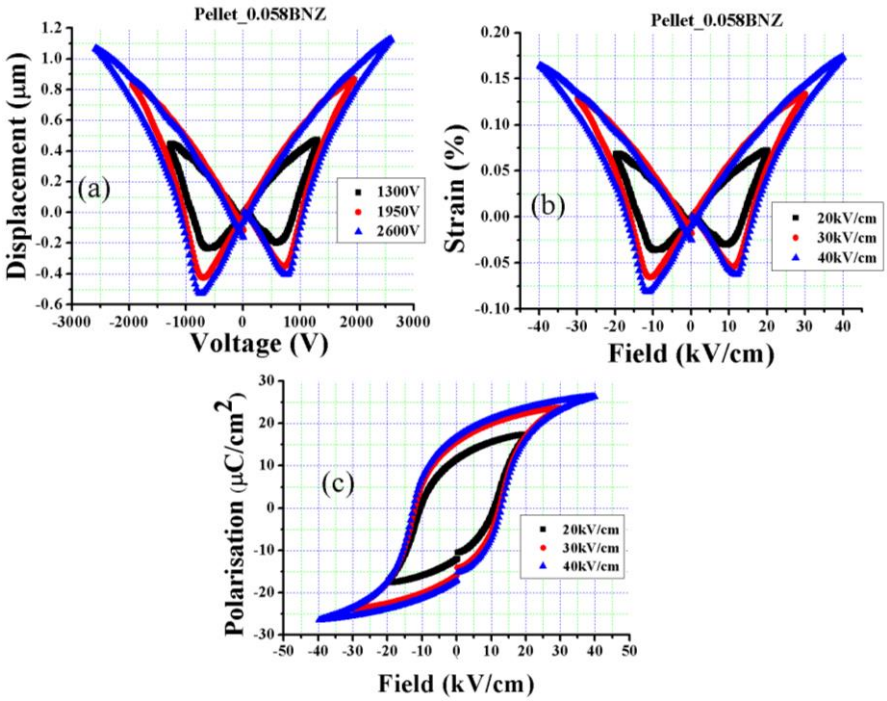

Figure 6-6 (a) Strain-Voltage, (b) Strain-Field & (c) Polarisation-Field Hysteresis loops of pellet sample (0.942KNN-0.058BNZ); measured at Sheffield Hallam University.

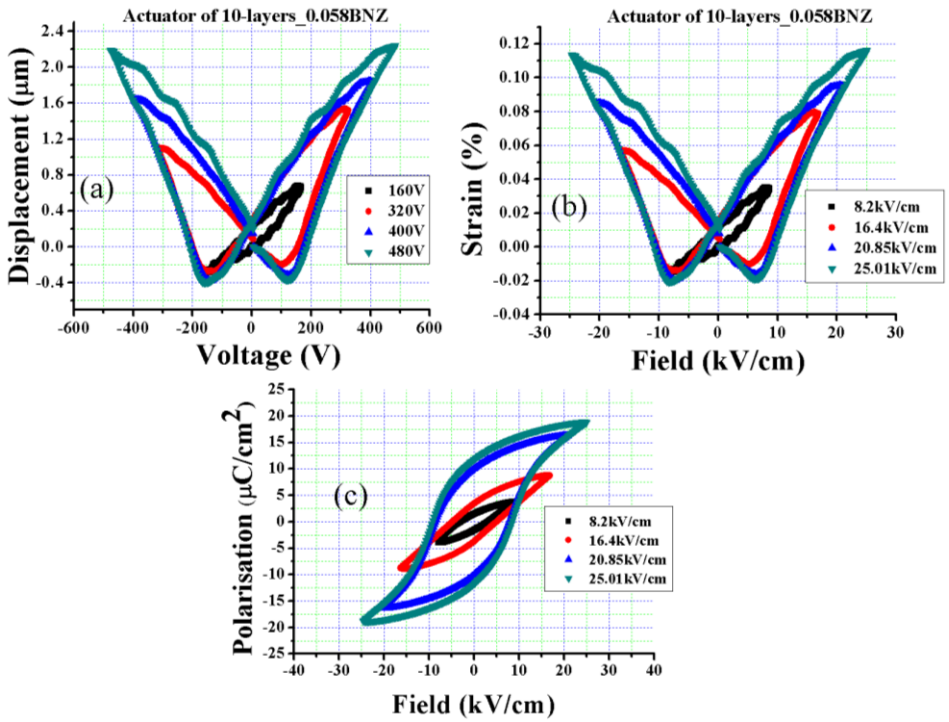

Figure 6-7 10-layers MLA sample of (0.942KNN-0.058BNZ) composition showing strain data & ferroelectric loops.

MLAs with 10 and 16 active layers of (0.942KNN-50/50-0.058BNZ) + ZrO_2 fabricated with Pt inner electrodes were characterised at high field. Strain and P-E loops of the 10-layer (Figure 6-7) MLAs saturated at lower voltage (25 kV/cm) than the pellet (40kV/cm). Total displacement (2.21μm / 10-layers), S_{max}(0.115% / layer), S_{neg}(0.20μm/ 10-layers or 0.010% /layer), d_{33}* (4604pm/V of 10-layers or 460.4pm/V per layer), P_s(19μC/cm^2 per layer), P_r(12μC/cm^2 per layer), and E_c (8.5kV/cm per layer) of device are observed respectively at 25 kV/cm[6]. The low drive field for the MLAs is particularly attractive for applications and in principle, these devices could operate at > 200ºC since T_C is around 300ºC. Nagata, Hajime at al. 2010 [37] fabricated MLAs based on 0.68($Bi_{0.50}Na_{0.50}$)TiO_3-0.04($Bi_{0.50}Li_{0.50}$)TiO_3-0.28($Bi_{0.50}K_{0.50}$)TiO_3 (BNLKT4-28) and reported d_{33}, S_{max} and

[6] S_{max}, S_{neg}, d_{33}*, d_{33}*(eff) are maximum strain per layer, negative strain per layer, ratio of S_{max} to E_{max} (maximum electric field) or inverse piezoelectric charge coefficient per layer and inverse piezoelectric charge coefficient per all layers respectively.

displacement of 130pC/N, 0.17% and 2.1μm, respectively at much higher applied electric field (70kV/cm).

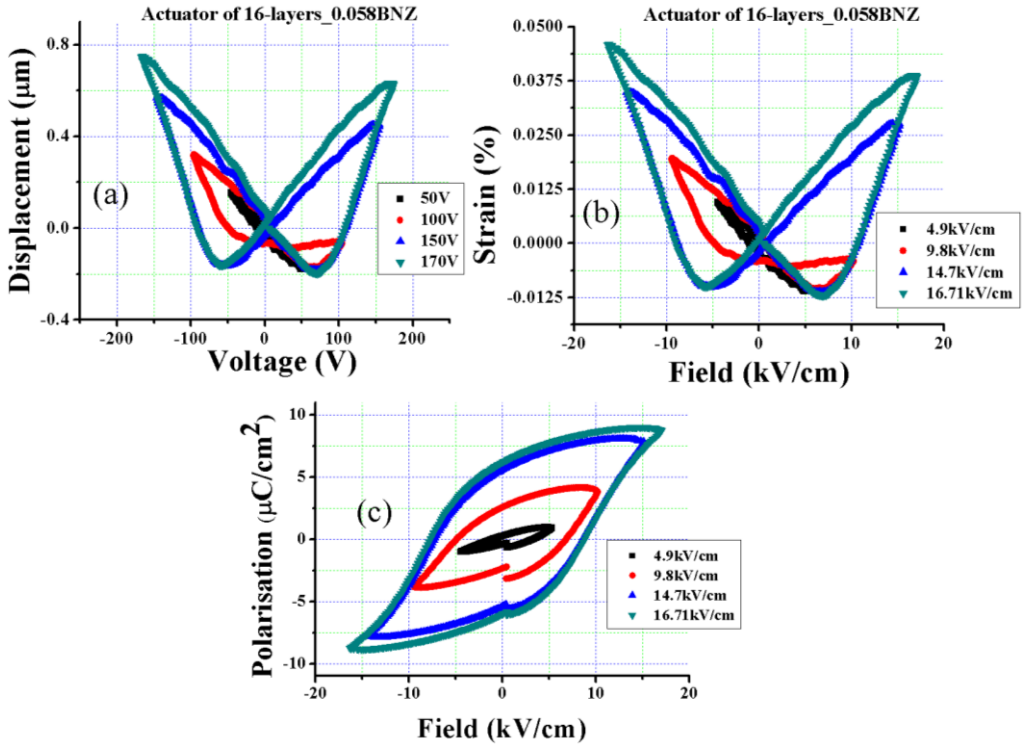

Figure 6-8 16-layers MLA sample of 0.942KNN-0.058BNZ compositions showing strain data & ferroelectric loops.

Each active piezoelectric layer in the 16-layer MLA (Figure 6-2b & Figure 6-8) is thinner than that in the 10-layer sample and could only sustain a weaker applied field (16.71 kV/cm) but the properties were similar and more symmetrical to the 10 layer actuators at the same respective electric field. Ferroelectric loops (Figure 6-8-c) at this applied voltage were beginning to saturate but higher voltages to achieve full saturation could not be applied without breakdown. Images obtained from scrap tape revealed more porosities in the green form than in the 10 layer samples, as shown in Figure 6-2-b. The total displacement (Figure 6-8-a) of the 16-layer sample was 0.70μm at relatively low volts (just 170V) with d_{33}* = 4118pm/V. It is proposed that

when the MLAs are fully optimised, they may be considered as low voltage actuators (≤ 200V) [38], within the current market.

Table 6-1 compares commercial PZT with those developed in the present study. The performance of KNN based ceramics are significantly worse than PZT-5H (Navy IV) and similar to PZT-5A (Navy II) but superior to PZT-4 (Navy-I) and PZT-8 (Navy-III). Comparison with other PbO-free ceramics is also shown in Table 6-1.

Table 6-1 Comparisons of general properties per layer (bulk) with well-established commercial type piezoelectric Ceramics

Piezoelectrics	**d_{33} (pC/N)**	**d_{33}* (pm/V)**	**tanδ**	**ε_r at RT,**	**T_C (°C)**	**References**
PZT-5A Nvy II	374	374		1700	350	[39]
PZT-5H Navy IV	593	585		3400	190	[39, 40]
PZT-4 Navy I		295		1300	325	[41]
PZT-8 Navy III		225		1000	300	[41]
KNN-Li (7%)	240	-	0.084	950	460	[42]
NBT-KBT-BT (MPB)	170	-	0.02	730	262	[43]
KNN-CZ 2 (MLCC)	160	360	-	1180	260	[20]
(KNN-0.058BNZ) + ZrO_2 (from Bulk & MLA)	250	423 & 460	0.028 & 0.041 at 1kHz	1812 & 1750 at 1kHz	300	This Study

6.4 Conclusions

Lead free KNN based MLAs were fabricated using the WMM method. To control volatilisation of K and Na, excess Zr^{4+} was utilised which additionally may have acted as an acceptor dopant in the system. At present, 10-layers and 16-layer MLAs with Pt internal electrodes generate 2500 and 3200 pC/N, respectively. Conversely, 10-layer MLAs can actuate with 2.21μm of displacement at moderately lower applied voltage (480V); and thin-layers actuator showed promising similar behaviour of applied maximum volts (170V). The effective d_{33}* of 10 and 16 layers were 4604pm/V and 4118pm/V, respectively. It is concluded therefore that for room temperature applications such as piezoelectric energy harvesting, KNN-BNZ offers a PbO-free alternative to PZT.

References

1. Zhang, S., F. Yu, and D.J. Green, *Piezoelectric Materials for High Temperature Sensors.* Journal of the American Ceramic Society, 2011. **94**(10): p. 3153-3170.
2. Wang, Y., et al., *High-Temperature Instability of Li- and Ta-Modified (K,Na)NbO_3Piezoceramics.* Journal of the American Ceramic Society, 2008. **91**(6): p. 1962-1970.
3. Lee, Y.-h., et al., *Piezoelectric Properties and Densification Based on Control of Volatile Mass of Potassium and Sodium in ($K_{0.5}Na_{0.5}$)NbO_3Ceramics.* Japanese Journal of Applied Physics, 2008. **47**(6): p. 4620-4622.
4. Lin, D., K.W. Kwok, and H.W.L. Chan, *Dielectric and piezoelectric properties of ($K_{0.50}Na_{0.50}NbO_3$–$BaZr_{0.050}Ti_{0.950}O_3$) lead-free ceramics.* Applied Physics Letters, 2007. **91**(14): p. 143513.

5. Zhao, Y., et al., *Low-temperature sintering of KNN with excess alkaline elements and the study of its ferroelectric domain structure.* Current Applied Physics, 2013. **13**(9): p. 2082-2086.

6. Tan, C.K.I., et al., *0.94($K_{0.5}Na_{0.5}$)NbO_3–0.06$LiNbO_3$ piezoelectric ceramics prepared from the solid state reaction modified with polyvinylpyrrolidone (PVP) of different molecular weights.* Ceramics International, 2012. **38**(3): p. 2513-2519.

7. Bafandeh, M.R., et al., *Improvement of piezoelectric and ferroelectric properties in (K,Na)NbO_3- based ceramics via microwave sintering.* Journal of Electroceramics, 2014. **33**(1-2): p. 128-133.

8. Wu, J., et al., *New potassium-sodium niobate lead-free piezoceramic: Giant-d_{33} vs. sintering temperature.* Journal of Applied Physics, 2014. **115**(11): p. 114104.

9. Zheng, T., et al., *Giant d_{33} in nonstoichiometric (K,Na)NbO_3-based lead-free ceramics.* Scripta Materialia, 2015. **94**: p. 25-27.

10. Donnelly, N.J. and C.A. Randall, *Pb loss in Pb(Zr,Ti)O_3 ceramics observed by in situ ionic conductivity measurements.* Journal of Applied Physics, 2011. **109**(10): p. 104107.

11. Zheng, H., et al., *Effects of strontium substitution in Nb-doped PZT ceramics.* Journal of European Ceramic Society, 2001. **21**: p. 1371-1375.

12. Reaney, I.M., *Octahedral tilting, domain structure and piezoelectricity in perovskites and related ceramics.* Journal of Electroceramics, 2007. **19**(1): p. 3-10.

13. Zheng, H., I.M. Reaney, and W.E. Lee, *Effects of Octahedral Tilting on the Piezoelectric Properties of Strontium-Barium-Niobium-Doped Soft Lead*

Zirconate Titanate Ceramics. Jounal of American Ceramic Society, 2002. **85**(9).

14. Malic, B., et al., *Influence of zirconia addition on the microstructure of $K_{0.5}Na_{0.5}NbO_3$ ceramics.* Journal of the European Ceramic Society, 2008. **28**(6): p. 1191-1196.
15. Hiroyuki Hayashi, S.K., et al., *Reliability of Nickel Inner Electrode Lead-Free Multilayer Piezoelectric Ceramics.* Japanese Journal of Applied Physics, 2012. **59**(09LD01).
16. Kui Yao , W.Z., *Improved preparation procedure and properties for a multilayer piezoelectric thick-film actuator.* Sensors and Actuators A: Physical, 1998. **71**: p. 139-143.
17. Alper Erturk, D.J.I., *Piezoelectric Energy Harvesting*. 2011: A John Wiley & Sons.
18. Uchino, K., *Materials issues in design and performance of piezo actuators:Overview.* Acta Metallurgica, 1998. **46**(11): p. 3745-3753.
19. Kim, M.-S., et al., *Lead-free NKN-5LT piezoelectric materials for multilayer ceramic actuator.* Journal of Electroceramics, 2008. **23**(2-4): p. 372-375.
20. Kawada, S., et al., *$(K_{0.5},Na_{0.5})NbO_3$-Based Multilayer Piezoelectric Ceramics with Nickel Inner Electrodes.* Applied Physics Express, 2009. **2**(11): p. 111401.
21. Gao, R., et al., *Investigation on co-fired multilayer KNN-based lead-free piezoceramics.* physica status solidi (a), 2014. **211**(10): p. 2378-2383.
22. Gao, R., et al., *A study on (K, Na) NbO_3based multilayer piezoelectric ceramics micro speaker.* Smart Materials and Structures, 2014. **23**(10): p. 105018.

23. El Hosiny Ali, H., et al., *Properties of multilayer composite thin films based on morphotropic phase boundary* $Pb(Mg_{1/3}Nb_{2/3})O_3$-$PbTiO_3$. Thin Solid Films, 2012. **520**(24): p. 7205-7211.

24. Kahoul, F., L. Hamzioui, and A. Boutarfaia, *The Influence of Zr/Ti Content on the Morphotropic Phase Boundary and on the Properties of PZT–SFN Piezoelectric Ceramics.* Energy Procedia, 2014. **50**: p. 87-96.

25. Wang, D., Hussain, F, Khesro, A, et al., *Composition and temperature dependence of piezoelectricity in* $(1-x)(K_{1-y}Na_y)NbO_3$-$x(Bi_{1/2}Na_{1/2})ZrO_3$ *lead-free ceramics.* American Ceramic Society, 2016.

26. Wang, Z., et al., *New Lead-Free* $(1-x)(K_{0.5}Na_{0.5})NbO_3$-$x(Bi_{0.5}Na_{0.5})ZrO_3$*Ceramics with High Piezoelectricity*. Journal of the American Ceramic Society, 2014. **97**(3): p. 688-690.

27. Weaver, P.M., et al., *High temperature measurement and characterisation of piezoelectric properties.* Journal of Materials Science: Materials in Electronics, 2015. **26**(12): p. 9268-9278.

28. Stevenson, T., et al., *Surface mapping of field-induced piezoelectric strain at elevated temperature employing full-field interferometry*. IEEE Trans Ultrason Ferroelectr Freq Control, 2015. **62**(1): p. 88-96.

29. Ceramics, M.T. http://www.morgantechnicalceramics.com/en-gb/datasheets/material-datasheets/. [cited 2016 09/16/2016].

30. Stevenson, T., et al., *Piezoelectric materials for high temperature transducers and actuators.* Journal of Materials Science: Materials in Electronics, 2015. **26**(12): p. 9256-9267.

31. Morozov, M.I. and D. Damjanovic, *Hardening-softening transition in Fe-doped Pb(Zr,Ti)O_3 ceramics and evolution of the third harmonic of the polarization response.* Journal of Applied Physics, 2008. **104**(3): p. 034107.

32. Chen, Y.-H., et al., *Mn-Modified Pb($Mg_{1/3}Nb_{2/3}$)O_3-$PbTiO_3$ Ceramics: Improved Mechanical Quality Factors for High-Power Transducer Applications.* Japanese Journal of Applied Physics Part 1, 2000. **39**(8): p. 4843-4852.

33. C. K. , K., *Dielectric Phenomena In Solids : With Emphasis on Physical Concepts of Electronic Processes*. 2004, USA: Elsevier Academic Press.

34. Damjanovic, D., *Chapter4, 'Hysteresis in Piezoelectric and Ferroelectric materials'* I. Mayergoyz and G.Bertotti (Eds.) ed. The Science of Hysteresis, ed. G. Bertotti, Mayergoyz, I.D., . Vol. 3. 2005: Elsevier.

35. Dragan, D., Demartin, M., *Contribution of the irreversible displacement of domain walls to piezoelectric effect in Barium Titanate and Lead Zirconate Titanate ceramics.* Journal of Physics: Condensed Matter, 1997. **9**: p. 4943-4953.

36. Brinkman, E., et al., *The Hidden use of Piezo Technology in Applications all around us*. 2011, The Netherlands: applied PIEZO, Stichting Applied Piezo.

37. Nagata, H., Hiruma, Y., Takenaka, T.,, *Electric-field-induced strain for ($Bi_{0.50}Na_{0.50}$)TiO3-based lead-free multilayer actuator.* Journal of Ceramic Society of Japan, 2010. **118**(8): p. 726-730.

38. APC, *First Steps Towards Piezoaction*. APC International Ltd.

39. efunda. *Lead Zirconate Titanate (PZT-5H): http://www.efunda.com/materials/piezo/material_data/matdata_output.cfm?Material_ID=PZT-5H*. [cited 2016 09/20/2016].

40. Wang, D., Y. Fotinich, and G.P. Carman, *Influence of temperature on the electromechanical and fatigue behavior of piezoelectric ceramics.* Journal of Applied Physics, 1998. **83**(10): p. 5342.

41. BOSTON Piezo Optics. *Ceramic Materials: General Characteristics; http://bostonpiezooptics.com/ceramic-materials-pzt*. [cited 2016 09/20/2016].

42. Hollenstein, E.D., Matthew Damjanovic, Dragan, Setter, Nava, *Piezoelectric properties of Li- and Ta-modified $(K_{0.5}Na_{0.5})NbO_3$ ceramics.* Applied Physics Letters, 2005. **87**(18): p. 182905.

43. Zang, S., Shrout, T.R., et al., , *Piezoelectric properties in $(K_{0.5}Bi_{0.5})TiO_3$-$(Na_{0.5}Bi_{0.5})TiO_3$-$BaTiO_3$ lead-free ceramics.* IEEE Transactions On Ultrasonics, Ferroelectrics, And Frequency Control, 2007. **54**(5): p. 910-917.

Chapter 7 Conclusions

7. Conclusions

KNN based compounds have been extensively studied for decades but most recently they have received attention as lead free replacements the PZT.

7.1. Undoped KNN

At the start of this study, undoped KNN was synthesized with different ratios of K^+ and Na^+ and fired in air and N_2. 95% relative density was obtained in these systems in air and N_2 utilising a conventional mixed oxide route. XRD of all undoped KNN ceramics and powders revealed an orthorhombic crystal structure with Bmm2 symmetry. Minor peaks of a tetragonal tungsten bronze structured secondary-phase (TTB) were also observed in air but not in N_2 sintered pellets. Impedance spectroscopy and thermo-power analysis confirmed that un-doped KNN was *p*- and *n*-type when sintered in air and N_2, respectively. Moreover, dielectric losses increased in N_2 sintering conditions, presumably due to the formation of oxygen vacancies and accompanying electrons. Optimum P_r, k_p and d_{33} were obtained for air-sintered samples with P_r=29μC/cm^2 for KNN_50/50_and d_{33}=125pC/N and k_p=0.38 for KNN_51/49. Equivalent samples sintered in N_2 had lower values of P_r, k_p and d_{33}. For applications, these properties were considered too low and therefore dopant strategies were pursued in an attempt to improve properties.

7.2. Single doped KNN

Acceptor dopants such as Mn^{2+} ($Mn_{Nb}^{\prime\prime\prime}$) and Ti^{4+} ($Ti_{Nb}^{\prime}$) at B-site of KNN were incorporated to modify properties but they both inhibited densification of KNN. Nonetheless, both acceptor species were soluble in the lattice, as revealed by XRD. Dielectric losses increased dramatically at lower frequency with increasing temperature by using acceptors, but were moderately lower at higher frequency.

These losses are likely associated with the formation of V_O, but the increase in porosity (decrease in density) may also play a role. A further B-site dopant (Sn^{4+}) was also attempted but was insoluble as evidenced by the appearance of secondary phase peaks in XRD data at low concentrations. Nevertheless, Sn^{4+} was an effective sintering aid in KNN-50/50 and improved its relative density.

Sr^{2+} was used as a donor ion on the A-site in $(K_{0.50}N_{0.50})_{1-x}$ Sr_xNbO_3 where $0.01 \leq x \leq 0.07$. Ceramic density improved with 1 mole% but at a higher sintering temperature. Sr^{2+} doped formulations showed higher conductivity which manifested itself in higher values of tan δ and leaky P-E loops. T_C of KNN-1Sr in N_2 decreased with respect to air sintered samples as observed in un-doped compositions.

Finally, isovalent Ta^{5+} doping was attempted. XRD data showed the structure to be tetragonal at room temperature with up to 30 mol% Ta^{5+} on the B-site but double-peaks were observed in relative permittivity plots even though XRD appeared to index based on a single perovskite phase. The simplest explanation is that Ta doped KNN is a two phase mix of Ta rich and Nb rich (with respect to the base composition) perovskite. The absence of a second perovskite phase in the XRD data may be explained by the identical ionic radius and thus resultant lattice parameter of Ta^{5+} (0.64 Å) and Nb^{5+} (0.69 Å)[1]. Despite their identical radius and charge, the difference in mass (Ta (180.95 amu) > Nb (92.90 amu))[2] accounts for a difference in polarizability with (4.75 $^{\circ}A^3$) Ta^{5+} > Nb^{5+} (3.98 $^{\circ}A^3$),[3] hence Ta has a lower T_C than the Nb rich phase and two peaks appear in the permittivity versus temperature curves. There was a marginal improvement in piezoelectric properties (d_{33} = 135pC/N) for 10 mol% Ta^{5+} but no significant enhancement was observed at > 10 mol% Ta^{5+}.

7.3. Co-doped KNN

Stoichiometric co-doping KNN was also investigated based on initial work reported in [4-8]. Bi^{3+} and Zr^{4+} were substituted onto the A- and B-site, respectively, to give the effective solid solution KNN-BNZ. The net result of this substitution was a dramatic increase in piezoelectric properties (d_{33}=315pC/N and k_p =0.45) at room temperature and compositions showed great promise for applications in stark contrast to singly doped compositions and hence were chosen for further work to develop multilayers.

7.4 Multilayers of co doped KNN

Multilayers of 10 and 16 layers with Pt electrodes were prepared for the first time from KNN-BNZ (where x=0.058) with trace excess of ZrO_2 to inhibit volatilisation and potentially act as an acceptor dopant. Commercial grade raw materials were used to demonstrate scalability and a new simple method (WMM) was utilised to improve lamination prior to binder burnout and densification. A Na/K (50/50) ratio was chosen such that the crystal structure was tetragonal at RT as determined by XRD and LCR data with T_{O-T} & T_{R-O} subambient. Optimum effective d_{33}, effective d_{33}* and displacement of 10-layers were recorded as 2500pC/N, 4604pm/V and 2.21μm, respectively, at 480V. These values compare well with commercial devices based on well-established such as PZT-4 and PZT-8 ceramics.

References

1. Shannon, R.D., *Revised Effective Ionic Radii and Systematic Studies of Interatomie Distances in Halides and Chalcogenides.* Acta Crystallographica Section A, 1976. **32**(5): p. 751-767.

2. Chemical Elements. *Periodic Table: Atomic mass:* http://www.chemicalelements.com/show/mass.html. 2016 [cited 2016 10/12/2016].

3. Shannon, R.D., *Dielectric polarizabilities of ions in oxides and fluorides.* Journal of Applied Physics, 1993. **73**(1): p. 348.

4. Wang, Z., et al., *New Lead-Free* $(1-x)(K_{0.5}Na_{0.5})NbO_3$-$x(Bi_{0.5}Na_{0.5})ZrO_3$*Ceramics with High Piezoelectricity.* Journal of the American Ceramic Society, 2014. **97**(3): p. 688-690.

5. Wu, J., et al., *New potassium-sodium niobate lead-free piezoceramic: Giant-*d_{33} *vs. sintering temperature.* Journal of Applied Physics, 2014. **115**(11): p. 114104.

6. Wang, X., et al., *Giant piezoelectricity in potassium-sodium niobate lead-free ceramics.* J Am Chem Soc, 2014. **136**(7): p. 2905-10.

7. Wang, X., et al., *Large* d_{33} *in* $(K,Na)(Nb,Ta,Sb)O_3$-$(Bi,Na,K)ZrO_3$ *lead-free ceramics.* Journal of Materials Chemistry A, 2014. **2**(12): p. 4122.

8. Zheng, T., et al., *Giant* d_{33} *in nonstoichiometric* $(K,Na)NbO_3$*-based lead-free ceramics.* Scripta Materialia, 2015. **94**: p. 25-27.

Chapter 8 Future Work

8.1 KNN multilayers

From previous research, some KNN compositions are compatible with cheap Ni inner electrodes [1, 2] but this necessitates firing multilayers in low $P(O_2)$ atmospheres to prevent oxidation of the Ni [3]. In this study, Pt internal electrodes were utilised and multilayers were fired in air. Some studies on bulk undoped KNN ceramics were performed in lower $P(O_2)$ using a N_2 atmosphere. The samples remained insulating but there was a clear effect on the conductivity with samples becoming lossier at lower frequencies and exhibiting *n*- rather than *p*-type behaviour. Typically, commercial Ni electrode MLCCs are fabricated in N_2 with up to 3%H_2, further reducing the $P(O_2)$ with respect to N_2.[4-7] It is anticipated that further increases in conductivity are likely at lower $P(O_2)$ and that dopants would be required to inhibit reduction. In MLCC technology, acceptor dopants such as Ca, Mg and Mn are often substituted onto the B-site to prevent reduction or at least suppress the migration of V_O. It is proposed that a similar dopant strategy could be afforded to permit the use of Ni electrodes and low $P(O_2)$ sintering. However, it should be noted that the use of Bi^{3+} as a dopant in these materials may well affect the stability of the ceramic with respect to the Ni electrode based on an assessment of the thermodynamics of NiO versus Bi_2O_3 in the Ellingham Diagram.[8] Further studies are therefore required to determine ideal dopants for the fabrication of KNN based multilayers using Ni based electrodes.

This study developed a simple low cost methodology for lamination in MLA fabrication referred to as the wet-method-multilayers (WMM) method. It is proposed that WMM is attempted for a wider range of multilayer applications. To date, Khesro et al.,2016 [9] (KBT based piezoelectric multilayers) and Nicholls (2016)[10]

($Li_{1/2}Nd_{1/2}TiO_3$ based multilayers) within the Functional Materials and Devices group at Sheffield have utilised this methodology and achieved significantly better densification in their respective multilayers.

8.2. Characterisation

Some TEM samples of undoped KNN fired in air and N_2 were prepared and some basic diffraction patterns obtained. However, more TEM is required to study the domain structure of compositions, particularly KNN-BNZ to give a comprehensive understanding of structure-properties and likely domain-switching. Although not included in the thesis, seed crystals (~500 μm) were also introduced in undoped KNN in an attempt to promote grain growth and improve piezoelectric properties. [1, 4]. An improvement was observed and further work is suggested in this area to optimise properties in KNN-BNZ and in particular to look at the relation between grain size and domain structure using TEM. A detailed study of the interfacial reactions and domain structure is also required for multilayers.

References

1. Kawada, S., et al., *$(K_{0.5},Na_{0.5})NbO_3$-Based Multilayer Piezoelectric Ceramics with Nickel Inner Electrodes.* Applied Physics Express, 2009. **2**(11): p. 111401.
2. Liu, C., et al., *Base metal Co-fired $(Na,K)NbO_3$ structures with enhanced piezoelectric performance.* Journal of Electroceramics, 2014. **32**(4): p. 301-306.

3. Peraldi, R., et al., *High temperature oxidation of high purity nickel: oxide scale morphology and growth kinetics.* Materials at High Temperatures, 2003. **20**(4): p. 649-655.

4. Hiroyuki Hayashi, S.K., et al., *Reliability of Nickel Inner Electrode Lead-Free Multilayer Piezoelectric Ceramics.* Japanese Journal of Applied Physics, 2012. **59**(09LD01).

5. Yamamatsu, J., et al., *Reliability of multilayer ceramic capacitors with nickel electrodes.* Journal of Power Sources, 1996. **60**: p. 199-203.

6. Kishi, H., Y. Mizuno, and H. Chazono, *Base-Metal Electrode-Multilayer Ceramic Capacitors: Past, Present and Future Perspectives.* Japanese Journal of Applied Physics Part 1, 2003. **42**: p. 1-15.

7. Herbert, J.M., *High permittivity Ceramics Sintered in Hydrogen.* Transactions of British Ceramic Society, 1963. **62**(8): p. 645.

8. MIT. *Ellingham Diagrams,* *http://web.mit.edu/2.813/www/readings/Ellingham_diagrams.pdf*. 2016 [cited 2016 10/13/2016].

9. Khesro, A., Wang, D, Hussain, F, et al., *Temperature Stable and Fatigue resistant Lead-free Ceramics for actuators* Applied Physics Letters, 2016. **109**(14).

10. Nicholls, S.J., *High Permittivity Ceramics for Dielectrically Loaded Applications*, in *Materials Science and Engineering*2016, University of Sheffield: Sheffield, UK.